





This is to certify that the

thesis entitled

Electronic Speckle Pattern

Interferometry and Applications In

Engineering Mechanics

presented by

Xiaolu Chen

has been accepted towards fulfillment of the requirements for

Master's degree in Mechanics

Hay L Cloud
Major professor

Date 24 Feb 1992

O-7639

MSU is an Affirmative Action/Equal Opportunity Institution

LIBRARY Michigan State University

PLACE IN RETURN BOX to remove this checkout from your record.

TO AVOID FINES return on or before date due.

	DATE DUE	DATE DUE	
SEP 25 1995		<u> </u>	
FATH I I I I I I I I I I I I I I I I I I I			
	<u>.</u>		

MSU is An Affirmative Action/Equal Opportunity Institution

ELECTRONIC SPECKLE PATTERN INTERFEROMETRY AND APPLICATIONS IN ENGINEERING MECHANICS

By Xiaolu Chen

A THESIS

Submitted to

Michigan State University
in partial fulfillment of the requirements
for the degree of

MASTER OF SCIENCE

Department of Materials Science and Mechanics

ABSTRACT

ELECTRONIC SPECKLE PATTERN INTERFEROMETRY AND APPLICATIONS IN ENGINEERING MECHANICS

By

Xiaolu Chen

Holographic interferometry (HI) techniques have been brought to near perfection and have solved a wide variety of practical problems. The techniques have, however, not received the general acceptance in industry as their potential should indicate. The major reluctance stems from the cumbersome and slow process of film recording and development, and from the method's sensitivity to environmental disturbances.

This paper describes the calibration and use of an Electronic Speckle Pattern Interferometry (ESPI) system which is a combination of holography, video recording, signal processing and computer technology. The major advantages of ESPI are fast recording (1/30 s), real time correlation fringe display, and computer controlled speckle pattern image processing with displacement calculation. ESPI also can display real time modal shape of a vibrating object. The theory of speckle pattern decorrelation and actual measurements obtained from ESPI are discussed in detail. Some results of using ESPI as a nondestructive test tool for composite material are presented. Conclusions and recommendations are presented.

To My Parents

ACKNOWLEDGMENTS

The author wishes to express his sincerest appreciation and gratitude to his academic advisor and major professor Gary Lee Cloud for his valuable guidance and encouragement during the course of this research.

The author also wishes to thank his wife Jianzhen Xie and newborn son Louie Chen for their patience, understanding, help and encouragement.

TABLE OF CONTENTS

	Page
LIST OF TABLES	vi
LIST OF FIGURES	vii
INTRODUCTION	1
CHAPTER 1 LASER SPECKLE AND ITS ROLE IN ESPI	6
1.1 Speckle and Its Origins	6
1.2 Size of Speckle	9
1.2.1 Objective Speckle Size	9
1.2.2 Subjective Speckle Size	10
1.3 The Brightness Distribution of Speckles	11
1.4 Coherent Combination of Speckle and Uniform Fields	13
1.4.1 Size	13
1.4.2 Brightness Distribution	13
1.5 Coherent and Incoherent Combination of Two Speckle Fields	14
1.6 Polarization Effects	16
1.7 Speckle Pattern Decorrelation	17
1.7.1 Out-of-plane Translation	19
1.7.2 In-plane Translation	20
1.7.3 Out-of-plane Rotation	21
1.7.4 In-plane Rotation	21

CHAPTER 2 DISPLACEMENT ANALYSIS AND OPTICAL SETUPS	22
2.1 Sensitivity Vector	22
2.2 Out-of-plane Displacement Sensitive Optical Setup	26
2.3 In-plane Displacement Sensitive Optical Setup	27
2.4 Two Special Cases	32
2.4.1 Pure Out-of-plane Displacement	32
2.4.2 Pure In-plane Displacement	34
2.5 Limitations of ESPI	35
2.5.1 Measurement Sensitivity	35
2.5.2 Object Size Limitations	36
2.5.3 Depth of Field	37
2.5.4 Surface Condition	37
2.6 Practical Optical Setups for ESPI	38
CHAPTER 3 ESPI SYSTEM	41
3.1 Introduction	41
3.2 Video System and Other Electronics in ESPI	41
3.3 Speckle Correlation Fringe Formation by Video Signal Subtraction	44
3.4 Speckle Correlation Fringe Formation by Video Signal Addition	46
3.5 The Measurement of Real Time Vibration Pattern	48
3.6 The Measurement of Dynamic Displacement	51
3.7 The Optimization of Light Intensity in ESPI	51
3.7.1 Two Speckle Beam Case	52
3.7.2 Smooth Reference Beam Case	52
3.8 Spatial Resolution of the Video System and Its Effect on ESPI	52
3.8.1 Spatial Resolution (two-speckled-beam case)	55
3.8.2 Spatial Resolution (smooth reference beam case)	56

3.8.3 General Conclusion60
3.9 Error Sources
3.10 Displacement Measurement Using Phase Information62
3.10.1 Principal Phase Determinationn
3.10.2 Phase Measurement62
3.10.3 Means of Phase Shifting64
3.10.4 Phase-measurement Algorithms65
3.10.5 Comparison of Phase Measurement Techniques74
3.10.6 Phase Unwrapping75
3.10.7 From Phase Change to Displacement
CHAPTER 4 NONDESTRUCTIVE TEST OF COMPOSITE USING ESPI78
4.1 Stressing Techniques
4.1.1 Mechanical Stressing
4.1.1 Mechanical Stressing
4.1.2 Thermal Stressing
4.1.2 Thermal Stressing
4.1.2 Thermal Stressing 79 4.1.3 Pressure Stressing 80 4.1.4 Acoustic Stressing 81
4.1.2 Thermal Stressing 79 4.1.3 Pressure Stressing 80 4.1.4 Acoustic Stressing 81 4.1.5 Vibration Excitation 81
4.1.2 Thermal Stressing 79 4.1.3 Pressure Stressing 80 4.1.4 Acoustic Stressing 81 4.1.5 Vibration Excitation 81 4.1.6 Microwave Excitation 81
4.1.2 Thermal Stressing 79 4.1.3 Pressure Stressing 80 4.1.4 Acoustic Stressing 81 4.1.5 Vibration Excitation 81 4.1.6 Microwave Excitation 81 4.2 NDT Results of Composite using ESPI 82
4.1.2 Thermal Stressing 79 4.1.3 Pressure Stressing 80 4.1.4 Acoustic Stressing 81 4.1.5 Vibration Excitation 81 4.1.6 Microwave Excitation 81 4.2 NDT Results of Composite using ESPI 82 4.2.1 Using Thermal Stressing 82
4.1.2 Thermal Stressing 79 4.1.3 Pressure Stressing 80 4.1.4 Acoustic Stressing 81 4.1.5 Vibration Excitation 81 4.1.6 Microwave Excitation 81 4.2 NDT Results of Composite using ESPI 82 4.2.1 Using Thermal Stressing 82 4.2.2 Using Gravity (creeping) 95
4.1.2 Thermal Stressing 79 4.1.3 Pressure Stressing 80 4.1.4 Acoustic Stressing 81 4.1.5 Vibration Excitation 81 4.1.6 Microwave Excitation 81 4.2 NDT Results of Composite using ESPI 82 4.2.1 Using Thermal Stressing 82 4.2.2 Using Gravity (creeping) 95

LIST OF TABLES

Table		Page
1.1	Fringe order N vs vibration amplitude	
	in time-average ESPI mode	50
1.2	Determination of the phase modulo 2π	76

LIST OF FIGURES

Figu	ure	Page
1.0	Step by step comparison between (A) real time	
	image holography and (B) ESPI system	4
1.1	A typical image plane speckle pattern	7
1.2	Formation of objective speckle	9
1.3	Formation of subjective speckle	10
1.4	Probability density functions of the brightness	
	distribution of a fully-developed speckle feild	12
1.5	Coherent combination of speckle field and uniform field	14
1.6	Incoherent combination of two speckle fields	16
1.7	Diagram for speckle decorrelation analysis	18
2.1	Position and propagation vectors	22
2.2	The variation of $\frac{d_m}{d_n}$ resulting from the change	
	of illuminating and viewing angle	25
2.3	Out-of-plane sensitive ESPI optical setup	
	using uniform reference beam	26
2.4	ESPI with reduced out-of-plane displacement sensitivity	27
2.5	The optical arrangement for in-plane displacement sensitive setup	28
2.6	An alternative optical setup of in-plane displacement measurement	30
2.7	A practical optical setup of an in-plane	
	displacement sensitive ESPI system	31
28	Pure out-of-plane displacement	32

2.9	The relationship between d_m and d to illumination	
	angle θ in pure out-of-plane case	33
2.10	Pure in-plane displacement	34
2.11	The relationship between d_m and d to illumination	
	angle θ in pure in-plane case	35
2.12	A smooth, in-line reference beam interferometer which	
	uses a beam splitter to combine the object and reference beams	39
2.13	A smooth, in-line reference beam interferometer based on	
	the hole-in-mirror principle	40
3.1	The block diagram of ESPI system	42
3.2	The first few cycles of the J_0^2 distribution which defines the	
	intensity distribution of time-averaged speckle fringes for a	
	sinusoidally vibrating surface	50
3.3	The general geometry of a smooth	
	reference beam interferometer	57
3.4	Schematic for measuring phase using a PZT mirror as the phase	
	shifter and sending data to a computer for the phase calculation	63
3.5	(1) CCD array with finite-sized detector element. (2) Detector	
	element much smaller than speckle size. (3) The size of	
	the detector element and speckle are almost equal. (4) Speckle	
	size is much smaller than the detector element	67
4.1	The ESPI system	83
4.2	Impact damaged composite (glass/epoxy) specimens used	
	in NDT using ESPI gravity and thermal stressing tech niques	84
4.3	Setup for NDT of composite using ESPI thermal (resistor) method	86
4.4	Setup for NDT of composite using ESPI thermal (steamer) method	87
45	Fringe pattern obtained when composite plate #7 is 'point heated'	

	at the center using a resistor heating device and then with	
	the heater removed	88
4.6	Fringe pattern obtained when composite plate #7 is heated	
	at the upper right corner using a resistor heating device	
	and then the heater is removed	89
4.7	Fringe pattern obtained when composite plate #7 is in free	
	expansion at ΔT about 8 °C (23-15) with Δt about 5 seconds	90
4.8	Fringe pattern of plate #9 when heated at the upper right	
	corner and then with the heater removed	91
4.9	The 3D plot of Figure 4.8	92
4.10	The 2D plot of Figure 4.8 of the section where the	
	damage spot is located	93
4.11	The 2D plot of Figure 4.8 of a arbitrary section	
	away from the damaged spot	94
4.12	Setup for NDT of composite using ESPI by gravity creeping method	96
4.13	Plate #3 creeping at room temperature with	
	fringe accumulation time $\Delta t = 5$ sec	98
4.14	Plate #9 creeping at room temperature with fringe	
	accumulation time $\Delta t = 30 \text{ sec}$	99
4.15	Plate #7 creeping at room temperature with fringe	
	accumulation time $\Delta t = 30$ sec	100
4.16	Impact damaged composite (glass/epoxy) specimens used in NDT	
	using ESPI time-average mode, speaker was used for excitation	101
4.17	Setup for vibration test using a speaker	102
4.18	Plate #1 vibrating at 173 Hz, (a) before impact, (b) after impact	103
4.19	Plate #1 vibrating at 707 Hz, (a) before impact, (b) after impact	104
4.20	Plate #1 vibrating at 942 Hz. (a) before impact. (b) after impact	105

4.21	Plate #6 vibrating at 100 Hz, (a) before impact, (b) after impact	106
4.22	Plate #6 vibrating at 300 Hz, (a) before impact, (b) after impact	107
4.23	Plate #6 vibrating at 388 Hz, (a) before impact, (b) after impact	108
4.24	Plate #6 vibrating at 451 Hz, (a) before impact, (b) after impact	109
4.25	Plate #6 vibrating at 761 Hz, (a) before impact, (b) after impact	110
4.26	Plate #6 vibrating at 805 Hz, (a) before impact, (b) after impact	111
4.27	Experimental setup for nondestructive inspection using ESPI's	
	time-average vibration mode. The composite being tested	
	is A s-4/828 mPDA, 18 plies, the depth of cut is 9 plies	112
4.28	The carbon fiber plate vibrating at 2057 Hz,	
	(a) plate without cuts, (b) plate with cuts	113
4.29	The carbon fiber plate vibrating at 8150 Hz,	
	(a) plate without cuts, (b) plate with cuts	114

INTRODUCTION

With the advent of the laser in 1960 and the holographic recording process, a unique technique which is called holographic interferometry (HI) was created to perform interferometric measurements on objects. HI was first demonstrated by Powell and Stetson [1] for vibration study. HI has many advantages as a measuring technique; as the wavelength of the laser light serves as the measuring unit, it is a noncontact, nondestructive method with very high sensitivity. In addition, the information is presented as a three-dimensional image of the test object which is covered with a fringe pattern. From the appearance of this pattern one can quickly determine the overall deformation and the location of stress concentrations. HI applications have been demonstrated by many authors[2-6]. In spite of these obvious advantages, industry in general has been slow to accept this new technique. HI has been mostly confined to research laboratories with some notable exceptions, e.g. Rolls-Royce [7] in England, Brown Boyeri in Switzerland and in the tire quality inspection area. The reasons for this, apart from the usual distrust towards new unfamiliar techniques, are in two aspects. First, the stability requirement in holography is not readily compatible with industry environments unless pulsed lasers are used. Second, the photographic recording process and subsequent development introduce an annoying time delay which prevents on-line inspection. Although self-developing and reusable recording media have been developed, there still remains a time delay between the recording and observation of the fringe pattern, and direct computer data processing is not applicable. In addition, the cost for consumable material is fairly high.

The essential of a hologram interferometer is that it records the complete pattern of waves emanating from the object, both in amplitude and phase, by combining it with a so-called reference beam. To measure deformation, wave patterns are recorded when the object surface is in its original and deformed states, and these are combined to give an interference fringe pattern related to the deformation that has taken place. The holographic process is used here only as an intermediate step in the acquisition of this fringe data, and unnecessary information relating to the three-dimensional shape and the surface reflectance of the object are included. The hologram stores far more information about the surfaces than is really necessary for measuring surface displacement.

For this reason it is natural to investigate the use of television systems to replace photographic recording materials and to use electronic signal processing and computer techniques to generate interference fringe patterns. This technique is called Electronic Speckle Pattern Interferometry (ESPI). The basic principle of ESPI was developed almost simultaneously by Macovski et al (1971) [8] in the United States, Schwomma (1972) [9] in Austria, and Butters and Leendertz (1971) [10] in England. The last group especially has pursued the development of the ESPI technique vigorously in both theoretical and practical directions. Later, another group in Norway headed by Ole Lokberg also started successful research and development in ESPI.

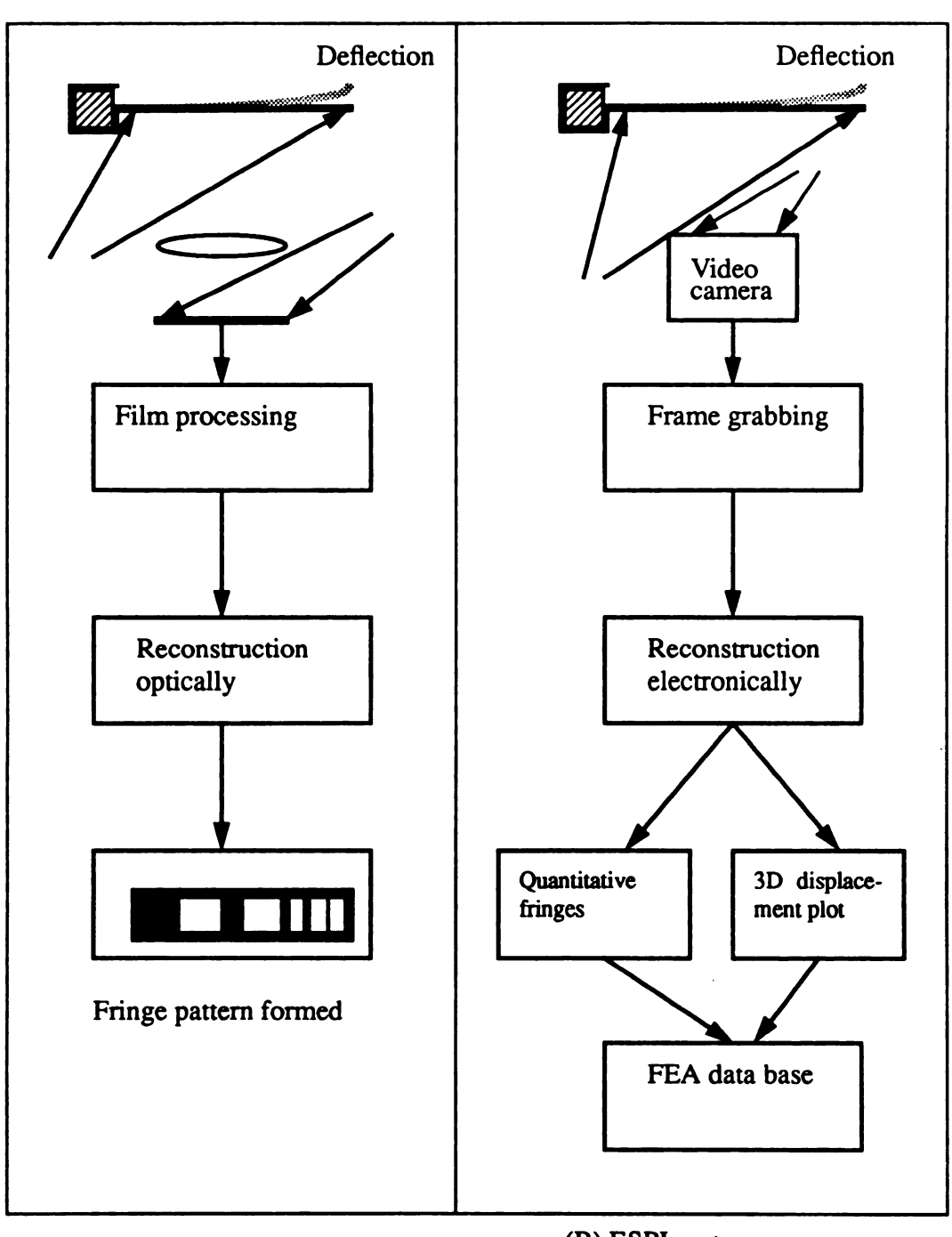
For speckle pattern interferometry, the resolution of the recording medium used need not be that high compared with that required for holography, since it is only necessary that the speckle pattern be resolved, and not the very fine fringes formed by the interference of object and holographic reference beam. The minimum speckle size is typically in the range 5 to $100 \, \mu m$, and it can be varied to some extent to suit the resolution limits of a TV camera without losing phase information about the surface position, so that a standard television camera may be used to record the speckle pattern. Thus, video processing may be used to generate correlation fringes equivalent to those obtained photographically.

The major feature of ESPI is that it enables real-time correlation fringes to be displayed directly upon a television monitor without recourse to any form of photographic processing and plate relocation. Furthermore, the vibration isolation is relaxed (only need 1/30 s to record a frame of speckle pattern) and no dark room is needed. A computer is used to control the entire process, to calculate the displacement and present results in graphical form. The advantages can be summarized as follows:

- 1. Does not require the highly stable environment necessary for conventional holographic interferometry.
- 2. System can be used in brightly lighted conditions, no dark room is needed.
- 3. Since no film and the processing of the film are needed, the material cost per experiment is very low.
- 4. People with little background in optics can operate the system.
- 5. The safety hazard is significantly lowered.
- 6. Expanded experimental capability.
- 7. High efficiency, automatic data processing, real-time result presentation.

Comparison of ESPI and HI

ESPI and image HI are compared step by step in Figure 1. The recording mechanism in holography is a film grain exposure which, after development, results in a proportional amplitude transmittance of the reconstruction wave. In ESPI the equivalence consists of a charge buildup which subsequently is transformed by the TV scan into a current proportional to the exposure. After first exposure, for HI one simply places the developed film (hologram) back into the reference wave. The interference pattern



(A) Image holography

(B) ESPI system

Fig. 1.0

Step by step comparison between (A) real time image holography and (B) ESPI system.

stored in the hologram now acts as a complex grating sending some of the light into a side order wave which is identical to the original object wave. Therefore we see a reconstructed image of the object which, upon deformation of the object, will create an interference fringe pattern. In ESPI we have to simulate the optical reconstruction by electronic processing of the video signal. Correlation fringes are obtained by electronic subtraction or addition and displayed on a TV monitor where we see the object covered with exactly the same bright and dark fringes as in holography, except that the image looks more coarse. Moreover, ESPI can calculate phase and displacement information and present the results in computer graphics very rapidly.

Chapter 1

Laser Speckle and Its Role in ESPI

Laser speckle is used as the phase information carrier in an ESPI system. Knowledge of its properties are very important for a good understanding of ESPI.

1.1 Speckle and Its Origins

Operation of the first continuous wave (cw) He-Ne laser in 1960 revealed an unexpected phenomenon; objects viewed in highly coherent light acquire a peculiar granular appearance. As illustrated in Figure 1.1, the detailed structure of this granularity bears no obvious relationship to the macroscopic properties of the illuminated object, but rather it appears chaotic and unordered, with an irregular pattern that is best described by the methods of probability and statistics [11].

The physical origin of the observed granularity, which we now know as "laser speckle", was quickly recognized by the early workers in the field [12-13]. The surfaces of most materials are extremely rough on the scale of an optical wavelength (0.6 microns). This includes most surfaces other than those which are polished to high optical quality. Speckle can also be produced by transmission through scattering objects such as ground glass, opal glass or particles in liquid. When laser light is reflected or scattered from such a surface, the optical wave arriving at any moderately distant point consists of many coherent components or wavelets, each arising from a different microscopic element of the surface. The distances travelled by these various wavelets may differ by several or many wavelengths if the surface is very rough. Interference of the dephased but coherent wavelets results in the granular pattern of intensity that is called speckle.

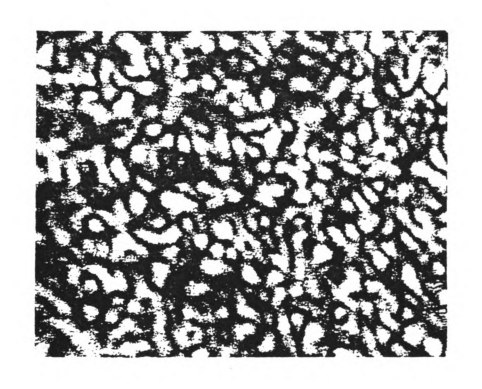


Fig 1.1

A typical image plane speckle pattern.

When the geometry is that of an imaging system, rather than the free-space propagation, the explanation must incorporate diffraction as well as interference. Even for a perfectly corrected (aberration-free) imaging system, the intensity at a given image point can result from the coherent addition of contributions from many independent surface areas. It is necessary only that the diffraction limited (amplitude) point-spread function of the imaging system be broad in comparison with the microscopic surface variations to assure that many de-phased coherent contributions add at each image point. Thus speckle can arise either from free-space propagation or from an imaging operation.

In this paper the speckle considered is "Gaussian speckle". The terminology "Gaussian speckle" is derived from the fact that, as a result of the rough surface approximation and the central limit theorem, the complex amplitude is a circular complex Gaussian process. This results in a negative exponential probability density function for the intensity. Within the limits of the necessary conditions, the statistics of a Gaussian speckle pattern are independent of the nature of the scattering medium; in particular, the surface roughness does not influence the statistics provided that the surface roughness is greater than the wavelength and that a large number (N) of scatterers contribute to the intensity at any image point (patch). For most practical applications this is generally the case.

On the other hand, if only a few independent scattering areas are present, then the speckle statistics do contain information about the scattering medium. Such "small-N" speckle usually has non-Gaussian statistics and hence the probability density function of intensity is usually not of the negative exponential type.

In the experimental measurement of the intensity in a speckle pattern, the detector aperture must of necessity be of finite size. Hence the measured intensity is always a somewhat smoothed or integrated version of the ideal point-intensity, and the statistics of

the measured speckle will be somewhat different than the ideal statistics of the speckle pattern.

1.2 Size of Speckle

1.2.1 Objective Speckle Size

The size of laser speckles, a statistical average of the distance between adjacent regions of maximum and minimum brightness, is always related to the aperture angle that the radiation subtends at the plane defining the speckle field. Thus, for example, the size (diameter) S_{obj} of the 'objective' speckles formed on a screen H at distance L by scattering of coherent light from a circular region of diameter D, see Figure 1.2, is given by [14,15],

$$S_{obj} = 1.22 \frac{L}{D} \lambda \tag{1.1}$$

where λ is the wavelength of the laser light.

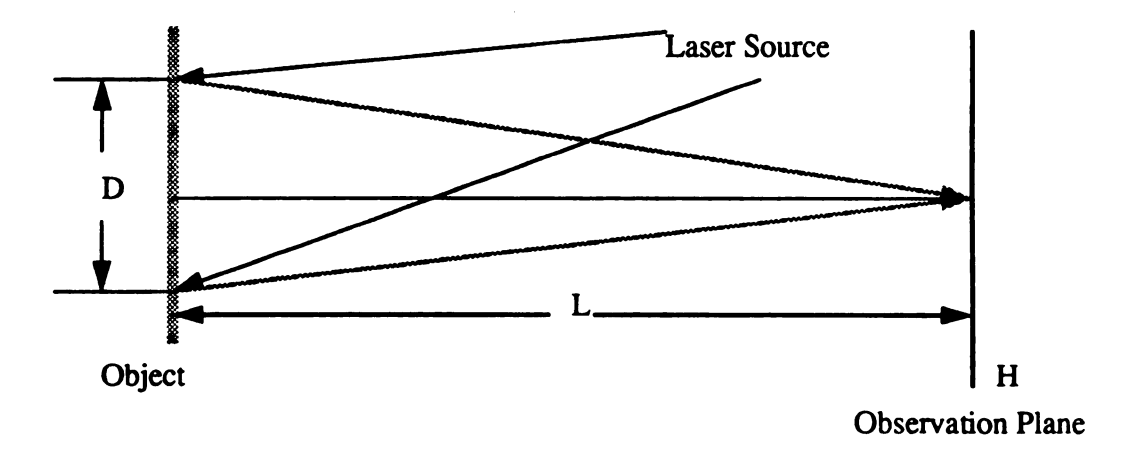


Fig. 1.2 Formation of Objective Speckle

1.2.2 Subjective Speckle Size

Alternatively, if the speckle field is formed by collecting the scattered radiation field with a lens and focusing it onto the screen (Figure 1.3) a 'subjective' speckle pattern is formed. The size S_{sub} of the individual speckles in this case is then related to the aperture ratio F of the lens (the f/number) and the magnification M of the lens. The speckle size in the image is then [16,17],

$$S_{sub} \cong 1.22 (1 + M) \lambda F, \qquad (1.2)$$

From simple lens theory, the speckle size on the scattering surface (object) is given by

$$S_{sub}^{o} \cong 1.22 (1 + M) \lambda \frac{F}{M}$$
, (1.3)

This is defined as the resolution element on object. Subjective speckle is the type that is used in ESPI and most other speckle metrology methods.

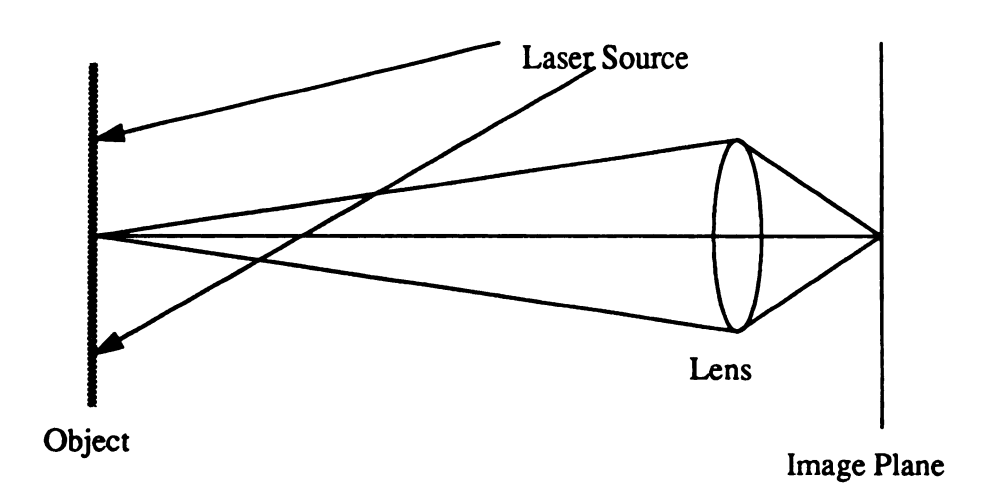


Fig. 1.3
Formation of subjective speckle

1.3 The Brightness Distribution of Speckles

The speckle is itself an interference phenomenon. There are two different speckle patterns. One called the 'fully-developed' speckle pattern develops only from interference of light that is all polarized in the same manner. The speckle field itself will then be similarly polarized. Surfaces at which polarized light is singly scattered, such as lightly abraded metal, generally give rise to polarized speckle fields, as do also lightly-scattering transmission elements such as ground glass. On the other hand, matte white paint surfaces or opal glass, into which the light penetrates and is multiply scattered, depolarize the light and thus do not generate a fully developed speckle pattern. The brightness distributions of the two speckle patterns are markedly different from each other.

The distribution of brightness of a fully-developed speckle pattern is governed by the negative exponential relationship [18]

$$p(I) = (\frac{1}{I_0}) \exp\left(-\frac{I}{I_0}\right), \qquad (1.4)$$

where p(I) is the probability that a speckle has brightness between the values I and (I+dI), and I_0 is the average brightness. This relationship is plotted in Figure 1.4, and it shows that the most probable brightness for a speckle is zero, i.e. there are more dark speckles in the field than speckles of any other brightness. It is this property that is of the greatest importance in distinguishing a fully-developed speckle pattern from one which is partially-developed.

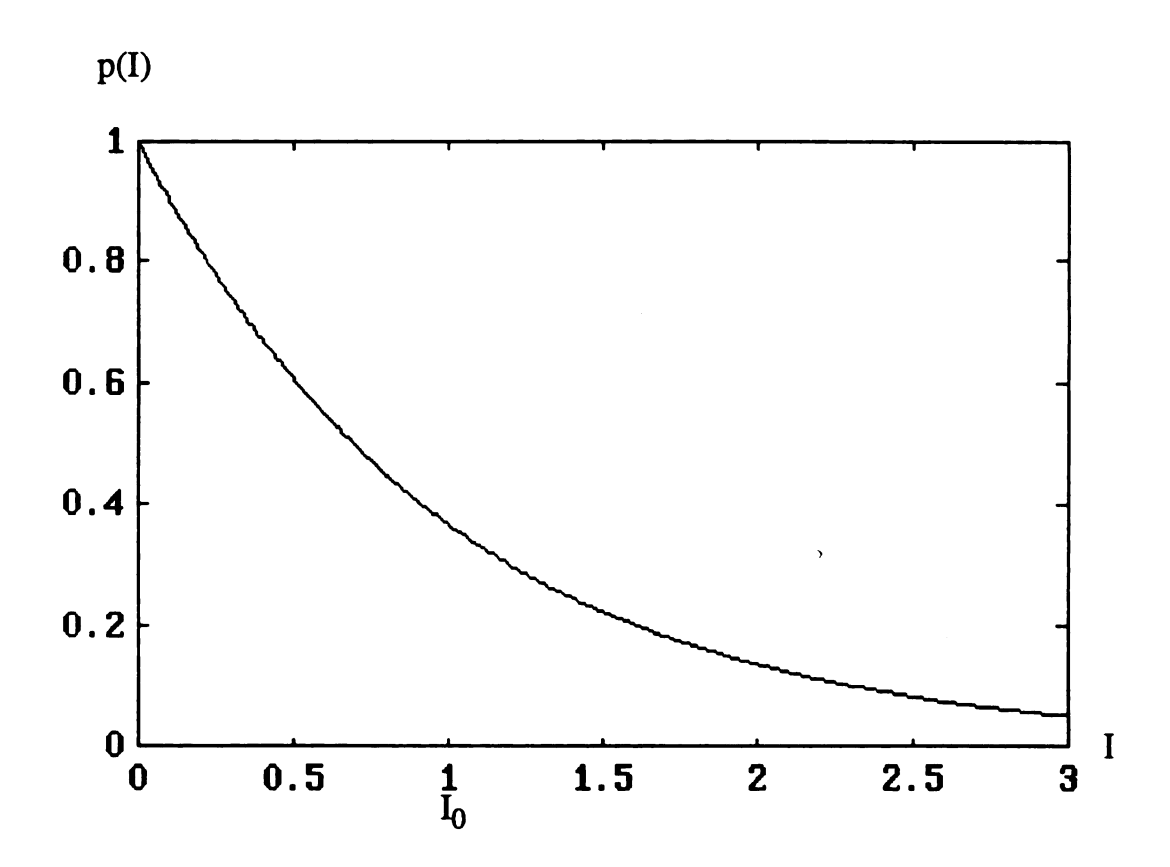


Fig 1.4

Probability density functions of the brightness distribution of a fully-developed speckle field

1.4 Coherent Combination of Speckle and Uniform Fields

In a typical ESPI system, a uniformly bright field of coherent radiation, which is the so called reference beam, is added to the speckle field. The addition of the reference field will affect both the size and the brightness distribution of the speckle field.

1.4.1 Size

When a reference beam is introduced the size of a speckle will approximately double. The reason for this involves the interference effect of adding a uniform strong wave to the speckle pattern in the direction of the optical axis. The size of a speckle without the addition of the reference beam corresponds roughly to the spacing of the interference fringes generated by waves coming from the opposite ends of a diameter of the speckle-forming pupil if an imaging system is used. When the strong reference wave is introduced, the principal interference effects will take place with respect to this central strong ray, so that the maximum angle between interfering rays is halved. The interference fringe spacing is doubled as is the size of the speckle.

1.4.2 Brightness Distribution

Burch [19] has considered the statistical distribution of brightness when the uniform field is added to the speckle pattern in varying proportions. A typical curve is shown in Figure 1.5, which shows the distribution when the average speckle brightness is equal to the reference field brightness. The mathematical relationship is expressed by

$$B(I) = \left(\frac{2}{I_0}\right) exp\left[-\left(1+2\frac{I}{I_0}\right)\right] J_0 \left[2\left(2\frac{I}{I_0}\right)^{\frac{1}{2}}\right]$$
 (1.5)

where J_0 is the Bessel function of zero order with imaginary argument. The important feature of this curve is that it does not differ greatly from the distribution curve for the speckle pattern alone; in particular, the most probable brightness is still zero.

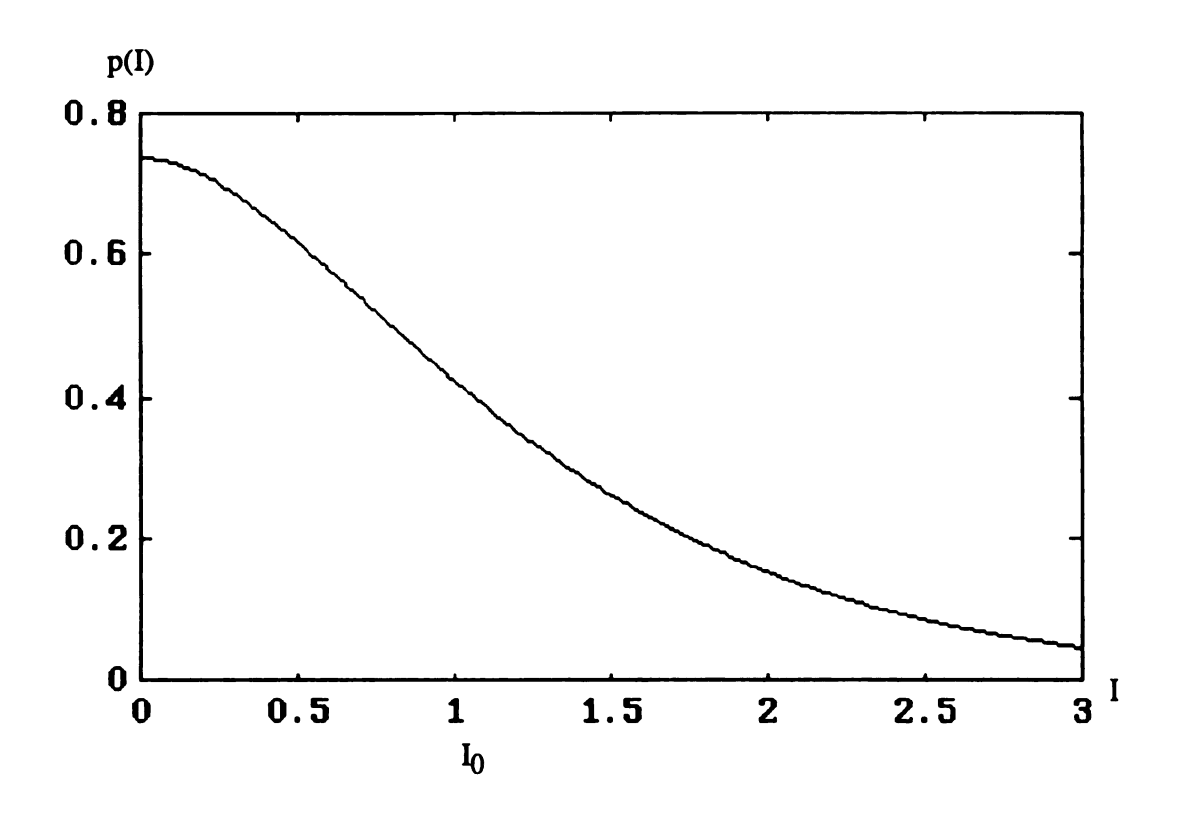


Fig 1.5

Coherent Combination of speckle field and uniform field

1.5 Coherent and Incoherent Combination of Two Speckle Fields

An important class of speckle interferometers, particularly those for measuring in-plane surface displacement, operate by the interference of two independent speckle patterns. When this occurs, the size of the speckles does not change appreciably, but their

brightness distribution may. In the case where the two original speckle fields are brought together coherently, the result will be a third speckle pattern, differing in detail from its two constituent patterns, but whose size and statistical brightness distribution remains the same. However, if the two original speckle fields are combined incoherently, the brightness distribution follows the equation [20],

$$p(I) = 4\left(\frac{I}{I_0^2}\right) exp(-2\frac{I}{I_0}),$$
 (1.6)

This relationship is plotted in Figure 1.6. It is seen that now there is a very low probability of a dark speckle occurring. Conceptually, this is not surprising, since when two intensity speckle patters are overlaid physically, there is a high probability that the bright areas of one pattern will be superimposed on to the dark areas of the other. Surfaces that completely depolarize the light will give a speckle pattern having a brightness distribution that agrees with the above equation, since any two orthogonally polarized components of the scattered light are incoherent with one another.

Although there is a striking statistical difference between the brightness distributions of coherently and incoherently summed speckle patterns, in practice it is not easy to distinguish the two visually.

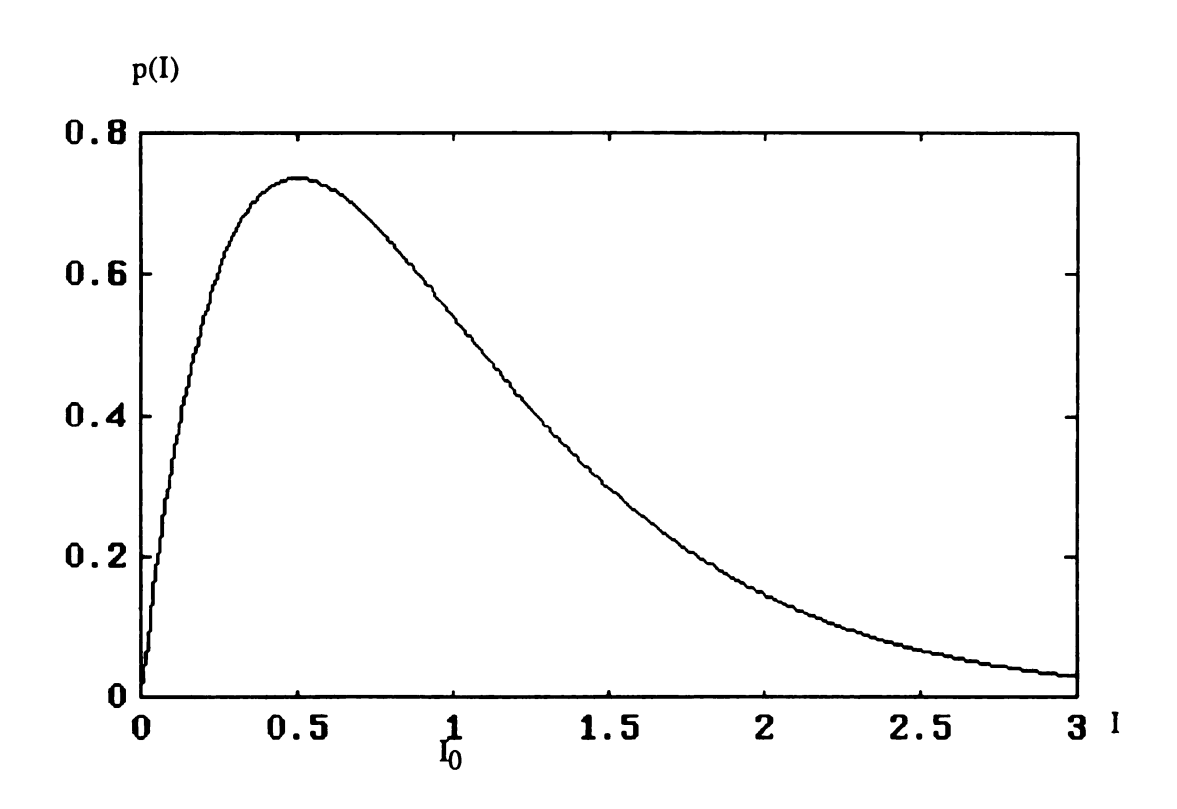


Fig. 1.6

Incoherent combination of two speckle fields.

1.6 Polarization Effects

Since phase information relies upon the formation of interferometric fringes formed by the constructive and destructive interference between the object and reference beams, the light in the two beams should have the same polarization. Laser beams polarized orthogonally to each other will not interfere. Most lasers are linearly polarized and this can, in some instances, cause problems in recording speckle patterns. Although both beams are derived from the same source, polarization changes can occur as a result of reflections. Fortunately, most diffuse objects scatter light in randomly polarized fashion, and there will always be components having the same polarization as the reference beam. For example, in the study on composites (carbon fiber and glass/epoxy), we found that they do not depolarize light; the light scattered has the same polarization as the reference light. Light scattered from white carton board will be partially depolarized. If a polarization problem exists, it can be rectified by the following methods.

- (1) Changing the surface properties of the object (e.g. paint it or spray with aluminum paint).
- (2) Rotating the plane of polarization in the reference or object beams to match each other by inserting a half-wave plate into either beam and rotating it until the extinction angle is the same for each beam when tested with a polarizing filter.
- (3) Circularly polarizing the light as it emerges from the laser by orienting a quarter-wave plate in the laser output beam.

1.7 Speckle Pattern Decorrelation

In the following discussion it is assumed that the illumination direction and the viewing direction are parallel with the normal of the object surface. This assumption is close to the real ESPI case. Refer to Figure 1.7 for the configuration used in this section.

In speckle pattern correlation interferometry, it is assumed that neither the displacements which give rise to the phase variation causing the fringes nor other displacements not contributing to this phase variation significantly alter the random phase and amplitude of the speckle pattern in the fringe observation plane. This is, however, an

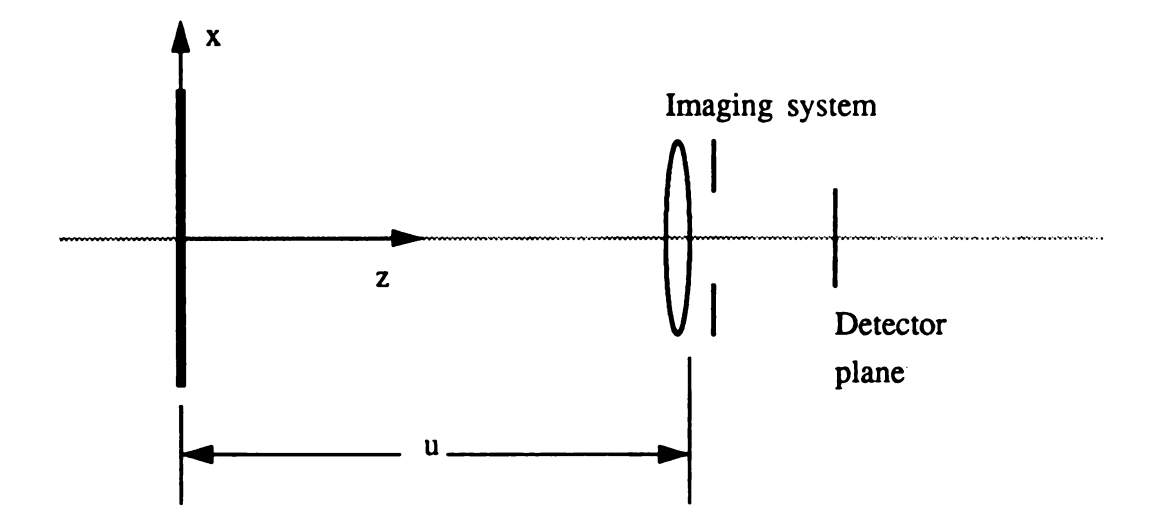


Fig. 1.7
Diagram for speckle decorrelation analysis.

approximation which is valid only when the displacements involved are less than some minimum value which depends on the kind of displacement involved and the viewing geometry. For example, in the case of in-plane displacement interferometry, a body may undergo in-plane strain together with out-of-plane rotation. The effect of the latter will be to reduce the contrast of the plane-strain fringes when the magnitude is sufficient to cause speckle pattern decorrelation. Another important factor which should be noted is that when the object deforms the resolution elements also move. If this movement is big enough to move across the detector element, it will 'lose the memory' of the speckle which contains the displacement information. Consider here the case in which the speckle and the detector element have the same size. The criterion to judge if there is decorrelation is as follows:

- (1) When the phase change across the resolution element is equal to or bigger than 2π , the speckle will be totally decorrelated.
- (2) When the resolution element moves across and out of the detector element, the detector will lose the memory of the displacement (phase) information carried by the speckles.
- (3) If the phase change or memory loss in either case is less than about one tenth of a corresponding critical values, the speckle is not decorrelated and no 'memory loss occurs'.

Four different cases are considered below in order to determine which factor is dominant for each.

1.7.1 Out-of-plane Translation

As the object is displaced along the viewing direction, the relative phase of the components of light scattered from a resolution element will also change. It can be shown that the maximum value of this phase change is 2π across the resolution element when the object moves by an amount Δz_1 given by (neglect the small quantities of second order)

$$\Delta z_1 \approx \frac{Mau^2}{1.22(1+M)fx} . \tag{1.7}$$

Here u is the object-to-lens distance, a is the aperture diameter, f is the focal length, M is the magnification of the imaging system.

It also can be shown that when the translation is

$$\Delta z_2 \approx 1.22 (1 + M) \frac{fu\lambda}{Max}, \qquad (1.8)$$

the detector will lose memory of the corresponding resolution element, which means the resolution element will move out of the detector element.

If M=1 / 15, u = 500 mm, f/a = 16 (typical numerical aperture used in ESPI), for x = 50 mm we will have

$$\Delta z_1 \approx 16009 \mu m$$
, and $\Delta z_2 \approx 1976 \mu m$.

So, in this case the 'memory loss' is more important, and we also can see that ESPI has large tolerance in the z direction. It will be shown in Chapter 3 that the tolerance above is more than enough in using an ESPI system.

1.7.2 In-plane Translation

When a body moves in its plane, the speckle pattern in the image plane also moves in proportion to the magnification of the viewing system. If the amount of the movement is small compared with the resolution element size, the change in the speckle pattern at a given point in the image plane is also small. It can be shown that the speckle pattern at a point is decorrelated when the object is translated by an amount Δx_1 , given by

$$\Delta x_1 \approx \frac{Mau}{1.22(1+M)f} . \tag{1.9}$$

The detector element will lose memory when

$$\Delta x_2 \approx 1.22 (1 + M) \frac{f\lambda}{Ma} . \tag{1.10}$$

As the object is translated in its plane, the speckle pattern is translated; it does not remain identical in form because the light scattered from a given point in the object is incident on the viewing lens at a different angle so that the displaced speckle pattern is not identical in form to the original pattern. When $\Delta x_1 = a$, the displaced speckle pattern is totally decorrelated with respect to the original pattern.

If M = 1/15, u = 500 mm, x = 50 mm and f/a = 16 we get

$$\Delta x_1 = 1601 \mu m, \qquad \Delta x_2 = 198 \mu m$$

again 'memory loss' is more sensitive.

1.7.3 Out-of-plane Rotation

When the resolution element is rotated by an angle θ about an axis lying in the object plane, the speckle pattern is decorrelated when θ is given by

$$\theta = \frac{\lambda}{q} \approx \frac{Ma}{1.22 (1+M)f} \tag{1.11}$$

where q is the resolution element diameter. For M = 1 / 15, f/a = 16, we obtain

$$\theta = 0.18^{\circ}$$
.

1.7.4 In-plane Rotation

An in-plane rotation of the object gives rise to an equivalent rotation of the speckle pattern. A point at a distance R from the center of rotation moves by $R\alpha$, where α is the angle of rotation; thus the speckle pattern is decorrelated when

$$\alpha \approx \frac{q}{R} = 1.22 (1 + M) \frac{\lambda f}{aMR},$$
(1.12)

for M = 1 / 15, f/a = 16, we obtain

$$\alpha = 0.23^{\circ}$$
.

From the above analysis, we conclude that the "memory loss" effect is more important than the decorrelation effect.

Chapter 2

Displacement Analysis and Optical Setups

This chapter discusses quantitative measurements using an ESPI system and some practical ESPI optical setups.

2.1 Sensitivity Vector

The sensitivity of ESPI measurement is governed by the orientation relation between three vectors, namely, the illumination vector, the displacement vector and the viewing vector [21]. In Figure 2.1, the object is illuminated by a point source located at O. Light is scattered by an object point P to an observer or viewing plane at point Q. When the object is displaced, so that the point P is displaced by L to P', the optical path from the source O to a point in the viewing plane via a given point P in the object is altered. The change in phase associated with this change in optical path is the basis of holographic and speckle correlation techniques for measuring surface displacements.

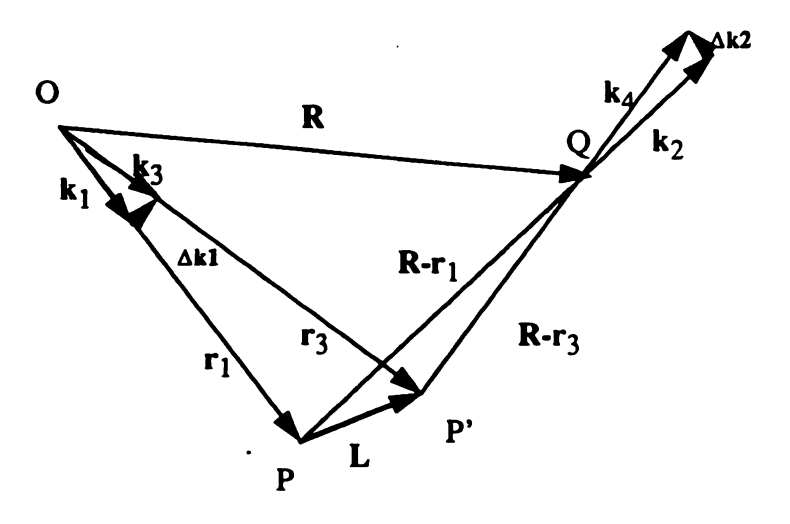


Fig. 2.1 Position and propagation vectors

Let δ represents the phase shift of light scattered by point P on the object in a particular direction. In Figure 2.1, several vectors are defined for use in determining the relation between δ and L. Vectors **R** and \mathbf{r}_1 lie in the plane defined by points O, P, and Q; and \mathbf{k}_1 and \mathbf{k}_2 are the propagation vectors of the light illuminating P and the light scattered toward the viewing plane, respectively. Since the magnitude of a propagation vector is $\frac{2\pi}{\lambda}$, the phases of the two light rays which reach the viewing plane are as follows:

$$\phi_1 = \mathbf{k}_1 \bullet \mathbf{r}_1 + \mathbf{k}_2 \bullet (\mathbf{R} - \mathbf{r}_1) + \phi_0 \tag{2.1}$$

$$\phi_2 = \mathbf{k}_3 \bullet \mathbf{r}_3 + \mathbf{k}_4 \bullet (\mathbf{R} - \mathbf{r}_3) + \phi_0 \tag{2.2}$$

Here ϕ_1 is the phase of the light scattered by P before displacement, ϕ_2 is the phase of the light scattered by P after displacement; and ϕ_0 is the arbitrary phase assigned to these rays at the point source O. The phase difference measured at the viewing plane is

$$\delta = \phi_2 - \phi_1 \ . \tag{2.3}$$

After displacement of P, the propagation vectors in the illumination and viewing directions are k_3 and k_4 . Define the small changes, $\Delta k1$ and $\Delta k2$, in these propagation vectors by

$$k_3 = k_1 + \Delta k1, \qquad k_4 = k_2 + \Delta k2.$$
 (2.4)

Combining the preceding equations gives

$$\delta = (\mathbf{k}_2 - \mathbf{k}_1) \bullet (\mathbf{r}_1 - \mathbf{r}_3) + \Delta \mathbf{k} \mathbf{1} \bullet \mathbf{r}_3 + \Delta \mathbf{k} \mathbf{2} \bullet (\mathbf{R} - \mathbf{r}_3) , \qquad (2.5)$$

In practical situations the magnitudes of \mathbf{r}_1 and \mathbf{r}_3 are much larger than $L = |\mathbf{r}_3 - \mathbf{r}_1|$; so, for practical purposes, $\Delta \mathbf{k} \mathbf{1} \perp \mathbf{r}_3$ and $\Delta \mathbf{k} \mathbf{2} \perp (\mathbf{R} - \mathbf{r}_3)$. Because of these relations, the last two scalar products in equation (2.5) vanish, and the phase difference becomes

$$\delta = (\mathbf{k}_2 - \mathbf{k}_1) \bullet \mathbf{L}, \tag{2.6}$$

*

This relation forms the basis of quantitative interpretation of the fringes of ESPI.

It is convenient to define the sensitivity vector K by,

$$\mathbf{K} = \mathbf{k}_2 - \mathbf{k}_1 \tag{2.7}$$

so that,

$$\delta = \mathbf{K} \bullet \mathbf{L}. \tag{2.8}$$

Thus, the phase change is

$$\Delta \phi = \frac{2\pi}{\lambda} \delta = \frac{2\pi}{\lambda} (\mathbf{K} \bullet \mathbf{L}). \tag{2.9}$$

In general the fringe pattern represents in-plane as well as out-of-plane displacement.

When illumination and viewing angle are small (less than 15°) to the normal of the object surface, we can write, to a very good approximation, that

$$\Delta \phi = \frac{2\pi}{\lambda} \left(\cos \theta_i + \cos \theta_v \right) d_z \tag{2.10}$$

where θ_i is the angle of object illumination to surface-normal, θ_v is the angle of viewing direction to surface-normal, and d_z is the displacement vector oriented within θ_i and θ_v . We can see here the phase is not only a function of displacement but also a function of illumination angle and viewing angle. Therefore, it is not possible to calculate the exact actual displacement in ESPI. For NDT applications this is not a concern.

Let d_m be the measured (calculated) displacement, we should have

$$\frac{d_m}{d_r} = \frac{\cos\theta_i + \cos\theta_v}{2} \tag{2.11}$$

The approximation relationship of d_m vs d_z is graphically illustrated in Figure 2.2.

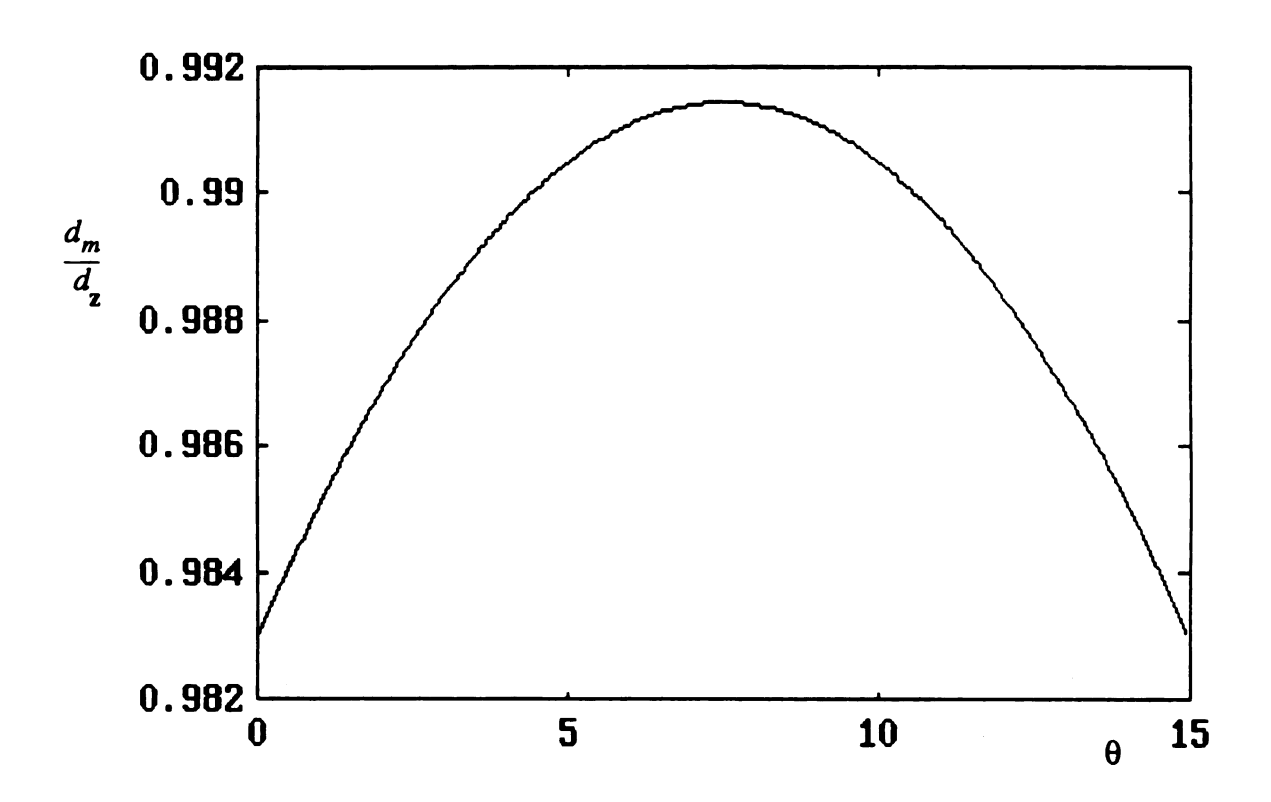


Fig. 2.2 The variation of (d_m/d_z) resulting from the change of illuminating and viewing angle

2.2 Out-of-plane Displacement Sensitive Optical Setup

A practical arrangement for out-of-plane sensitive measurement is shown in Figure 2.3

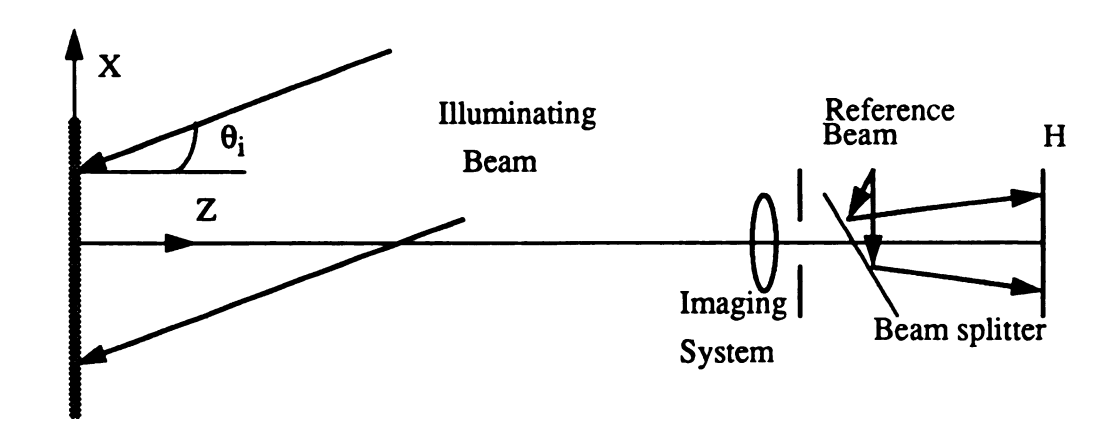


Fig. 2.3
Out-of-plane sensitive ESPI optical setup

Here the object is illuminated by the object beam at an angle θ_i to the surface normal and an image is formed by the lens L at image plane H. A diverging spherical reference wave is added to the image by the beam splitter B. When the object is displaced, the change in the phase of the object beam relative to the reference beam is given by equation (2.10) with $\theta_{\nu} = 0$, so that this setup is sensitive to out-of-plane displacement. ESPI is based on this setup but with a diverging illuminating beam.

Reduced out-of-plane displacement sensitivity may be obtained using the optical arrangement shown in Figure 2.4. The correlation phase factor is now given by

$$\Delta \phi = \frac{2\pi}{\lambda} \left(\cos \theta_{i1} - \cos \theta_{i2} \right) d_z \tag{2.11}$$

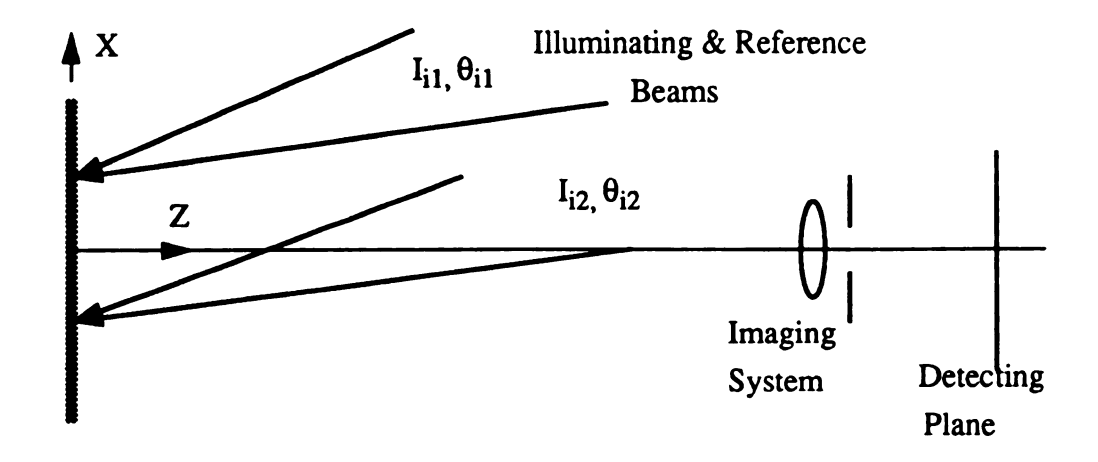


Fig. 2.4

ESPI with reduced out-of-plane displacement sensitivity

where θ_{i1} and θ_{i2} are the angles of inclination of the two illuminating wavefronts I_{i1} and I_{i2} to the surface normal of the object. Viewing is in the normal direction. When the difference between θ_{i1} and θ_{i2} are small, $(\cos\theta_{i1} - \cos\theta_{i2})$ becomes small and contours of out-of-plane displacement fringes, typically of the order of 10 μ m, may be observed. Displacements of this magnitude may cause speckle pattern decorrelation, and this fact limits the degree of desensitization.

2.3 In-plane Displacement Sensitive Optical Setup

The arrangement shown in Figure 2.5 gives fringes which are sensitive to in-plane displacement. Here the object lies in the x, y plane and is illuminated by two plane wavefronts, I_{i1} and I_{i2} inclined at equal and opposite angles, θ , to the x-axis surface-normal. The positive y-axis points out of the page and the center of the viewing lens aperture lies on the z-axis.

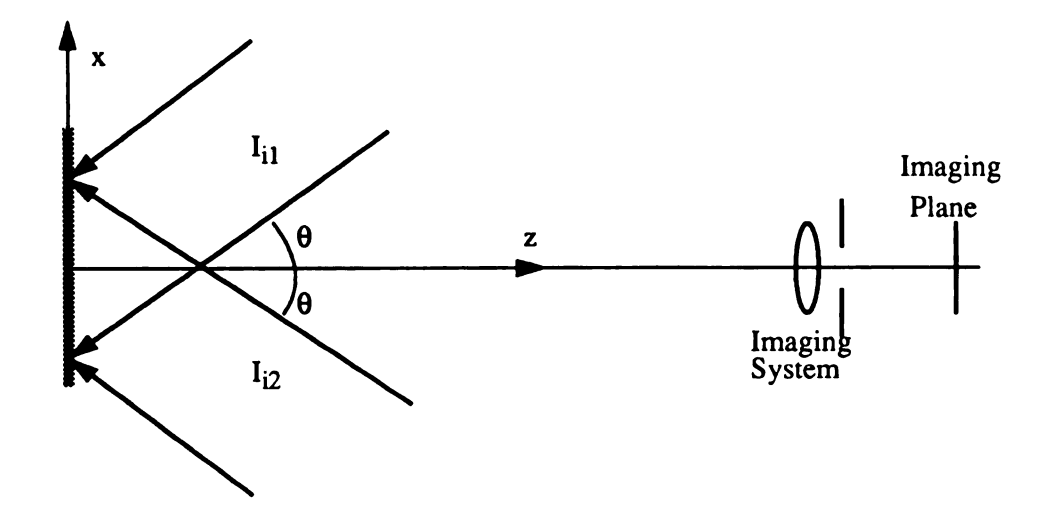


Fig. 2.5

The optical arrangement for in-plane displacement sensitive measurement

When an element is displaced by a distance d(dx, dy, dz) the relative phase change of the two beams is given by

$$\Delta \phi = \frac{4\pi}{\lambda} d_{\mathbf{x}} \sin \theta. \tag{2.12}$$

The relative phase of I_{i1} and I_{i2} is constant over planes lying parallel to the yz-plane so that the displacement components dy and dz lying in those planes will not introduce a relative phase change. This form of interferometer therefore allows in-plane displacement distributions to be observed independently in the presence of out-of-plane displacements.

Similarly, y-axis illumination geometry in which the object is illuminated at equal angles to the y-axis will form a fringe pattern where

$$\Delta \phi = \frac{4\pi}{\lambda} d_y \sin \theta \tag{2.13}$$

In order to determine all the components of the plane strain tensor, the fringe spacing measurements must be taken from both illumination geometry fringe patterns.

A third in-plane displacement sensitive geometry may be used. In this setup the object lies in the xy-plane and is illuminated by plane wave-fronts I_{i1} and I_{i2} propagating in the xz-plane and yz-planes at equal angles θ to the surface-normal. Viewing is in the normal z-direction. This is referred to as the orthogonal arrangement and it can be shown that

$$\Delta \phi = \frac{4\pi}{\lambda} (d_x + d_y) \sin \theta . \qquad (2.14)$$

In practice it is difficult to utilize the in-plane measurement described above. The reason is that large optical components are needed in order to study sizeable objects.

Two practical in-plane sensitive setups are illustrated in Figure 2.6 and Figure 2.7.

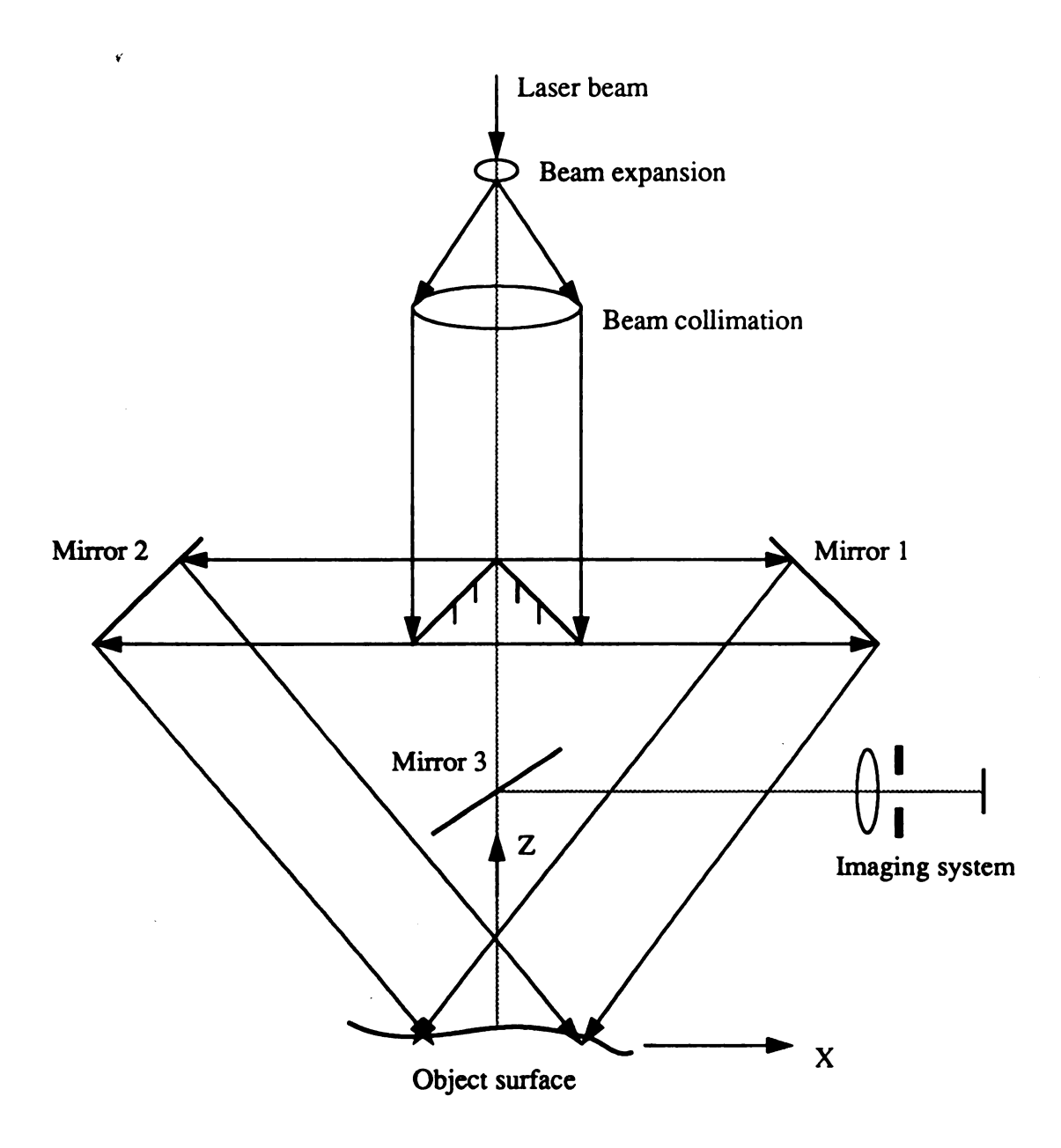
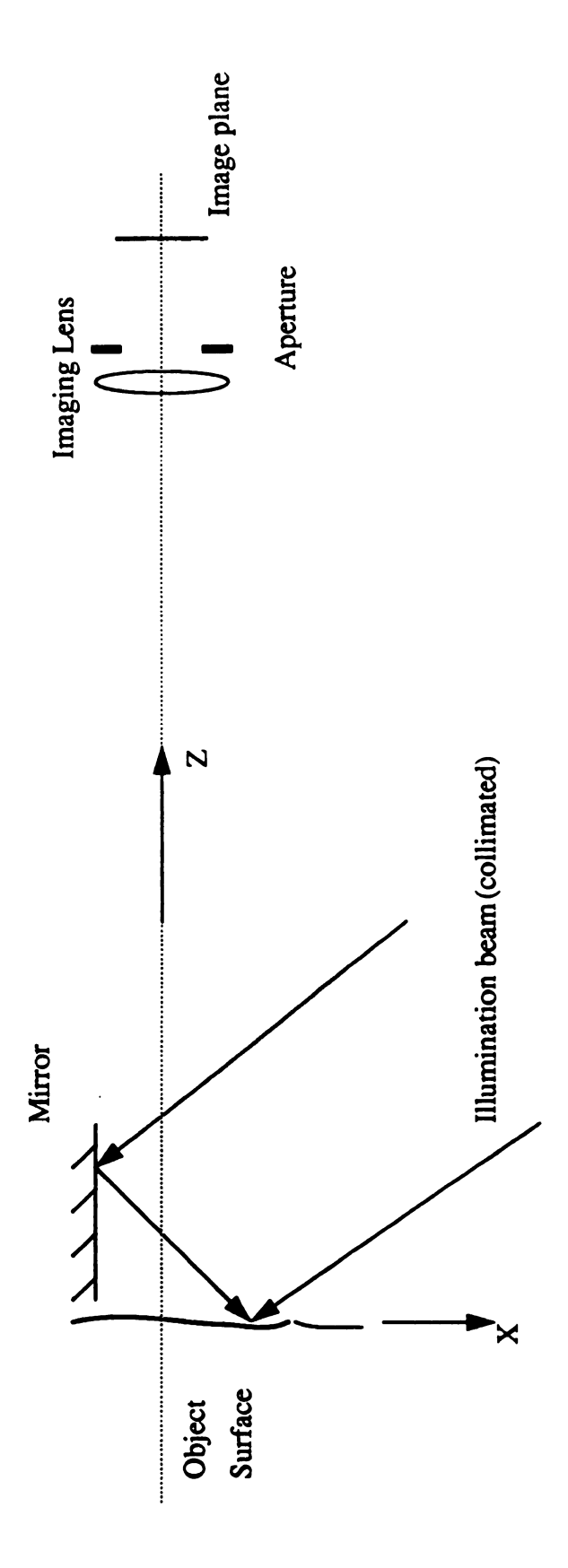


Fig. 2.6

An alternative optical setup of in-plane displacement sensitive ESPI system



A practical optical setup of an in-plane displacement sensitive ESPI system

Fig. 2.7

2.4 Two Special Cases

In order to get more understanding about what an ESPI system really measures, we analyze two special cases -- pure out-of-plane and pure in-plane. In this analysis, diverging spherical illumination and viewing parallel with surface normal are used.

2.4.1 Pure Out-of-plane Displacement

In this case, the displacement vector is parallel with the viewing vector (Figure 2.8).

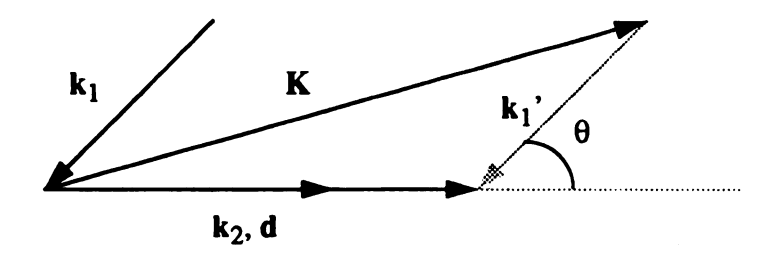


Fig. 2.8

Pure out-of-plane displacement

Here d is the displacement vector and K ($\mathbf{k}_2 - \mathbf{k}_1$) is the sensitivity vector, where \mathbf{k}_2 is the viewing vector, \mathbf{k}_1 is the illuminating vector and \mathbf{k}_1 ' is parallel with \mathbf{k}_1 . \mathbf{k}_1 , \mathbf{k}_1 ' and \mathbf{k}_2 are unit vectors.

Now the question is how the angle θ affects the measured displacement d_m . From Figure 2.8, we can derive a relationship between the measured displacement and the actual displacement. This is given by

$$d_m = \mathbf{d} \bullet \mathbf{K} = \frac{(1 + \cos \theta)}{2} d, \qquad (2.15)$$

here d is the actual displacement. The relationship between d_m and d for angle θ less than 15° is plotted in Figure 2.9. We can see there is a good approximation when θ is small.

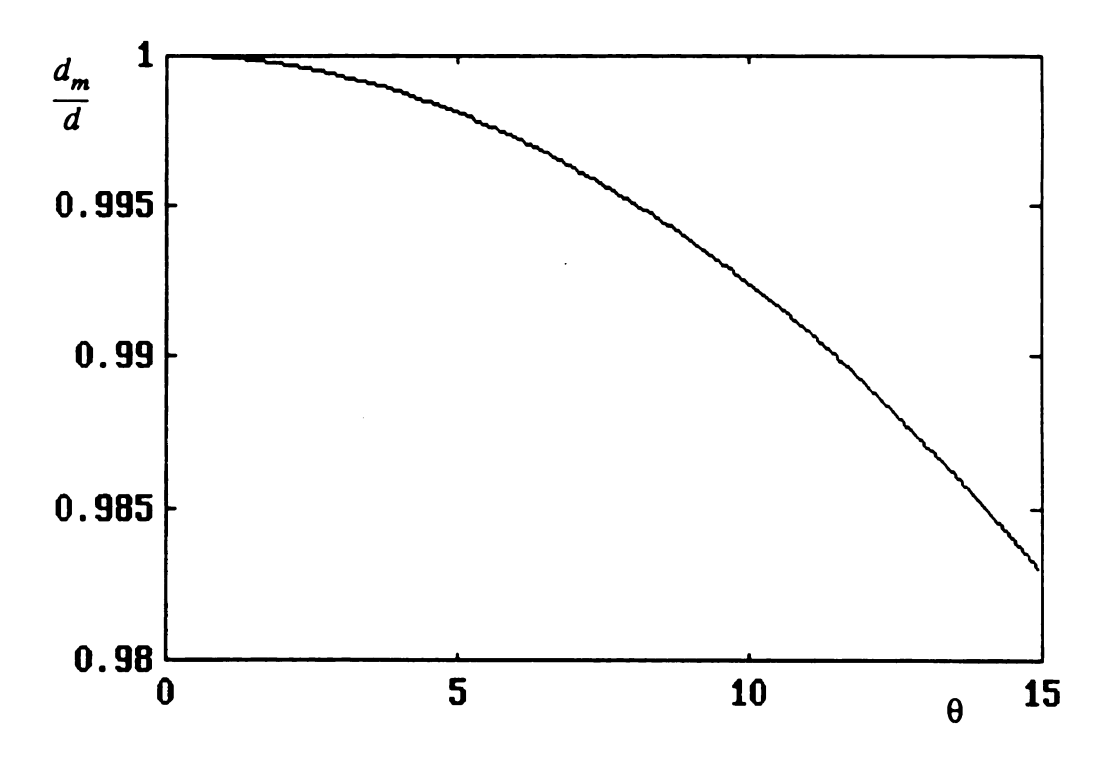


Fig. 2.9

The relationship between d_m and d to illumination angle θ in pure out-of-plane case

2.4.2 Pure In-plane Displacement

Here, the displacement vector is normal to the viewing vector k_2 (Figure 2.10)

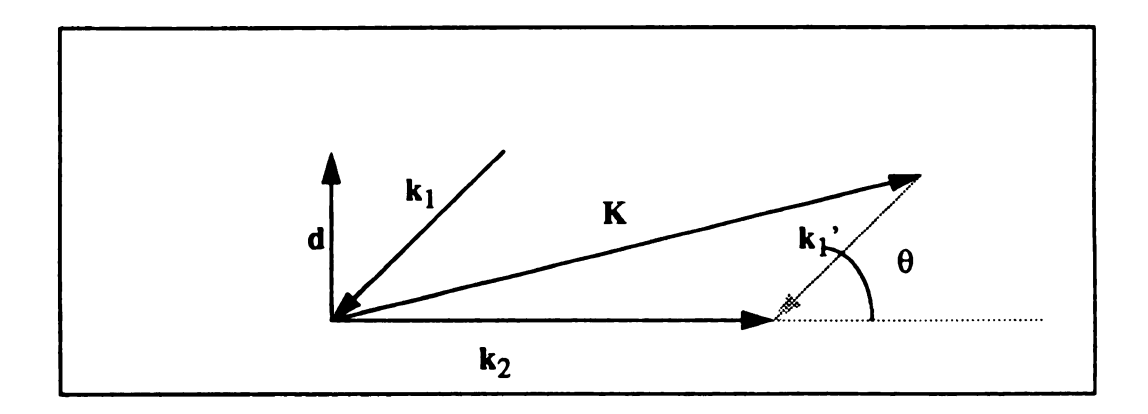


Fig. 2.10

Pure in-plane displacement

In this case, the relation between measured and actual displacement is given by

$$d_m = \mathbf{d} \cdot \mathbf{K} = (\sin \theta) d. \tag{2.16}$$

Note that the setup is a typical out-of-plane ESPI. For a pure in-plane displacement, only a small portion of the displacement will be sensed. The relationship between the measured displacement d_m and the actual displacement d for θ less than 15° is plotted in Figure 2.11.

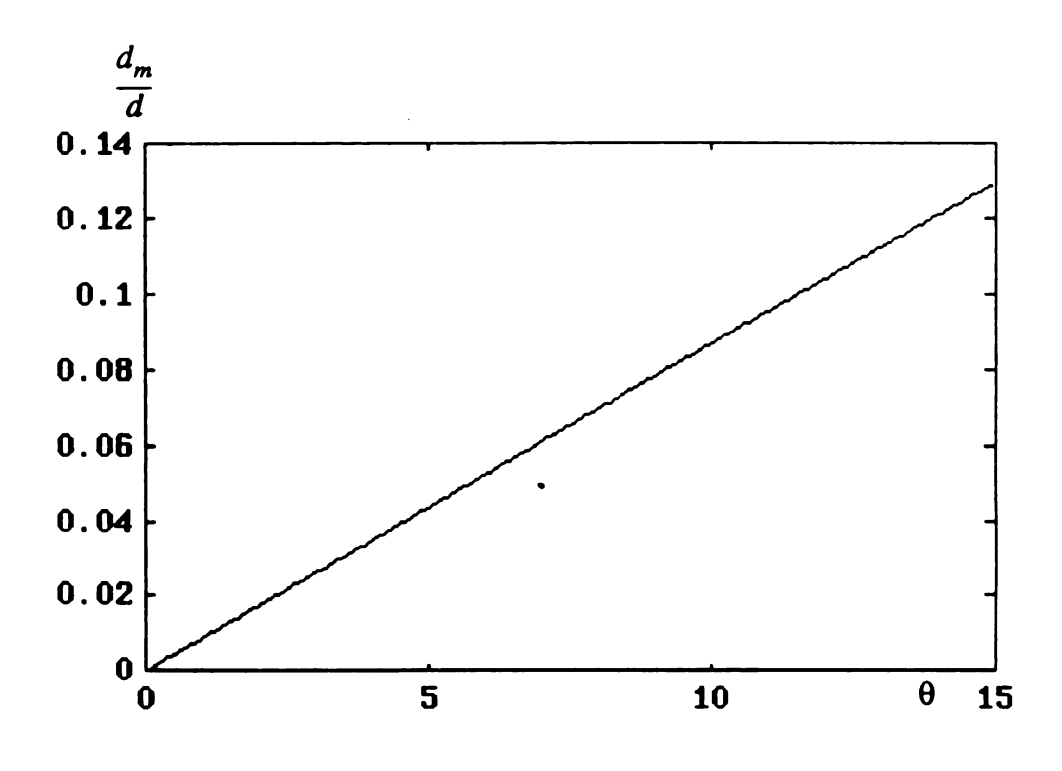


Fig. 2.11

The relationship between d_m and d to illumination angle θ in pure in-plane case

2.5 Limitations of ESPI

The main factors which limit the range of measurements that can be made using the various ESPI methods are discussed below.

2.5.1 Measurement Sensitivity

ESPI can be used to give fringes which represent lines of either in-plane or out-of-plane displacement. The fringe sensitivity for an in-plane interferometer is calculated from equation (2.12) to be $\lambda/(2\sin\theta)$, where λ is the wavelength of the light used and θ is the angle of incidence of the illuminating beams. Out-of-plane interferometers may give fringes representing constant displacements at intervals of the order of $\frac{1}{2}\lambda$, or they may be

desensitized up to about hundreds of microns. It is not possible to detect less than one fringe accurately with a conventional ESPI system, so that this value represents the maximum sensitivity of the system.

We shall show in chapter 3 that the fringe spacing on the TV camera must be less than 1/120 of the screen width; this restriction limits the displacement gradient and also the total displacement which can be observed. The visibility of the fringes obtained using time-averaged ESPI to observe out-of-plane vibrations falls off rapidly with increasing vibration amplitude unless stroboscopic illumination or other techniques are used.

2.5.2 Object Size Limitations

The maximum area which can be inspected in one view is limited by the laser power available and the camera sensitivity. There is no reason why a larger area can not be inspected if sufficient laser power is available, but the mechanical stability of the system and the coherence of the laser also limit the performance of the system.

When in-plane measurements are being made, the illuminating wave-fronts must be plane if fringes of uniform sensitivity are to be obtained. Unless a large collimating lens is used for large areas, the fringe pattern interpretation will be rather difficult. When the surface of the object being inspected is not flat, it can be shown that the fringes may have sensitivity to out-of-plane movements.

In order to observe fringes on a small area, a relatively large deforming force must be applied, and this is likely to give rise to rigid body translations, which cause speckle decorrelation and hence a reduction in fringe visibility. The same applies to displacements to which the interferometer does not have fringe sensitivity or has little sensitivity.

Decorrelation and memory loss (essentially decorrelation) due to in-plane translations and rotations increase as the magnification of the viewing system is increased. Thus, decorrelation of the speckle, causing a reduction in fringe visibility, is likely when ESPI is

used at high magnification. Fringes have been observed on an area of 0.05 mm² in an out-of-plane ESPI system [21]

2.5.3 Depth of Field

Because the ESPI system must use a high F-number (small aperture) viewing system, the depth of field of the system is high, so the depth of field is generally not a restriction in ESPI.

2.5.4 Surface Condition

It has been assumed throughout this discussion that the surface under examination does not alter microscopically during the course of the measurement. If it does so, through oxidation, re-crystallization, or other factors, de-correlation of the speckle will result. Additionally, the nature of the scattering surface itself can lead to a much greater dependence of the speckle pattern upon a tilt of the surface. For surfaces like abraded metal, the scattering from the surface is 'two-dimensional'(only scattered once). When the light penetrates to some extent into the 'surface' the light is then scattered three-dimensionally within the material, so that path changes resulting from a small tilt of the surface will vary in a random fashion from point to point. This occurs for such materials as paints, paper and cardboard, and many organic substances. The net effect is that the tolerance on the allowable tilt is much narrower when a multiple-scattering surface is being studied than when the light is only scattered once.

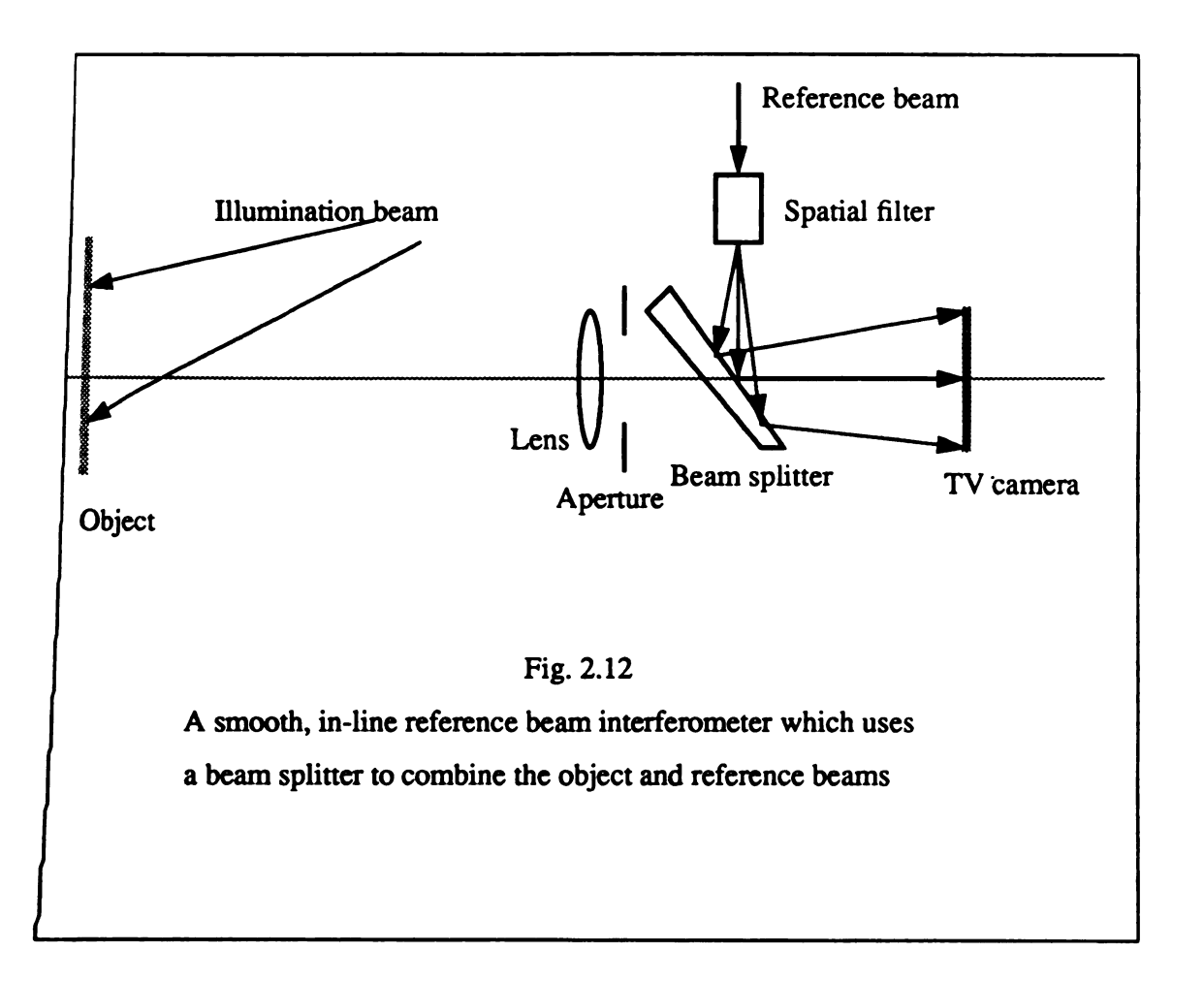
Another consideration of practical importance relates to the type of surface required for measurement of in-plane displacement using double illumination interferometry. Due to the high angles of incidence of the two illuminating beams, it is evident that the surface being studied must be totally diffusing, with no enhanced scattering in the specular direction. For this reason the object very often has to be coated with a matt white paint.

2.6 Practical Optical Setups for ESPI

There are two basic ways of combining the object and reference beams in an ESPI system for out-of-plane measurement. These are shown in Figures 2.12 and 2.13 respectively.

In Figure 2.12, the unexpended input reference beam is filtered and expanded by a spatial filter to remove extraneous optical noise and create a spherical wavefront. This well conditioned beam is particularly important for use in the addition mode (explained in chapter 3). The reference beam then is reflected onto the TV camera target by a small-angle wedge (about 1°) beam splitter. The rear face of the beam splitter is anti-reflection coated in order to suppress secondary reflections. The point of divergence of the reference wave-front is made conjugate with the mid-point of the maximum focal range to take care of the two extreme focal conditions. Light scattered from the object is collected by the viewing lens and an image is formed in the plane of the TV camera's target where it interferes with the reference wavefront. This system suffers from the disadvantage that dust particles which tend to collect upon the beam splitter, together with any small blemishes due to imperfect cleaning, act as light scattering centers. These cause reference beam noise and hence degrade the quality of addition fringes. In the subtraction mode of ESPI, this is not a serious problem.

Another arrangement which considerably reduces the reference beam noise is shown in Figure 2.13. The unexpended reference beam is pre-expanded by lens L₁ and focussed down through a mirror-with-pinhole. The reference beam is aligned by translating the lens L₂ so that its focal point coincides with the pinhole. The small hole in the mirror does not degrade the image quality unless a significant fraction of the light transmitted by the viewing lens is incident on the hole. The point of divergence of the reference beam and the center of the viewing lens are clearly not conjugate in this arrangement, but since



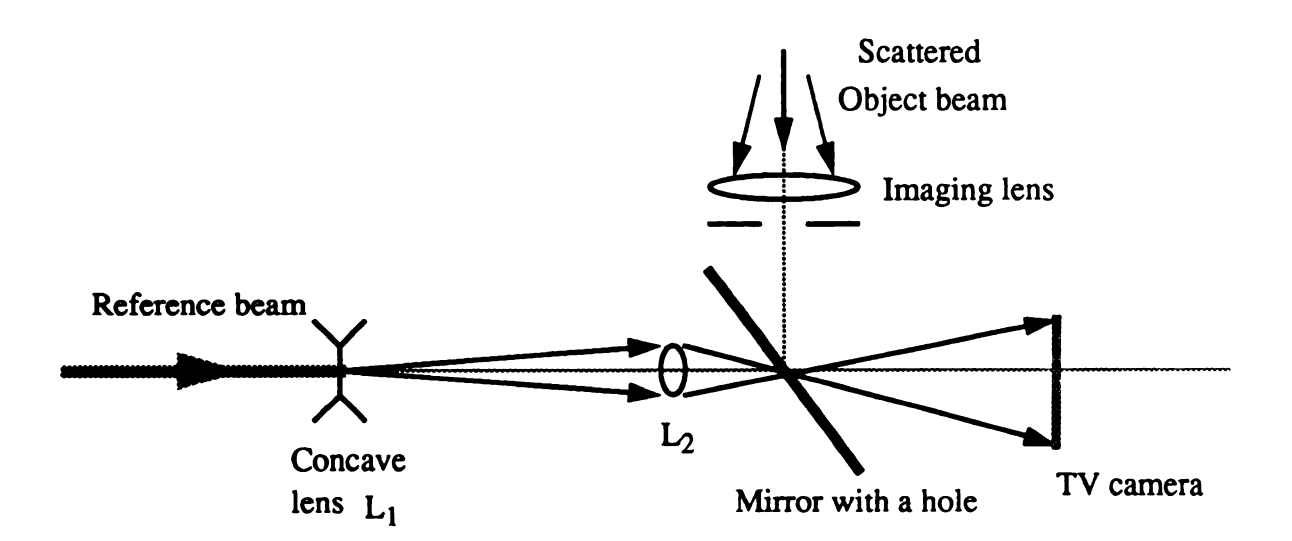


Fig. 2.13
A smooth, in-line reference beam interferometer based on the hole-in-mirror principle

the tolerance along the optical axis direction is large, this layout can be made to function within the limits specified by equation (3.32).

Chapter 3

ESPI System

In this chapter we will discuss the electronic part of an ESPI system. Considered are the video processing, resolving power of the system, and phase measuring techniques.

3.1 Introduction

As stated in the introduction, for speckle pattern correlation interferometry the resolution of the recording medium used need be only relatively low compared with that required for holography, since it is only necessary that the speckle pattern be resolved, and not the very fine fringes formed by the interference of object beam and reference beam. The speckle size can be adjusted to suit the resolution of the TV camera (a CCD is usually used in ESPI). Thus, video processing may be used to generate correlation fringes equivalent to those obtained photographically. The major feature of ESPI is that it enables real-time correlation fringes to be displayed directly upon a television monitor without recourse to any form of photographic processing, plate relocation, etc. This comparative ease of operation allows the technique of speckle pattern correlation interferometry to be extended to considerably more complex problems of the real world. Some of the advantages have been mentioned in the introduction. A block diagram of a typical ESPI system is illustrated in Figure 3.1.

3.2 Video System and Other Electronics in ESPI

The video system comprises the television camera, signal processing and picture storeage unit, and display monitor. The aim of the system design is to obtain maximum

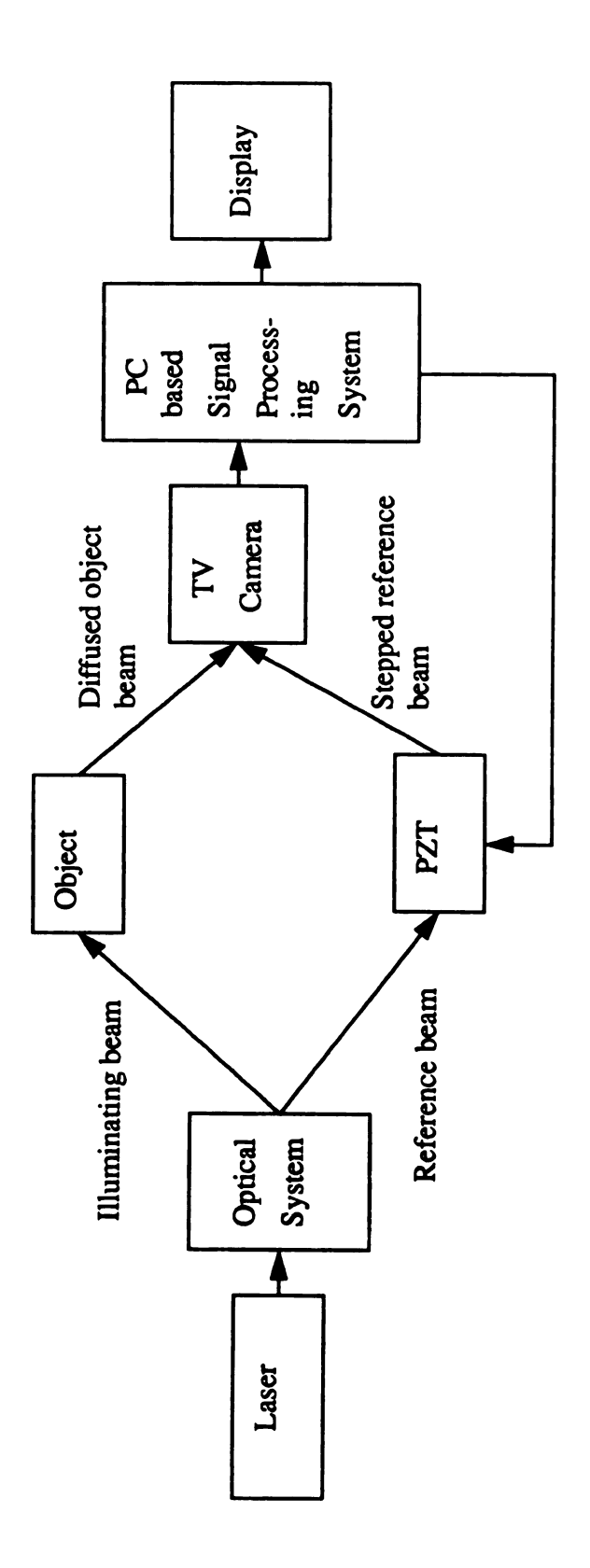


Fig. 3.1
The block diagram of ESPI system

43

visibility fringes. Electronic noise and, in particular, high frequency noise should be minimized. Since the cost of a laser increases approximately in proportion to the output power, it is important to optimize the sensitivity of the video system.

The most noise-sensitive part of the signal processing is at the first stage of video signal amplification, which is carried out at the camera head amplifier, so that this section of the system must be carefully designed. Usually, DC-coupling is used to link the output signal to a high-impedance and low-noise device such as an FET, which is connected directly to the detector plate (CCD array).

The CCD camera is used in modern ESPI systems because it has (1) wide range of linearity; (2) low noise at low light intensity; (3) high signal-to-noise ratio; (4) and peak spectral response about 0.6 µm.

The vertical resolution is determined by the number of scan lines, which is fixed when a standard video system is used. The frequency response of the system should be such that the horizontal spatial resolution is as good as the vertical resolution.

A video system converts an image which is formed on the detector plate of a television camera into an equivalent image on a television monitor screen. With light incident on the CCD array, a charge pattern will build up corresponding to the intensity distribution of the incident light. Charge is then transferred from collection site to collection site by changing potentials within what is essentially an insulator. The output will give rise to voltage signal. A standard television system has 525 vertical lines in total, and a complete scan is performed at a rate of 30 frames per second (U.S. standard). For a standard video camera the active area of the camera is about 13 x 10 mm, so that the image must be reduced to this size. After amplification and the addition of timing pules, the camera signal is used to modulate an electron beam which scans the screen of a television monitor so that the brightness of the screen is made to vary in the same way as the

44

intensity of the original image varies. Ideally, the brightness of the monitor should vary linearly with the intensity of the original image. The exact relationship between the monitor and original image intensities is a complicated function of the electronic processing as well as the brightness and contrast controls of the television monitor. In the analysis of the video display of speckle correlation fringes, it will be assumed that (a) the camera output voltage is linearly proportional to the image intensity and (b) that the monitor brightness is proportional to the camera output voltage.

Intensity correlation fringes in ESPI are observed by a process of video signal subtraction or addition. In the subtraction process, the television camera video signal corresponding to the interferometer image plane speckle pattern of the undisplaced object is stored electronically. The object is then displaced and the live video signal, as detected by the television camera, is subtracted from the stored picture. The output is then high-pass filtered, rectified and displayed on a television monitor where the correlation fringes may be observed live. In this process, sophisticated software may be used to process the fringe data, calculate the desired information, and display it graphically on the screen. For the addition method, the light fields corresponding to the two states are added at the image plane of the camera. The television camera detects the added light intensity, and the signal is full-wave rectified and high-pass filtered as in the subtraction process. Again the correlation fringes are observed on the television monitor.

3.3 Speckle Correlation Fringe Formation by Video Signal Subtraction

The detector plate of the camera is located in the image plane of the speckle interferometer. Under these conditions the output signal from the television camera, as obtained with the object in its initial state, is recorded in the computer's RAM memory. The object is then displaced and the live camera signal is subtracted electronically from the stored signal. Those areas of the two images where the speckle pattern remains correlated will give a resultant signal of zero, while uncorrelated areas will give non-zero

signals. We can see this by considering the intensities I_{before} and I_{after} given by equations before and after displacement [23]

$$I_{before} = I_r + I_o + 2\sqrt{I_r I_o} \cos \phi \tag{3.1}$$

$$I_{after} = I_r + I_o + 2\sqrt{I_r I_o} \cos(\phi + \Delta\phi)$$
 (3.2)

where ϕ is the phase difference between the reference beam and the object beam before the displacement. $\Delta \phi$ is the phase change caused by the displacement. If the output camera signals V_{before} and V_{after} are proportional to the input image intensities, then the subtracted signal is given by

$$V_{s} = (V_{before} - V_{after}) \propto (I_{before} - I_{after})$$

$$= 2\sqrt{I_{r}I_{o}} \left[\cos\phi - \cos(\phi + \Delta\phi)\right]$$

$$= 4\sqrt{I_{r}I_{o}}\sin(\phi + \frac{1}{2}\Delta\phi)\sin(\frac{1}{2}\Delta\phi)$$
(3.3)

This signal has negative and positive values. The television monitor will, however, display negative-going signals as areas of blackness. To avoid this loss of signal, V_s is rectified before being displayed on the monitor. The brightness on the monitor is then proportional to $|V_s|$, so that the brightness B at a given point in the monitor image is given by

$$B = 4K \left| \sqrt{I_r I_o} \sin \left(\phi + \frac{1}{2} \Delta \phi \right) \sin \left(\frac{1}{2} \Delta \phi \right) \right|$$
 (3.4)

where K is a constant.

If the brightness B is averaged along a line of constant $\Delta \phi$, it varies between maximum and minimum values B_{max} and B_{min} given by

$$B_{max} = 2K\sqrt{I_{p}I_{o}}, \quad \Delta \phi = (2n+1)\pi, \quad n = 0, 1, 2, 3$$
 (3.5a)

$$B_{min} = 0,$$
 $\Delta \phi = 2n\pi,$ $n = 1, 2, 3$ (3.5b)

To enhance the fringe clarity, the signals should be high-pass filtered to improve fringe visibility by removing low frequency noise together with variations in mean speckle intensity.

3.4 Speckle Correlation Fringe Formation by Video Signal Addition

In this case, the two speckle patterns derived from the object in its two states are added together on the camera detector plate. The two images do not need to be superimposed simultaneously since a given camera tube has a characteristic persistence time (about 0.1 second for a standard tube), so that the camera output voltage will be proportional to the added intensities if the time between the two illuminations is less than the appropriate persistence time. This technique is employed for the observation of time-averaged fringes when studying vibrations, and it is also used with a dual-pulsed laser.

When the two speckle patterns are added together, areas of maximum correlation have maximum speckle contrast and, as the correlation decreases, the speckle contrast falls. It reduces to a minimum, but non-zero, value where the two patterns are uncorrelated. This is seen as follows:

The voltage V_a is proportional to $I_{before} + I_{after}$ and is given by

$$V_a \propto (I_{before} + I_{after}) = 2I_r + 2I_o + 4\sqrt{I_r I_o} \cos(\phi + \frac{1}{2}\Delta\phi) \cos\frac{1}{2}\Delta\phi$$
 (3.6)

The contrast of the speckle pattern can be defined as the standard deviation of the intensity. For a line of constant $\Delta \phi$, this may be shown to be [24]

$$\sigma_{ro} = 2 \left[\sigma_r^2 + \sigma_o^2 + 8 \langle I_r \rangle \langle I_o \rangle \cos^2 \frac{1}{2} \Delta \phi \right]^{\frac{1}{2}}$$
(3.7)

where $\langle I_r \rangle$ and $\langle I_o \rangle$ are the intensities of the speckle pattern averaged over many points in the reference and object speckle pattern fields respectively, and

$$\sigma_r = \sqrt{\langle I_r^2 \rangle - \langle I_r \rangle^2} = \langle I_r \rangle$$
 $\sigma_o = \sqrt{\langle I_o^2 \rangle - \langle I_o \rangle^2} = \langle I_o \rangle$
(3.8)

 σ_r and σ_o are the standard deviations of I_r and I_o . It is seen that σ_{ro} varies between maximum and minimum values given by

$$[\sigma_{ro}]_{max} = 2 [\sigma_r^2 + \sigma_o^2 + 2I_r I_o]^{\frac{1}{2}}, \quad \Delta \phi = 2n\pi, \quad n = 0, 1, 2$$
 (3.9a)

$$\left[\sigma_{ro}\right]_{min} = 2\left[\sigma_r^2 + \sigma_o^2\right]^{\frac{1}{2}}, \qquad \Delta \phi = (2n+1)\pi, \ n = 0, 1, 2$$
 (3.9b)

While the contrast of the added intensities varies, the mean value along a line of constant $\Delta \phi$ is the same for all $\Delta \phi$, and is given by

$$\langle I_{before} + I_{after} \rangle = 2 \langle I_r \rangle + 2 \langle I_o \rangle$$
 (3.10)

Thus, when the sum of the two speckle patterns is directly displayed on the television monitor, the average intensity is constant, and the variation in correlation is shown as a variation in the contrast of the speckle pattern but not in its intensity. The DC component

of the signal is removed by filtering, and this signal is then rectified. The resulting monitor brightness can then be considered to be proportional to σ_{ro} , so that

$$B = K \left[\sigma_r^2 + \sigma_o^2 + 2 \langle I_r \rangle \langle I_o \rangle \cos^2 \frac{1}{2} \Delta \phi \right]^{\frac{1}{2}}$$
(3.11)

Hence the intensity of the monitor image varies between maximum and minimum values given by equations (3.9a) and (3.9b). Comparison of equations (3.5a) and (3.5b) shows that the fringe minima obtained with subtraction correspond to fringe maxima obtained using addition. It can also be seen that subtraction fringes have intrinsically better visibility than addition fringes, since the subtraction fringes have zero intensity, while addition fringes do not. However, when addition is used to observe the fringes, a video storeage is not required. Vibration fringes can also be produced by the time-average subtraction technique, which gives more clear fringes [25].

3.5 The Measurement of Real Time Vibration Pattern

For vibration pattern measurement, the ESPI is operated in time-average mode. In time-averaged mode the images are being taken while the object is vibrating. At a given time, t, the intensity in the image plane is given by I(t) where

$$I(t) = I + I_o + 2\sqrt{I_r I_o} \cos\left[\theta + \frac{4\pi}{\lambda}a(t)\right]$$
 (3.12)

where a(t) represents the position of a given point on the object at time t. The intensity is averaged over time τ to give

$$I_{\tau} = I_r + I_o + \frac{1}{\tau} 2 \sqrt{I_r I_o} \int_0^{\tau} \cos \left[\theta + \frac{4\pi}{\lambda} a(t)\right] dt$$
 (3.13)

When this is evaluated for a sinusoidal vibration,

$$a(t) = a_0 \sin \omega t$$
 (where $2\pi/\omega \ll \tau$)

we get

$$I_{\tau} = I_{r} + I_{o} + 2\sqrt{I_{r}I_{o}}J_{o}^{2}(\frac{4\pi}{\lambda}a_{o})\cos\theta$$
 (3.14)

The value of I_{τ} averaged along many speckle patterns is constant over the whole image, but it can be seen that the contrast of the speckle will vary as the value of the J_0^2 function varies. When J_0^2 has a value of zero, the intensity varies only as I_0 varies; whereas when J_0^2 has a maximum value, the intensity varies with variation in I_0 and

$$2\sqrt{IJ_o}\cos\theta. \tag{3.15}$$

Figure 3.2 shows the J_0^2 distribution.

Correlation fringes are thus observed which map out the variation in a_0 , the amplitude of the vibration across the object surface. The fringe minima correspond to the minima of the Bessel function. Table 1 shows the relation between the fringe order N and the vibration amplitude a.

In the time-averaged mode, the phase information of the vibration components is lost due to the averaging of the displacements over a vibration cycle. This limitation is eliminated if stroboscopic technique is used [26]. Another way to record the phase information is to use a dual-pulsed laser [27], or to move the PZT mirror in the reference beam path at the same vibration frequency [28].

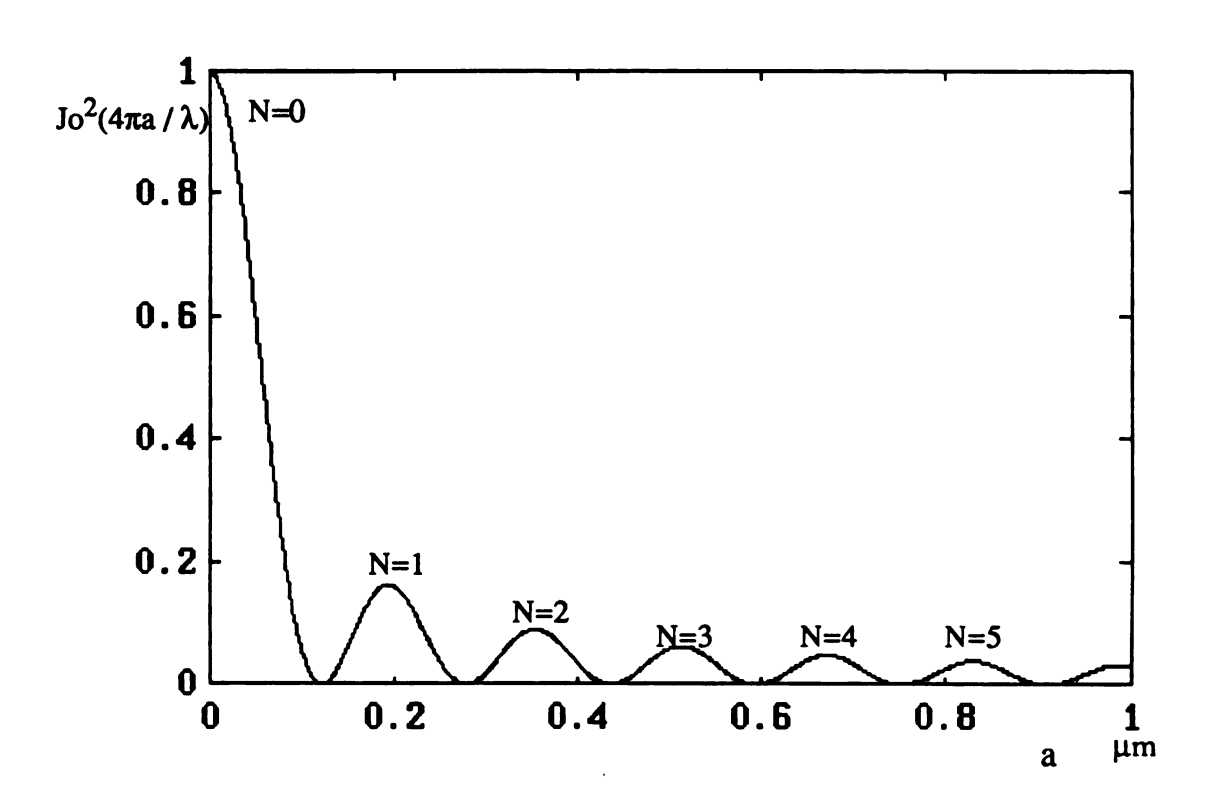


Fig. 3.2 The first few cycles of the ${\rm J_0}^2$ distribution which defines the intensity distribution of time-averaged speckle fringes for a sinusoidally vibrating surface

N (fringe order)	a (amplitude, μm)
0	0
1	0.19
2	0.35
3	0.51
4	0.67
5	0.83
	-

Table 1
Fringe order N vs vibration amplitude in time-average ESPI mode.

3.6 The Measurement of Dynamic Displacements

When taking a speckle picture in ESPI it is necessary that all the components are stable to considerably better than a wavelength during the exposure time (1/30 second). So, only static or quasi-static displacements can be measured using continuous lasers. With the use of a dual-pulsed laser, ESPI can be extended to the measurement of dynamic displacements. The dual pulsed technique can also be used to measure large amplitude periodic displacements. If, for example, the period of oscillation is 10^{-3} second, a pulse separation of 10 μ s will enable 0.01 of the overall amplitude to be measured in a single recording. This procedure extends the range of vibration measurement to amplitudes approaching $10^3 \lambda$.

3.7 The Optimization of Light Intensity in ESPI

For a given type of TV camera, a certain minimum intensity is required to create a camera voltage output which can be detected above the background electronic noise. An increase in the incident intensity gives an increased output camera voltage until the intensity reaches the camera saturation level, beyond which the output voltage remains constant for any further increase in incident intensity.

The intensity of the speckle pattern varies randomly across the image, and, to avoid losing information from the speckle pattern, the overall intensity should be below the saturation level of the camera for all of the useful picture area. If the mean value and the standard deviation of the speckle pattern are given by $\langle I_t \rangle$ and σ_t , then, when

$$\langle I_t \rangle + 2\sigma_t < I_{sat} \tag{3.16}$$

the intensity will be less than the saturation level of the camera for 95% of the image. Here I_{sat} is the camera's saturation intensity.

3.7.1 Two Speckle Beam Case

When two speckled beams are used in a subtraction correlation system, the mean intensities of the two beams at the image plane should be equal, and the combined peak intensities should be approximately equal to the camera saturation intensity.

3.7.2 Smooth Reference Beam Case

Based on our experience, the best results are obtained when the reference beam intensity is set as,

$$\frac{1}{4}I_{sat} \le \langle I_r \rangle \le \frac{1}{2}I_{sat} \tag{3.17}$$

This depends on the signal-to-noise ratio and and the threshold set in the software. The sum of the intensities should be such that the peak intensities are near the saturation level of the camera.

3.8 Spatial Resolution of the Video System and Its Effect on ESPI

The spatial resolution and dynamic range of video systems are considerably less than those of photographic and holographic emulsions. These factors affect the design of speckle pattern interferometers which use video systems to display the correlation fringes.

The ability of the video system to resolve fine detail in the image is limited. Thus, if a coarse black and white grid is imaged on the face plate of the TV camera, an equivalent grid will be observed on the monitor. As the spacing of the grid is reduced, the contrast of the grid observed on the monitor is reduced; and when the grid spacing is sufficiently small, no grid structure is observed on the monitor.

The limit to the spatial resolution in the vertical direction is governed by the number of scan lines. A standard system having 525 lines and an active face plate area of about 13 x10 mm should have a minimum vertical resolution of ~20 µm on the face plate.

The resolution in the horizontal direction is governed by the temporal frequency response of the video system, which is determined by the electronic design of the system. Typically, this frequency response is fairly uniform up to 4 MHz and falls to a very low value at 10 MHz. The temporal frequency response is clearly related to the spatial frequency in the image. A sinusoidal intensity distribution in the image plane of spatial frequency 10⁶/ WNM mm⁻¹ will give a sinusoidal output voltage of 1 MHz, where

W = width of the active face plate area in mm

N = number of scan lines

M = number of frames per second

For a standard TV system, 1 MHz corresponds to a spatial frequency of \sim 5 mm⁻¹ (spacing \sim 200 μ m).

A grid having a 20 μ m spacing in the horizontal direction will give an output voltage of frequency 9.45 MHz. Since the frequency response is very low at 10 MHz, 20 μ m can also be taken as the upper limit of the spatial resolution in the horizontal direction.

It was assumed in deriving equations (3.4) and (3.11), which describe the variation in monitor brightness to give subtraction and addition correlation fringes, that the random variations in I_r , I_o are fully resolved by the television camera, so that the camera signal from a given point in the image is proportional to the intensity at that point. When the points are not fully resolved, the output voltage is a function of the intensity of the image averaged over the resolution area of the camera, and the effect of this averaging is to reduce the standard deviation or contrast of the output voltage [29]. Consider, for example, the case of two speckle patterns whose intensities have the same mean value and standard deviations, one of which is fully resolved by the TV camera and the other of which is only partially resolved. The output camera signals will have the same mean

values across the image, but the standard deviation of the signal will be less for the partially resolved pattern. If the speckles are sufficiently small, the output signal will be uniform. It will be shown below that the effect of this reduction in the standard deviation of the output signal is to reduce the visibility of the correlation fringes.

From equations (3.4) and (3.5) the correlation fringes are seen to arise from the variation with $\Delta \phi$ of the standard deviation of the subtracted or added signals; if the contrast of the individual signals is reduced, the standard deviation of the subtracted or added signals is also reduced, and the visibility of the correlation fringes is decreased. If we write the output camera signal as

$$V_{r,o} = V_0 + (V_{corr})_{r,o} (3.18)$$

where V_0 arises from the $(I_r + I_o)$ term and $(V_{corr})_{r,o}$ arises from the $2\sqrt{I_1I_2}\cos\phi$ and $2\sqrt{I_1I_2}\cos(\phi + \Delta\phi)$ terms, then, since V_0 remains unchanged when the object is displaced, it is a noise term. Consequently, the correlation fringe visibility is maximized when the standard deviation of $(V_{corr})_{r,o}$ is maximized. We can write the value of $(V_{corr})_{r,o}$ at a given point in the image as

$$(V_{corr})_{r,o} = k \langle \sqrt{I_{r}I_{o}} \cos (\phi + \Delta \phi) \rangle \Delta A$$
 (3.19)

where k is a constant, and $\Delta \phi$ is the phase difference between the reference beam and the object beam. ΔA is the resolution area of the camera.

If the variation of ϕ over the resolution area is very much less than 2π , then the value of $(V_{corr})_{r,o}$ for constant $\Delta \phi$ varies between $\pm [k\langle \sqrt{I_r I_o} \cos \Delta \phi \rangle]_{max}$. When the value of ϕ varies by ϕ or more over the resolution area, then the value of ϕ over the whole image is approximately zero, and in this case correlation fringes are not observed.

Thus, the spatial frequency distribution of $\cos \phi$ must be such that the components of that distribution are at least partially resolved by the video system.

3.8.1 Spatial Resolution (Two-speckled-beam case)

When the two wavefronts I_r and I_o are speckled, the spatial frequency distribution of the combination of the two beams will be similar to that of I_r or I_o . The maximum spatial frequency f_{max} of the distribution is determined by the diameter of the viewing lens aperture a, and is given by the equation

$$\frac{1}{f_{max}} \approx 1.22 (1 + M) \frac{\lambda v}{a},$$
 (3.20)

where v is the lens-to-image distance. M is the magnification of the lens. If the object-to-viewing-lens distance is considerably greater than the lens-to-image distance, the lens equation gives that v = f. The minimum speckle size s_{min} is then given by

$$s_{min} = \frac{1}{f_{max}} \approx 1.22 (1 + M) \lambda (NA)$$
 (3.21)

where NA = $\frac{f}{a}$ is the numerical aperture of the viewing lens.

If the smallest spot resolved by the video system is 20 μ m, corresponding to a spatial frequency of 50 mm⁻¹, then, to resolve fully the spatial frequencies arising from the speckle distribution, we must have

Thus, quite a small aperture must be used if the scale of the speckle pattern is to be large enough to be fully resolved by the video camera.

If the numerical aperture of the lens is reduced below this value, the spatial frequency of the speckle pattern will increase and it will no longer be fully resolved. However, the amount of light transmitted through the lens will increase, so that the value of V_{corr} does not necessarily decrease. An exact analysis of the relationship between V_{corr} and the viewing lens aperture diameter is quite difficult. However, the optimum value can be readily found in practice simply by adjusting the aperture size until maximum speckle contrast is obtained.

3.8.2 Spatial Resolution (smooth reference beam case)

In this system, I_o is a random speckle intensity, while I_r is nominally uniform across the image plane. The phase difference ϕ between I_o and I_r is given by

$$\phi = \phi_s + \frac{2\pi l_{op}}{\lambda} - \left[\phi_r + \frac{2\pi l_{o^*p}}{\lambda}\right]$$

$$= \phi_s - \phi_r + \frac{2\pi}{\lambda} \left(l_{op} - l_{o^*p}\right)$$
(3.22)

where O is the center of the aperture of the viewing lens, O' is the point from which the reference beam appears to diverge, and P is a point in the image plane (see Figure 3.3). ϕ_r is the phase of reference beam at O' and is constant across that beam, while ϕ_s is the random phase at O. l_{op} and $l_{o'p}$ are the distances from O and O' to P.

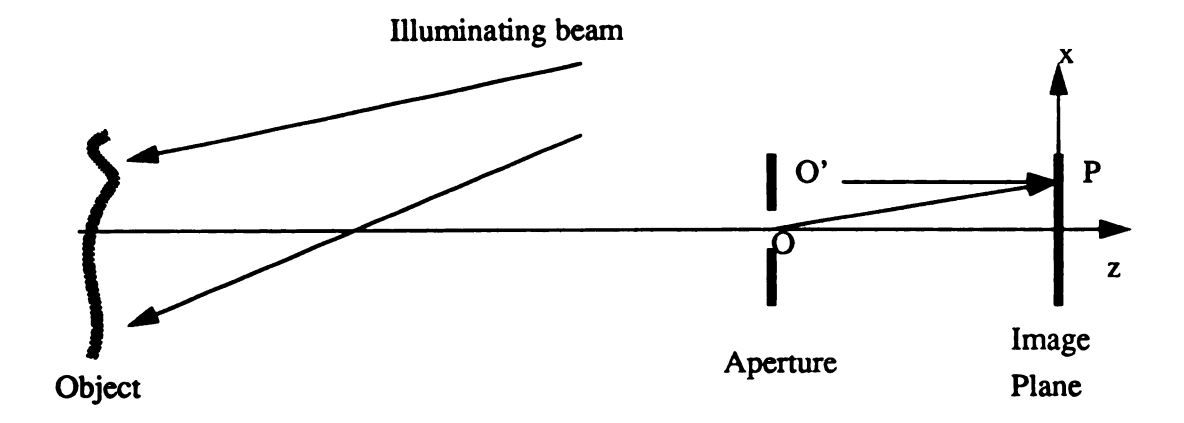


Fig. 3.3

The general geometry of a smooth reference beam interferometer

It was pointed out that if ϕ varies by 2π or more within the resolution diameter of the resolution area of the camera, the correlation signal V_{corr} will be very small. The variation in ϕ_s is governed by the viewing lens aperture diameter, as in the case of the two-speckled beams system, and a suitable aperture ensures that it does not vary too rapidly. Clearly, the variation in the last term $\Omega = \frac{2\pi}{\lambda} \left(l_{op} - l_{o'p}\right)$ with P must be such that Ω varies by considerably less than 2π over the diameter of the resolution area. If O and O' are coincident, Ω is zero so that, if possible, this condition should be satisfied (O and O' are then referred to as being conjugate).

To determine the departure from conjugacy that can be tolerated, we assume that the coordinates of O and O' are $(0, 0, l_0)$ and $(\Delta x, 0, l_r)$; the resolution diameter is x_r . When Δx , $\Delta l = l_0 - l_r << l_0$, we have;

$$l_{op} - l_{o'p} \approx \left(l_o + \frac{x^2}{2l_o}\right) - \left[l_r + \frac{(x - \Delta x)^2}{2l_r}\right]$$
 (4.23)

Neglecting second order terms of Δx and Δl , we have;

$$l_{op} - l_{o'p} \approx \Delta l + \frac{x\Delta x}{l_o} - \frac{x^2 \Delta l}{2l_o^2}$$
(3.24)

It is seen that a lateral displacement, Δx , of O' with respect to O produces a linear variation in ϕ across the image plane. ϕ varies by 2π across an interval δx given by;

$$\delta x = \frac{l_o \lambda}{\Delta x} \tag{3.25}$$

If this is to be resolved by the video system, δx should be considerably greater than x_r , i.e.;

$$x_r \ll \frac{l_o \lambda}{\Delta x}$$
 (3.26)

or

$$\Delta x \ll \frac{l_o \lambda}{x_-} \tag{3.27}$$

Thus, the lateral departure from conjugacy must be less than that specified by the equation (3.27). For a lens-to-image distance of 100 mm and $x_r = 20 \mu m$, we have

$$\Delta x \ll 3.2 \text{ mm}.$$

A longitudinal departure from conjugacy of Δl gives rise to a variation in ϕ which varies as x^2 . The maximum gradient of ϕ occurs at the edge of the image. Here it can be seen that the distance δx in which ϕ varies by 2π is given (taking absolute value) by;

$$\delta x = \frac{\lambda l_o^2}{x \Delta l} \tag{3.28}$$

If this is to be resolved, we must have;

$$\frac{\lambda l_o^2}{r \Lambda l} \gg x_r \tag{3.29}$$

OI

$$\Delta l \ll \frac{\lambda l_o^2}{x x_t} \tag{3.30}$$

Let x take its maximum value, which is equal to the half width of the active area of the camera tube, typically about 5 mm. For a lens-to-image distance of 100 mm and $x_r = 20$ um, we have;

$$\Delta l \ll 63 \text{ mm}$$

To optimize the visibility of the correlation fringes, Δx and Δl should be made as small as possible. It is seen that displacements in the lateral direction give rise to much more rapid variation of ϕ than equivalent variations in the longitudinal direction, so that the lateral shift in particular should be minimized. It is not difficult in practice to do this. In addition, the size of the viewing lens aperture should be adjusted to give optimum speckle contrast.

If $x_r = 20 \,\mu\text{m}$, because the speckle size is doubled resulting from the interference with the reference beam, the aperture needed to make the speckle size equal to the detector element size can be reduced to,

$$(NA) = 13$$

3.8.3 General Conclusion

Because of resolution limitations, the use of a television camera to observe speckle correlation fringes requires the use of a small aperture in the viewing lens and results in relatively large speckles. This affects the performance of the interferometer in two ways.

First, the spacing of the correlation fringes must be greater than approximately 1/120 of a screen width. This follows because when the fringe spacing becomes comparable to the minimum speckle size, the fringe visibility decreases and drops to zero when they are equal. A minimum ratio of fringe spacing to speckle size of about five is necessary to give reasonably visible fringes. Since the minimum speckle size is about $20 \mu m$, then the minimum fringe spacing is of the order of $100 \mu m$. This corresponds to a fringe spacing of 1/120 of a target plate of $12 \mu m$ width. Hence a maximum of $120 \mu m$ fringes of uniform spacing should, in theory, be observable. With a fringe pattern of variable spacing, the maximum number under optimum viewing conditions is found in practice to be about 50. If the number of fringes in one full screen is greater than 50, it will likely give rise to fringe counting error.

Second, the use of a small aperture means that the system is not very efficient in light usage compared with the equivalent photographic speckle correlation system.

However the speed and convenience of video processing compared with photographic processing generally outweighs these disadvantages. One also can use a laser with greater power. Most systems use a 10-15 mw laser. A high power laser such as an Argon laser can also be used for testing large objects.

3.9 Error Sources

Several possible sources of error and their contributions to measurement inaccuracy are listed below:

1. Frequency instability of the light source;

This instability may cause λ to change slightly, but this effect is very small and negligeable.

2. Reference phase error;

This is the deviation for the *i*th shift or step between the actual and desired values of α_i , by carefully calibrating the PZT used, this error can be eliminated.

3. Detector nonlinearity;

In technical manuals for detectors, the nonlinearity of the detector is often described as: $I_i = I_i^r$ (0 < r < 1). For CCD detectors the nonlinearity is negligible ($r \approx 1$), but for vidicon tubes the nonlinearity can be considerable ($r \approx 0.7$). A CCD camera is commonly used in ESPI system.

4. Instability of the light source;

The light source intensity during recording of the frames may vary from one frame to another. When the laser is already warmed up this error is negligeable.

5. Environment disturbances, vibration and air turbulence;

By looking at live correlation fringes, we can see the disturbances; if they do not affect the fringe pattern, then it does not matter.

6. Noise of the detector output and quantization noise of the measured intensity;

For a CCD camera this is very small and negligeable.

3.10 Displacement Measurement Using Phase Information:

3.10.1 Principal Phase Determination

As shown in Figure 3.4. The light from a He-Ne laser is split into object and reference beams by a beam splitter. The object beam is further expanded by an objective lens and filtered by a pin-hole to illuminate the object. Diffusely scattered light from the object is collected by an imaging lens and imaged on the detector plate of a TV camera. The reference beam is also expanded and filtered through a spatial filter to interfere with the speckle image of the object on the detector plate of a TV camera.

If the detector elements are several times larger than the smallest speckles in the pattern, the modulation that is generated by changing the phase of the reference beam is reduced. This reduction is offset by the increased light level on the detectors, so there is a trade-off between light level and modulation [30]. The best result can be determined by experiment.

In order to calculate the phase information, a mirror mounted on a PZT device is placed in the reference beam path to artificially change the optical path difference between reference and object beam. The light intensity of the interference speckle image pattern is sampled to yield a digital picture made up of 512 x 512 sample points. Each sample point is quantized to 256 discrete gray levels. The digital picture is stored in a digital frame memory at a speed of 1/30 sec. Further processing depends on the application and calculation algorithm.

3.10.2 Phase Measurement

In order to detect the deformation, phase-measurement interferometry (PMI) is used. Although the basic techniques for phase-measurement interferometry have been known for many years [31-39], it is only recently that PMI has become of practical use. Two

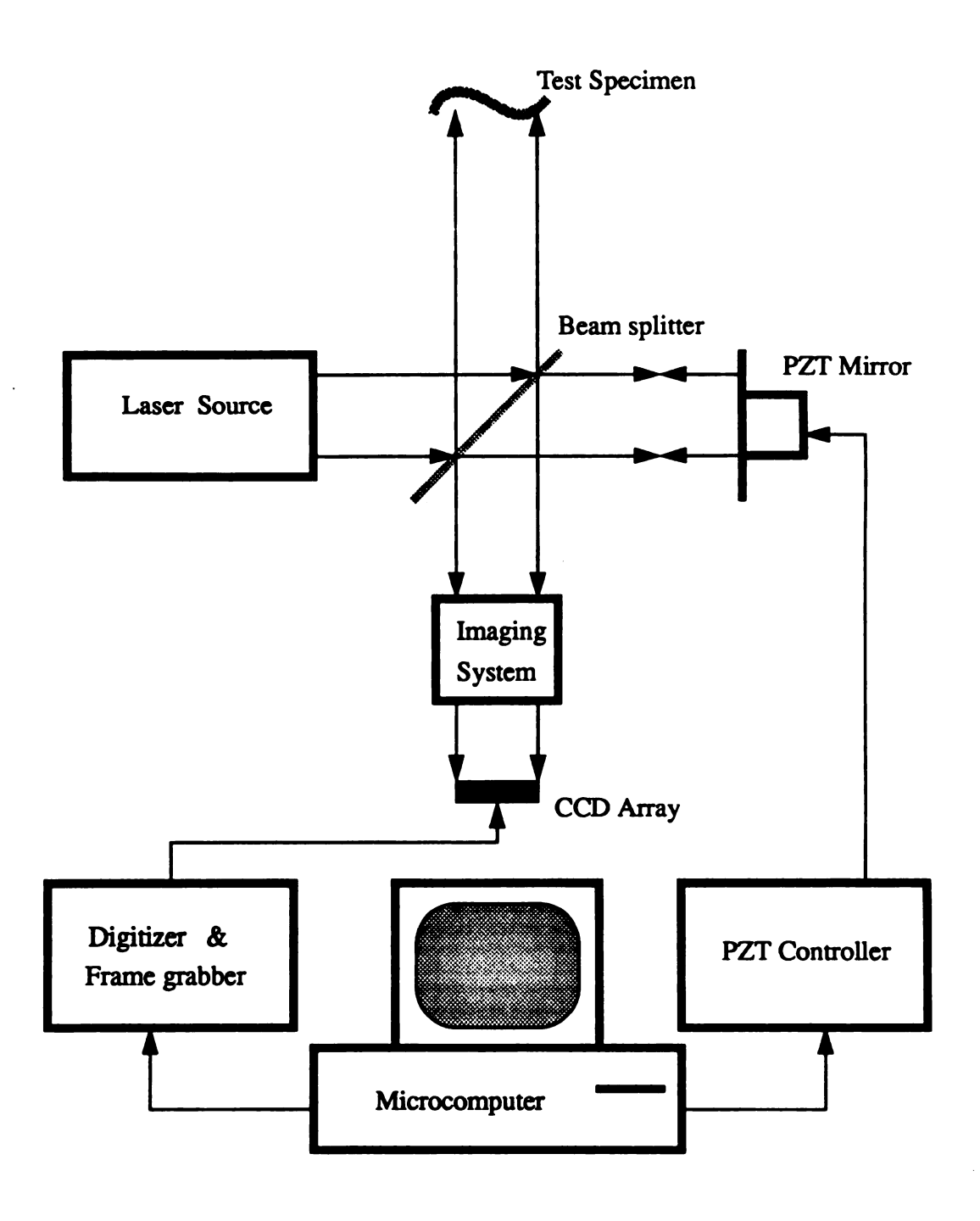


Fig. 3.4

Schematic for measuring phase using a PZT mirror as the phase shifter and sending data to a computer for the phase calculation.

major developments make this possible, namely, solid-state detector arrays and fast microprocessors. When a detector array is used to detect fringes, and a known phase change (can be unknown for Carre technique) is induced between the object and reference beams, the phase of a wavefront may be directly calculated from recorded intensity data. Generally, a number of data frames are recorded as the reference beam phase is changed in a known manner. The data are fed into a computer where the phase at each detector point is calculated. Information about the test surface is geometrically related to the calculated wavefront phase.

The direct measurement of phase information has many advantages over simply recording interferograms and then digitizing them. First, the precision of phase measurement techniques is ten to a hundred times greater than that of digitizing fringes. Second, it is simple. A detector array is placed at the image plane, and a phase-shifting device is placed in the reference beam. Using solid-state detector arrays, data can be taken very rapidly, thereby reducing errors due to air turbulence or vibration. Third, automatic fringe enhancement, counting and ordering can be carried out using microcomputers. Full field displacement information can be calculated using pipe-line processing in a very fast fashion.

3.10.3 Means of Phase Shifting

There are many ways to determine the phase of a wavefront. For all techniques a temporal phase modulation (or time-dependant relative phase shift between the object and reference beams in an interferometer) is introduced to perform the measurement. By measuring the speckle pattern intensity as the phase is shifted, the phase of the wavefront can be determined with the aid of a computer-controlled electronic processing system.

Phase modulation in an interferometer can be induced by moving a mirror, tilting a glass plate, moving a grating, rotating a half-wave plate or analyzer, or by using an

acousto-optic or electro-optic modulator [34, 40, 41]. Phase shifters such as moving mirrors, gratings, tilted glass plates, or polarization components can produce continuous as well as discrete phase shifts between the object and reference beams.

The most common and straightforward phase-shifting technique is the placement of a mirror pushed by a piezo-electric transducer (PZT) in the reference beam [38]. Many brands of PZTs are available to move a mirror linearly over a range of several microns. A high-voltage amplifier is used to produce a linear ramping signal from 0 to several hundred volts. If there are nonlinearities in the PZT motion, they can be accounted for by using a programmable waveform generator. If a phase-stepping technique is preferred to a continuous modulation, any calibrated PZT can be used because only discrete voltage steps are needed.

3.10.4 Phase-measurement Algorithms

Phase-measurement techniques using analytical means to determine phase all have some common denominators. These techniques shift the phase of one beam in the interferometer with respect to the other beam and measure the intensity of an interference pattern at many different relative phase shifts. To make these techniques work, the interference pattern must be sampled correctly to obtain sufficient information to reconstruct the wavefront. The detected intensity modulation as the phase is shifted can be calculated for each detected point to determine if the data point is good (sufficient modulation)

Fringe modulation is a fundamental problem in all phase-measurement techniques [42]. When a fringe pattern is recorded by a detector array, there is an output of discrete voltages representing the average intensity incident upon the detector element over the integration time. As the relative phase between the object and reference beams is shifted, the intensities read by the detector element should change. Because any array samples the image over a finite number of discrete points, the maximum image spatial frequency that

can be unambiguously transformed is the Nyquist frequency, at which each sensing element corresponds to either a maximum or a minimum in the image. Therefore, if we have at least one detector element for each speckle, the Nyquist frequency condition will be satisfied. However, if there is one fringe over the area of the detector element, there will be no modulation. Figure 3.5 illustrates three different cases; (2) indicates a highly sampled condition where speckle size is much larger than the detector element; this gives highly detailed modulation output. (3) represents the sufficiently sampled case, where the speckle and the detector element have almost the same size and the output has high modulation. (4) shows the undersampled case where the speckles are much smaller then the detector element and the output has low modulation. Thus the detector size influences the recorded fringe modulation, whereas the detector spacing determines if the wave front can be reconstructed without phase ambiguities.

Many different algorithms have been published for the determination of wavefront phase [30 -35, 38-39, 43-46]. Some techniques step the phase a known amount between intensity measurements, whereas others integrate the intensity while the phase is being shifted. Both types are phase-shifting techniques. The first is the so-called phase-stepping technique, and the second is usually referred to as an integrating-bucket technique. A minimum of three measurements is necessary to determine the phase, since there are three unknowns in the interference equation;

$$I = I_r + I_o + 2\sqrt{I_r I_o} \cos \phi \tag{3.31}$$

These unknowns are the reference beam intensity I_r , the object beam intensity I_o and the phase difference ϕ between the reference beam and object beam. The phase shift between adjacent intensity measurements can be anything between 0 and π as long as it is constant (for phase-stepping method) or linear (for integration method).

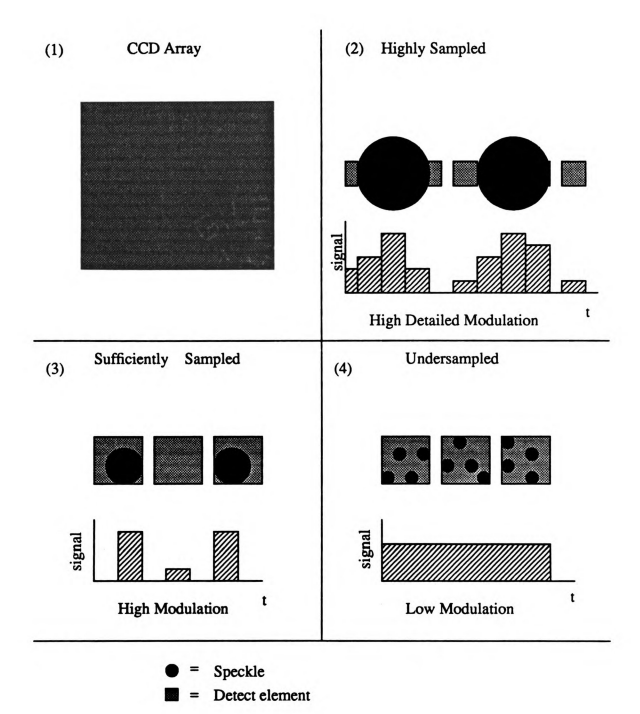


Fig 3.5

 CCD array with finite -sized detectors.
 Detector element much smaller than speckle size.
 The size of detector element and speckle are almost equal.
 Speckle size is much smaller than detector element. In general, N measurements of the intensity are recorded as the phase is shifted. For the general technique the phase shift is assumed to change during the detectors' integration time, and this change is the same from data frame to data frame. The amount of phase change from frame to frame may vary, but it must be known by calibrating the phase shifter or measuring the actual phase change. Unless discrete phase steps are used, the detector array will integrate the fringe intensity data over a change in relative phase of Δ. One set of recorded intensities may be written as [45];

$$I_{i}(x,y) = \frac{1}{\Lambda} \int_{(\alpha_{i} - \Delta/2)}^{(\alpha_{i} + \Delta/2)} I_{0}(x,y) \left\{ 1 + \gamma_{0} \cos[\phi(x,y) + \alpha(t)] \right\} d\alpha(t)$$
 (3.32)

where $I_0(x, y)$ is the average intensity at each detector point (DC component), γ_0 is the modulation of the fringe pattern, α_i is the average value of the relative phase shift for the *i*th exposure, and $\phi(x, y)$ is the phase of the wavefront being measured at the point (x, y). The integration over the relative phase shift Δ makes this expression applicable for any phase-shifting technique. After integrating this expression the recorded intensity is found to be;

$$I_{i}(x,y) = I_{0}(x,y) \left\{ 1 + \gamma_{0} \left(\frac{\sin \left[(1/2) \Delta \right]}{\left[(1/2) \Delta \right]} \right) \cos \left[\phi(x,y) + \alpha_{i} \right] \right\}$$
 (3.33)

It is important to note that the only difference between integrating the phase and stepping the phase is a reduction in the modulation of the interference fringes after detection. If the phase shift were stepped ($\Delta \approx 0$) and not integrated, we have;

$$\left(\sin\frac{1}{2}\Delta\right)/\left(\frac{1}{2}\Delta\right) = 1\tag{3.34}$$

Therefore, phase stepping is a simplification of the integrating method. At the other extreme, if $\Delta = 2\pi$, there would be no modulation of the intensity. Since this technique relies on a modulation of the intensities as the phase is shifted, the phase shift per exposure needs to be between 0 and π .

For a total of N recorded intensity measurements, the phase can be calculated using a least-squares technique. This type of approach can be found in references [44, 45, 47]. First, equation (3.33) is rewritten in the form

$$I_{i}(x, y) = a_{0}(x, y) + a_{1}(x, y) \cos \alpha_{i} + a_{2}(x, y) \sin \alpha_{i}$$
 (3.35)

where

$$a_0(x, y) = I_0(x, y)$$
 (3.36)

$$a_1(x, y) = I_0(x, y) \gamma_0 \frac{\sin[(1/2)\Delta]}{[(1/2)\Delta]} \cos\phi(x, y)$$
 (3.37)

$$a_2(x, y) = I_0(x, y) \gamma_0 \frac{\sin[(1/2)\Delta]}{[(1/2)\Delta]} \sin\phi(x, y)$$
 (3.38)

The unknowns of this set of equations are $I_0(x, y)$, γ_0 and $\phi(x, y)$. The least-squares solution to these equations is

$$\begin{vmatrix} a_0(x, y) \\ a_1(x, y) \\ a_2(x, y) \end{vmatrix} = A^{-1}(\alpha_i) B(x, y, \alpha_i),$$
 (3.39)

where

$$A(\alpha_i) = \begin{bmatrix} N & \Sigma \cos \alpha_i & \Sigma \sin \alpha_i \\ \Sigma \cos \alpha_i & \Sigma (\cos \alpha_i)^2 & \Sigma \cos \alpha_i \sin \alpha_i \\ \Sigma \sin \alpha_i & \Sigma \cos \alpha_i \sin \alpha_i & \Sigma (\sin \alpha_i)^2 \end{bmatrix},$$

and

$$B(\alpha_i) = \begin{bmatrix} \Sigma I_i(x, y) \\ \Sigma I_i(x, y) \cos \alpha_i \\ \Sigma I_i(x, y) \sin \alpha_i \end{bmatrix}$$

The matrix A needs to be calculated and inverted just once because it is dependent only on the phase shift. The phase at each point in the speckle pattern is determined by evaluating the value of B at each point and then solving for the coefficients a_1 and a_2 . Finally, we obtain

$$\tan\phi(x,y) = \frac{a_2(x,y)}{a_1(x,y)} = \frac{I_0 \gamma_0 \frac{\sin[(1/2)\Delta]}{[(1/2)\Delta]} \sin\phi(x,y)}{I_0 \gamma_0 \frac{\sin[(1/2)\Delta]}{[(1/2)\Delta]} \cos\phi(x,y)}$$
(3.40)

This phase calculation assumes that the phase shifts between measurements are known and that the integration period Δ is constant for every measurement.

Besides a reduction in intensity modulation due to the integration over a change in phase shift, the finite size of the detector element will also contribute to a reduction in intensity modulation. To make reliable phase measurements, the incident intensity must modulate sufficiently at each detector point to yield an accurate phase. The recorded intensity modulation can be calculated from the intensity data using the equation,

$$\gamma(x,y) = \gamma_0 \frac{\sin[(1/2)\Delta]}{[(1/2)\Delta]} = \frac{\sqrt{a_1(x,y)^2 + a_2(x,y)^2}}{a_0(x,y)}$$
(3.41)

This expression can be used to determine if a data point will yield an accurate phase measurement or if it should be ignored.

3.10.4.1 Three-step technique

Since there are three unknowns in the equation (3.31), a minimum of three sets (exposures) of recorded fringe data are needed to reconstruct a wavefront; the phase can then be calculated from a known phase shift of α_i per exposure. There are two common choices for the phase shift value, namely, $\Delta = \frac{\pi}{2}$ and $\Delta = \frac{2\pi}{3}$.

(a) When $\alpha_i = \frac{1}{4}\pi$, $\frac{3}{4}\pi$, and $\frac{5}{4}\pi$, that is N = 3, $\Delta = \frac{1}{2}\pi$. The three intensity measurements may be expressed as [24].

$$I_1(x, y) = I_0(x, y) \left(1 + \gamma \cos\left[\phi(x, y) + \frac{1}{4}\pi\right]\right)$$
 (3.42)

$$I_1(x, y) = I_0(x, y) \left(1 + \gamma \cos\left[\phi(x, y) + \frac{3}{4}\pi\right]\right)$$
 (3.43)

$$I_1(x, y) = I_0(x, y) \left(1 + \gamma \cos \left[\phi(x, y) + \frac{5}{4}\pi\right]\right)$$
 (3.44)

When discrete steps are used, $\gamma = \gamma_0$, and when the phase is integrated over a $\frac{1}{2}\pi$ phase shift per frame, $\gamma = 0.9\gamma_0$. The phase at each point is then simply;

$$\phi(x,y) = \arctan\left(\frac{I_3(x,y) - I_2(x,y)}{I_1(x,y) - I_2(x,y)}\right)$$
(3.45)

and the intensity modulation is;

$$\gamma(x,y) = \frac{\sqrt{[I_1(x,y) - I_2(x,y)]^2 + [I_2(x,y) - I_3(x,y)]^2}}{2I_0}$$
(3.46)

(b) If a phase shift of 120° ($\frac{2}{3}\pi$) is used, $\alpha_i = -\frac{2}{3}\pi$, 0, $\frac{2}{3}\pi$, and $\Delta = \frac{2}{3}\pi$. We have

$$\phi(x,y) = \arctan\left(\frac{\sqrt{3}(I_3(x,y) - I_2(x,y))}{2I_1(x,y) - I_2(x,y) - I_3(x,y)}\right)$$
(3.47)

for the integration method, $\gamma = 0.83 \gamma_0$, and the detected intensity modulation is

$$\gamma(x,y) = \frac{\sqrt{3[I_3(x,y) - I_2(x,y)]^2 + [2I_1(x,y) - I_2(x,y) - I_3(x,y)]^2}}{2I_0}$$
(3.48)

3.10.4.2 Four-step Technique

This is a common algorithm for phase calculations [17]. In this case $\alpha_i = 0$, $\frac{1}{2}\pi$, π , and $\frac{3}{2}\pi$. $\gamma = \gamma_0$ for the four-step technique and $\gamma = 0.9 \gamma_0$ for the integration technique ($\Delta = \frac{1}{2}\pi$). Note that integrating the phase produces a very small effect for a $\frac{1}{2}\pi$ phase shift per exposure. Thus, linearly ramping the phase shifter while taking measurements makes more sense than stepping and waiting for the reference beam to

settle down. Using calculations similar to that for three-step technique, the phase at each point for the four-step method is

$$\phi(x,y) = \arctan\left(\frac{I_4(x,y) - I_2(x,y)}{I_1(x,y) - I_3(x,y)}\right)$$
(3.49)

and the recorded modulation can be calculated from,

$$\gamma(x,y) = \frac{\sqrt{[I_4(x,y) - I_2(x,y)]^2 + [I_1(x,y) - I_3(x,y)]^2}}{2I_0}$$
(3.50)

One nice thing about this technique is that by using pipe-line image processing (using look-up tables) the noise due to the speckles can be removed, which gives noticeable fringe visibility improvement [49].

3.10.4.3 Carre Technique

In the previous equations the phase shift is known either by calibrating the phase shifter or by measuring the amount of phase shift each time it is moved. Carre [31] presented a technique of phase measurement that is independent of the amount of phase shift. It assumes that the phase is shifted by α between consecutive intensity measurements to yield four equations

$$I_1(x, y) = I_0(x, y) \left\{ 1 + \gamma \cos \left[\phi(x, y) - \frac{3}{2} \alpha \right] \right\}$$
 (3.51)

$$I_2(x, y) = I_0(x, y) \left\{ 1 + \gamma \cos \left[\phi(x, y) - \frac{1}{2} \alpha \right] \right\}$$
 (3.52)

$$I_3(x, y) = I_0(x, y) \left\{ 1 + \gamma \cos \left[\phi(x, y) + \frac{1}{2} \alpha \right] \right\}$$
 (3.53)

$$I_4(x, y) = I_0(x, y) \left\{ 1 + \gamma \cos \left[\phi(x, y) + \frac{3}{2} \alpha \right] \right\}$$
 (3.54)

where the phase shift is assumed to be linear. with time. From these equations the phase at each point can be calculated by,

$$\phi(x,y) = \arctan \frac{\sqrt{[3(I_2 - I_3) - (I_1 - I_4)][(I_2 - I_3) + (I_1 - I_4)]}}{(I_2 + I_3) - (I_1 + I_4)}$$
(3.55)

For this technique the intensity modulation is,

$$\gamma = \frac{1}{2I_0} \sqrt{\frac{\left[(I_2 - I_3) + (I_1 - I_4) \right]^2 + \left[(I_2 + I_3) - (I_1 + I_4) \right]}{2}}$$
(3.56)

where this equation assumes that α is near $\frac{1}{2}\pi$. An obvious advantage of the Carre technique is that the phase shifter does not need to be calibrated. It also has the advantage of working when a linear phase shift is introduced in a converging or diverging beam where the amount of phase shift varies across the beam.

3.10.5 Comparison of Phase Measurement Techniques

In general, the integration methods give the same results as the phase-stepping methods except in the case of nonlinear phase-shift errors, where the integration method is superior. The Carre algorithm is the best to use where phase-shifting errors are present, and the four-step technique is the best for eliminating effects due to second and third order detection nonlinearities.

3.10.6 Phase Unwrapping

Because of the nature of arctangent calculations, the equations presented for phase calculation are sufficient for only a modulo π calculation. To determine the phase modulo 2π , the signs of quantities proportional to $\sin \phi$ and $\cos \phi$ must be examined. For all techniques but Carre's [42], the numerator and denominator give the desired quantities. Table 2 shows how the phase is determined by examining the signs of these quantities after the phase is calculated modulo $\frac{1}{2}\pi$ using absolute values in the numerator and denominator to yield a modulo 2π calculation. Once the phase has been determined to be modulo 2π . The phase ambiguities due to the modulo 2π calculation can be removed by comparing the phase difference between adjacent pixels. For reliable removal of discontinuities the phase must not change by more than π between adjacent pixels. As long as the data are sampled as described in the sampling requirements, the wavefront can be reconstructed.

For the Carre technique, simply looking at numerators and denominators is not sufficient to determine phase modulo 2π [42]. It is somewhat complicated and will not be discussed here.

Any phase unwrapping needs some reference point, that is a point to start. If the reference point is a fixed point, say a point in the fixture which holds the object being tested, the calculated phase change will be an absolute value. Otherwise, the calculated phase change would be relative value.

To calculate the displacement, the phases before and after displacement are subtracted from each other. These phase values have been unwrapped before the subtraction.

$$\Delta \phi(x, y) = \phi_2(x, y) - \phi_1(x, y) \tag{3.57}$$

TABLE 2 Determination of the phase modulo 2π . Range of phase values Numerator Denominator Adjusted phase $[\sin \phi]$ [cos ф] positive positive φ positive negative π - Φ negative negative $\pi + \phi$ negative positive $2\pi - \phi$ 0 anything π π positive 0

negative

0

Of course, if we are interested only in the surface shape, we do not need to measure the deformed stage of the object and do the phase subtraction. What we need to do is to measure the phase of the stable object and do the phase unwrapping.

3.10.7 From phase change to displacement

Once the phase change is known, the corresponding displacement can be determined from the phase information. The surface displacement H at the location (x, y) is

$$H(x,y) = \frac{\Delta \phi(x,y) \lambda}{2\pi (\cos \theta_i + \cos \theta_y)}$$
 (3.58)

where λ is the wavelength of illumination, and θ_i and θ_v are the angles of illumination and viewing with respect to the surface normal. We can see here that the illumination and viewing directions will affect the measured value. The detailed relationships between actual and measured displacement have been discussed in chapter 2.

Chapter 4

Nondestructive Test of Composite Using ESPI

In this chapter we will first discuss some commonly used stressing techniques for nondestructive testing (NDT) using optical interferometry, then some NDT experimental results on composite material using ESPI will be presented.

The most successful methods of nondestructive testing at present would be pitch-catch, pulse-echo ultrasonics, and dye-penetrant enhanced x-ray radiography. Use of any of these non-destructive evaluation techniques requires that some forethought be given to the type of failure mode likely to be encountered. With both ultrasonic methods, liquids are generally used to carry acoustic waves into the panel. Similarly, the radiopaque penetrant used in radiography is also a liquid. The penetration of these liquids into the fracture surface can constitute a form of chemical contamination. A new NDT method urgently needed. The ESPI technique has a great potential to become a new generation of NDT tool.

4.1 Stressing Techniques

The object under test can be mildly stressed in several ways, which include mechanical stressing, thermal excitation, pressurization, and acoustic or mechanical vibration. The method employed would depend upon the object itself, the type of defect to be detected, and the accessibility of the object.

4.1.1 Mechanical Stressing

Mechanical stressing refers to loading the test objects in simple tension, compression, torsion, bending, or by applying point loads. Mechanical shakers also have been used for

79

object vibration analysis. The approach chosen for a particular test will depend upon object geometry and the particular type of defect being sought. Many of the techniques mentioned above have been utilized in conventional holographic interferometry, and they can also be used in ESPI. Tension and bending loading have been used to locate fabric cuts, delaminations, and overlaps in flat sheets of fiberglass reinforced plastics.

Grunewald et al. [50] have demonstrated that the sensitivity of flaw detection in this type of application depends on the relative orientation of the flaw and the applied stress, and also the depth of the flaw below the fibers. One method which has fairly wide acceptance is the use of mechanical shakers for vibration analysis.

For NDT of composites, the most simple mechanical loading setup maybe is to use gravity force. In this setup, the specimen is placed with minimum supporting force or just allowed to stand freely by itself. This method will be discussed later in this chapter.

When designing a mechanical loading device, care should be taken to ensure the mechanical stability of the fixture. Before and after stressing the specimen, the fixture should not deform in comparison with the wavelength. Otherwise, the fixture will introduce fringes to the speckle pattern of interest.

4.1.2 Thermal Stressing

Thermal stressing has been used for various applications of holographic nondestructive testing. This technique is used to observe mechanical deformation which occurs in response to changes in temperature. The test object can be heated by a heating device such as a hot air gun, quartz heater, infrared lamp or even a resister. It also can be cooled by evaporation after a volatile substance like alcohol has been sprayed on it. Air spaces created by debonds conduct less heat than do regions where a good bond exists, so the temperature field itself is distorted. Similar thermal distortion can be caused by crushed honeycomb cores, voids, delaminations, or by other nonhomogeneities in composite materials.

Some other applications with thermal stressing are the inspection of electronic components and circuit boards [51-53].

In our experimental study, we found that using steamed air (vapor) to introduce temperature into material, especially composite material, is very effective. The steamed air can be directed to a localized area, or spread to a large area easily.

Creating a small temperature difference (ΔT about 10 °C) between the specimen and the ambient, then allowing the specimen to expand freely or under some constraint was also found to be very effective and easy to do. A small refrigerator was used in our study.

4.1.3 Pressure Stressing

Burchett [54] has studied the applicability of holographic interferometry to nondestructive testing of carbon composite cylinders by using pressurization.

The pressurization method is ideal for pressure vessels and other structures that can be pressurized. With the double-exposure technique, the structure under test is pressurized between the exposures. The sequence of the exposures is immaterial. The structure may also be initially pressurized and then additionally pressurized. Pressurization usually does not introduce intolerable rigid-body motion. Internal pressurization may also be employed to inspect honeycomb structures. Honeycombs are generally sealed and therefore can be pressurized easily. By drilling a small hole through the skin, the structure can be internally pressurized through the hole. The hole is then mended after testing. The technique may be developed into a method for inspecting honeycombs in an aircraft in the field. A permanent access of pressurization may be built in the structures for regular inspection in service.

Some commercial HI systems for nondestructive testing of automotive and aircraft tires utilize pressure and vacuum stressing. The objective of this testing is to locate a variety of flaws such as separations, broken belts, debonds, and voids that can occur in tires. A

differential vacuum between holographic exposures induces a slight change in the overall tire shape and also causes a bulging at debond regions, which contain entrapped air.

This appears to be the most satisfactory method for holographic inspection of tires [55].

ESPI can also be used in these areas with similar procedures.

4.1.4 Acoustic Stressing

Ultrasonic waves can be used to introduce a mechanical and internal stressing condition. This technique can be used for NDT on a composite material. Note that some kind of medium is needed for coupling ultrasound into the specimen.

4.1.5 Vibrational Excitation

Vibrational excitation is useful for detecting debonds in composite materials and for disclosing inhomogeneites in materials or structures. The technique can be used in two ways; First, the entire structure being analyzed can be vibrated in a resonant mode. This creates bending stresses or torsional stresses which may cause anomalous deformation near flaws such as voids, delamination or matrix crushing. This method has been used to test turbine blades [56] and to detect flaws in fiberglass-reinforced plastics [45]. Second, debonds near the surface, for example, between the skin and the core of a honeycomb panel, create a locally flexible structure which can be caused to resonate.

4.1.6 Microwave Excitation

Microwave stressing is used to detect the presence of moisture in materials. Between the exposures, the object is excited by microwaves having the frequency which excites water molecules. The microwave excitation causes the moisture in the materials to heat up and this induces highly localized deformation detectable by ESPI. This method of stressing is only applicable to nonmetallic materials.

4.2 NDT Results of Composite Using ESPI

In this study, we mainly used three stressing techniques--thermal stressing, gravity force and vibration excitation. Composites studied were glass/epoxy plate and carbon fiber (A s-4/828 mPDA) plates.

The objective was to gain more understanding about how the defect (damage) is affecting the mechanical, thermal and dynamic properties. The ESPI system used is illustrated in Figure 4.1.

4.2.1 Using Thermal Stressing

Refer to Figure 4.2 for the specimens used in this analysis. Thermal stressing technique is especially suitable for the NDT of composites. This is based on the following factors:

4.2.1.1 Fundamentals

(1) Fibers have significantly smaller coefficients of thermal expansion (CTE), the CTE of glass fiber is 5.0 x 10⁻⁶/K, while a typical epoxy value is 54 x 10⁻⁶/K. Carbon and graphite fibers are anisotropic in thermal expansion. The CTE are usually extremely small, either positive or negative, of the order of 0.9 x 10⁻⁶/K. It follows that a unidirectional fiber composite has very small CTE in the fiber direction because the fibers will restrain matrix expansion. On the other hand, transverse CTE will be much larger because the fibers move with the expanding matrix and thus provide less restraint to matrix expansion.

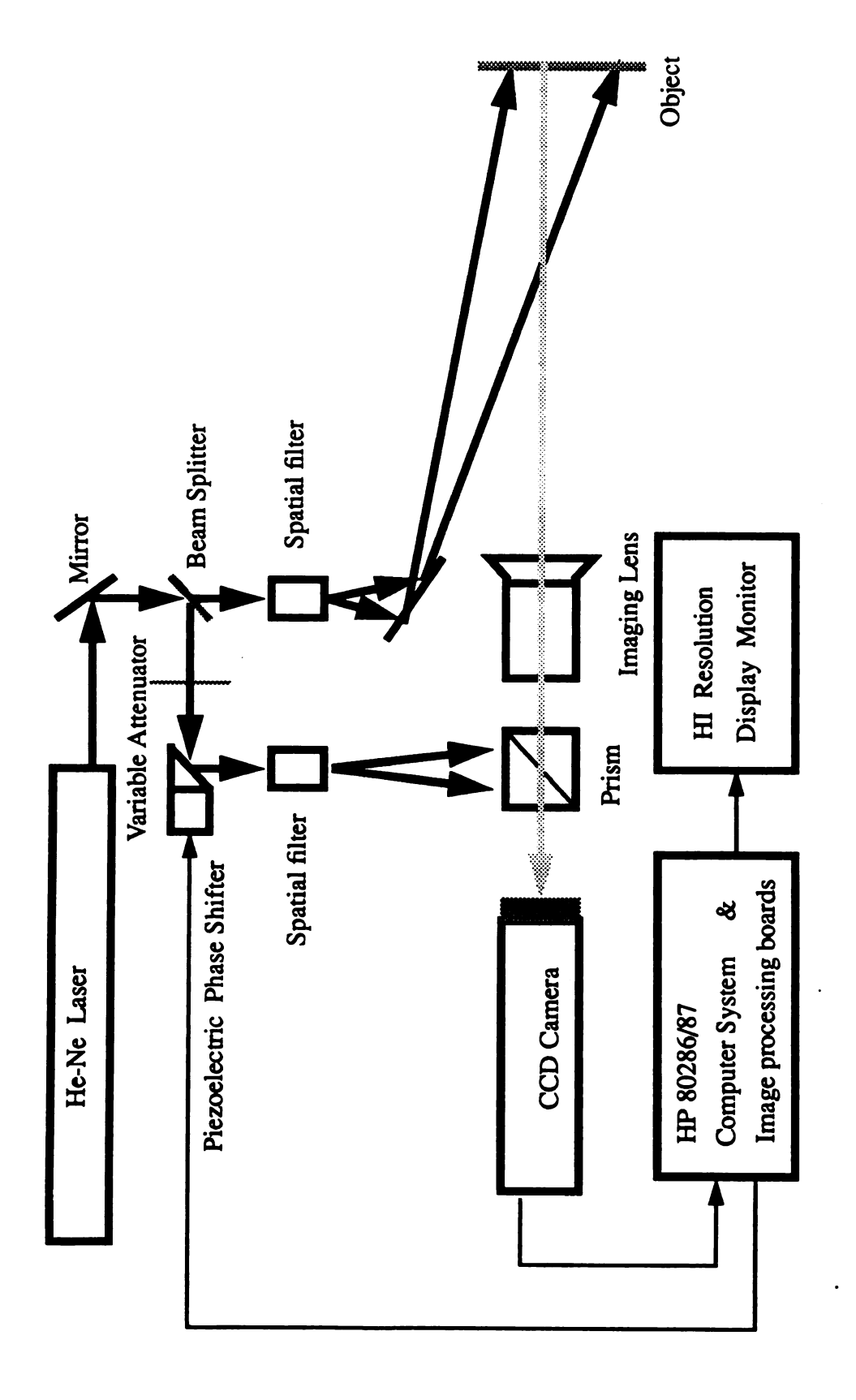


Fig. 4.1 The ESPI system

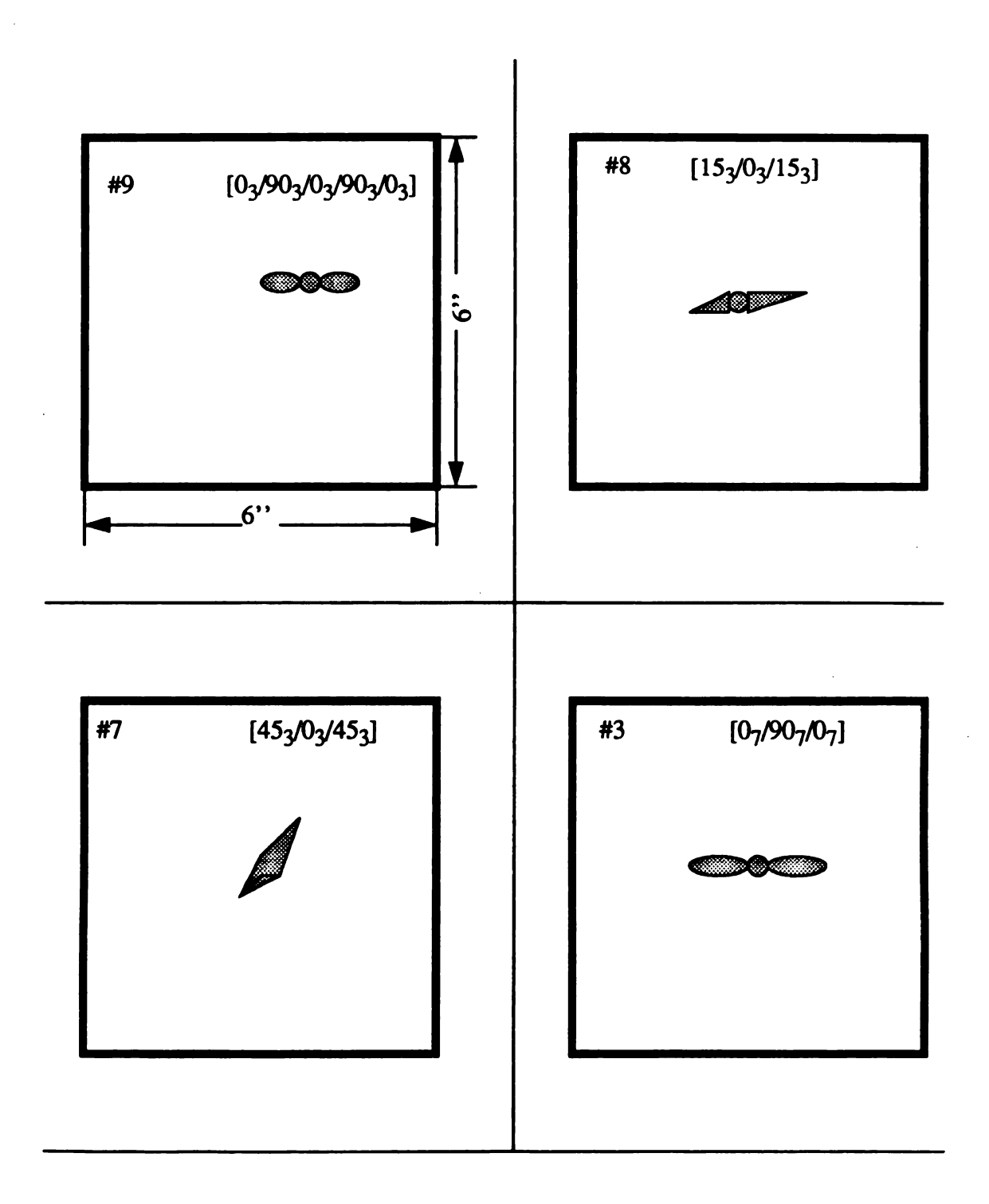


Fig. 4.2
Impact damaged composite (glass/epoxy)specimens used in NDT using ESPI gravity and thermal stressing techniques

These phenomena are of considerable practical importance, particularly for laminates made of unidirectionally reinforced layers. When such a laminate is heated, the expansion of any layer is prevented by the adjacent laminae because the fiber directions in all layers are different. This causes internal stresses that could be considerable, even when the laminate is allowed to expand freely.

(2) All polymetic matrix viscoelastic properties, such as creep and relaxation, are significantly temperature dependent. This will also introduce deformations when there is a temperature change.

No mater how complicated the stress field is, looking at the large scale, the stress introduced displacement field should be uniform if the composite plate is uniform. So, for NDT we are looking for any irregularities.

4.2.1.2 Heating Devices

Three devices were used for thermal study.

- (1) A resistor (25 ohms and 12 W) with adjustable current was used. The temperature was controlled at about 60 °C (see Figure 4.3 for the setup). During the heating process, the resistor was at a distance of 2 to 3 mm from the specimen.
- (2) Steamed air (vapor) was generated from a coffee pot and conducted through a flexible plastic pipe towards the specimen (see Figure 4.4 for the setup). Vapor can be brought to a localized small area or spread to the entire specimen.
- (3) A small refrigerator was used to create a uniform temperature gradient between the specimen and the ambient. The temperature difference used was about 8 to 12 °C.

4.2.1.3 Results

Results are presented in Figures 4.5 - 4.11. Please refer to Figure 4.2 for the configurations of the specimens. The 'free expansion' results were actually the

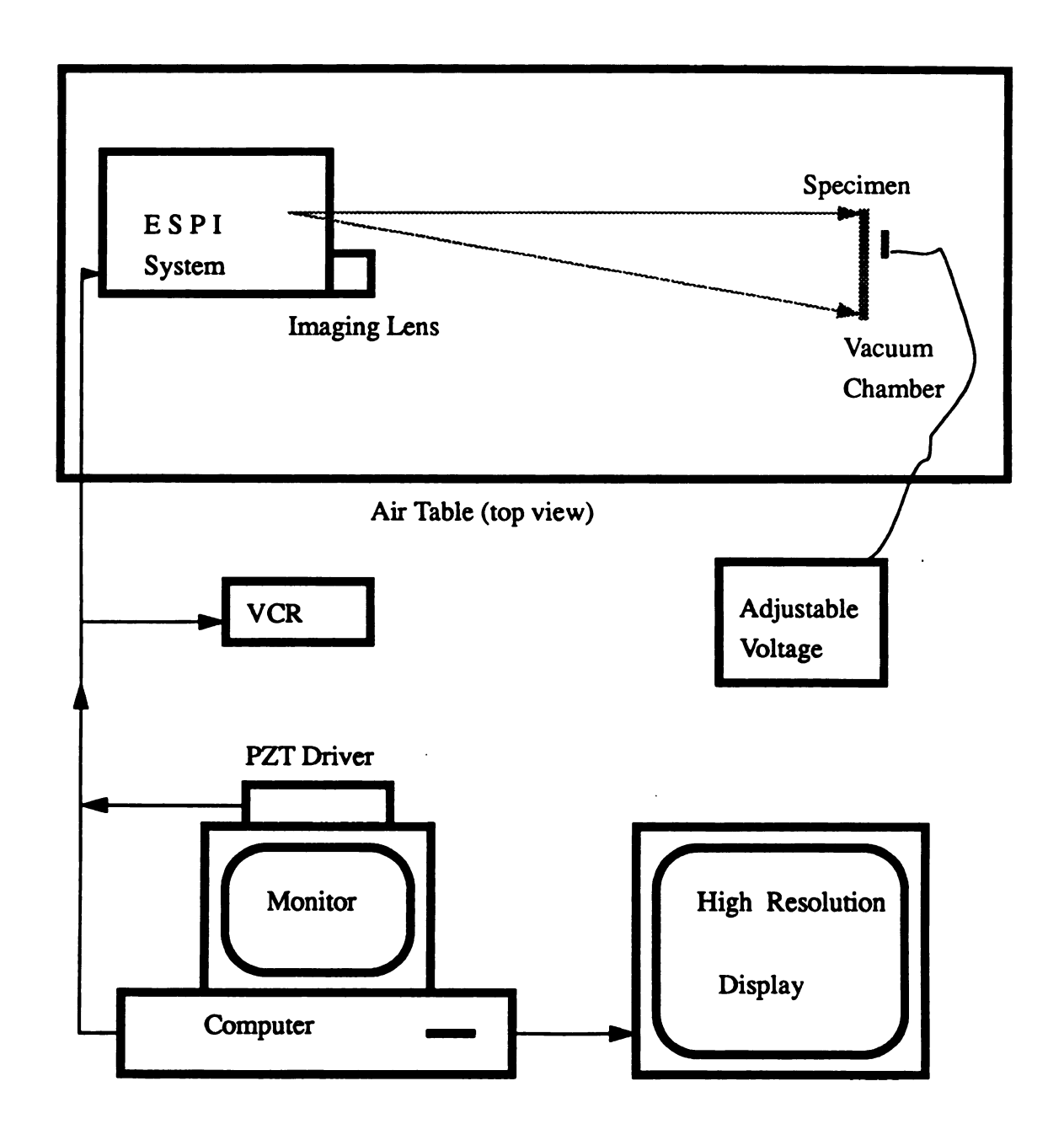


Fig. 4.3
Setup for NDT of Composite using ESPI thermal (resistor) method

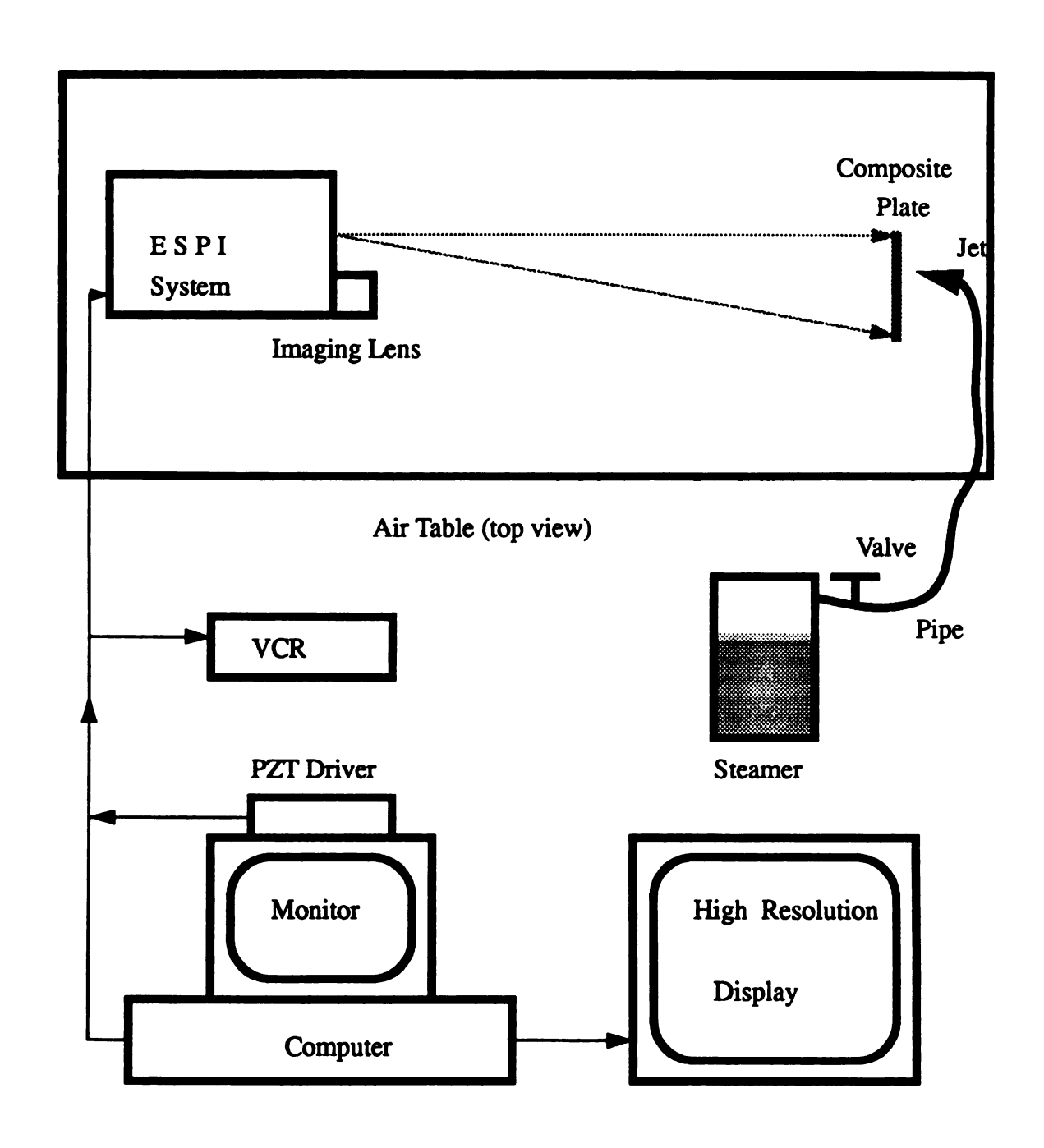


Fig. 4.4
Setup for NDT of composite using ESPI thermal (steamer) method

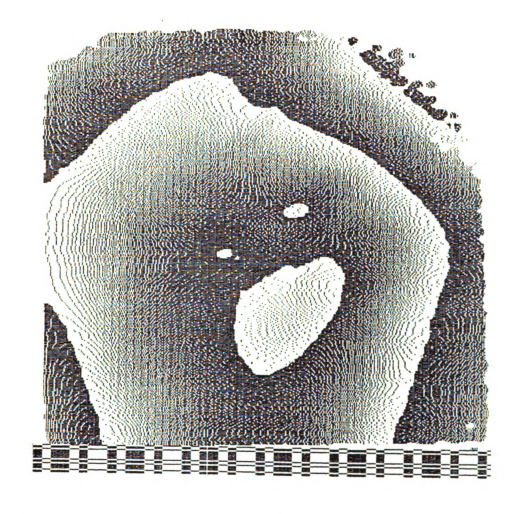


Fig. 4.5

Fringe pattern obtained when composite plate #7 is 'point heated' at the center using a resistor heating device and then with the heater removed.

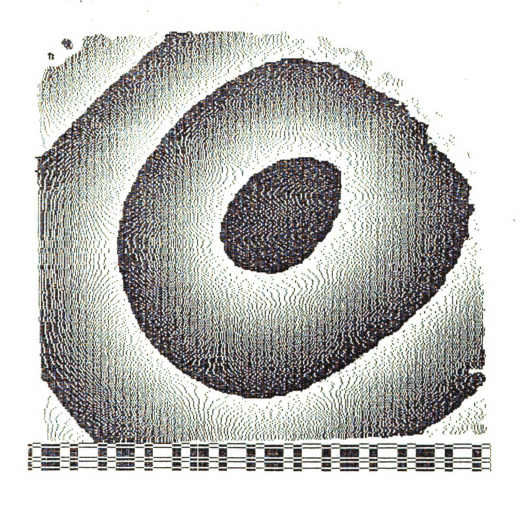


Fig. 4.6

Fringe pattern obtained when composite plate #7 is heated at the upper right corner using a resistor heating device and then the heater is removed.



Fig.~4.7 Fringe pattern obtained when composite plate #7 is in free expansion at ΔT about 8 °C (23-15) with Δt about 5 seconds.

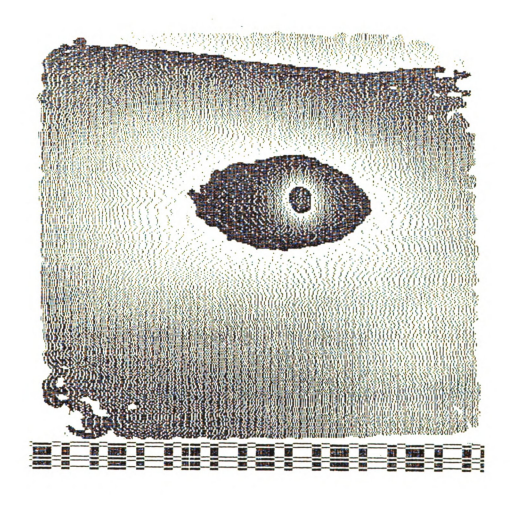
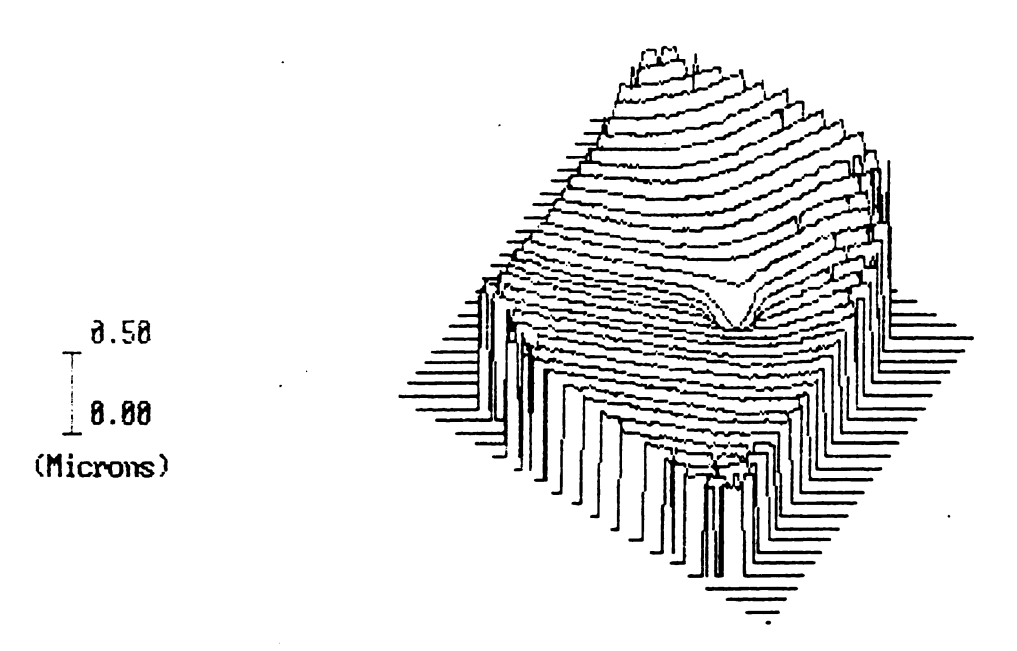


Fig. 4.8

Fringe pattern of plate #9 when heated at the upper right corner and then with the heater removed.

Peak to valley : 0.88 Microns



3-D 'ISOMETRIC' PLOT OF OUT OF PLANE DISPLACEMENT

Fig. 4.9
This is the 3D plot of Figure 4.8.

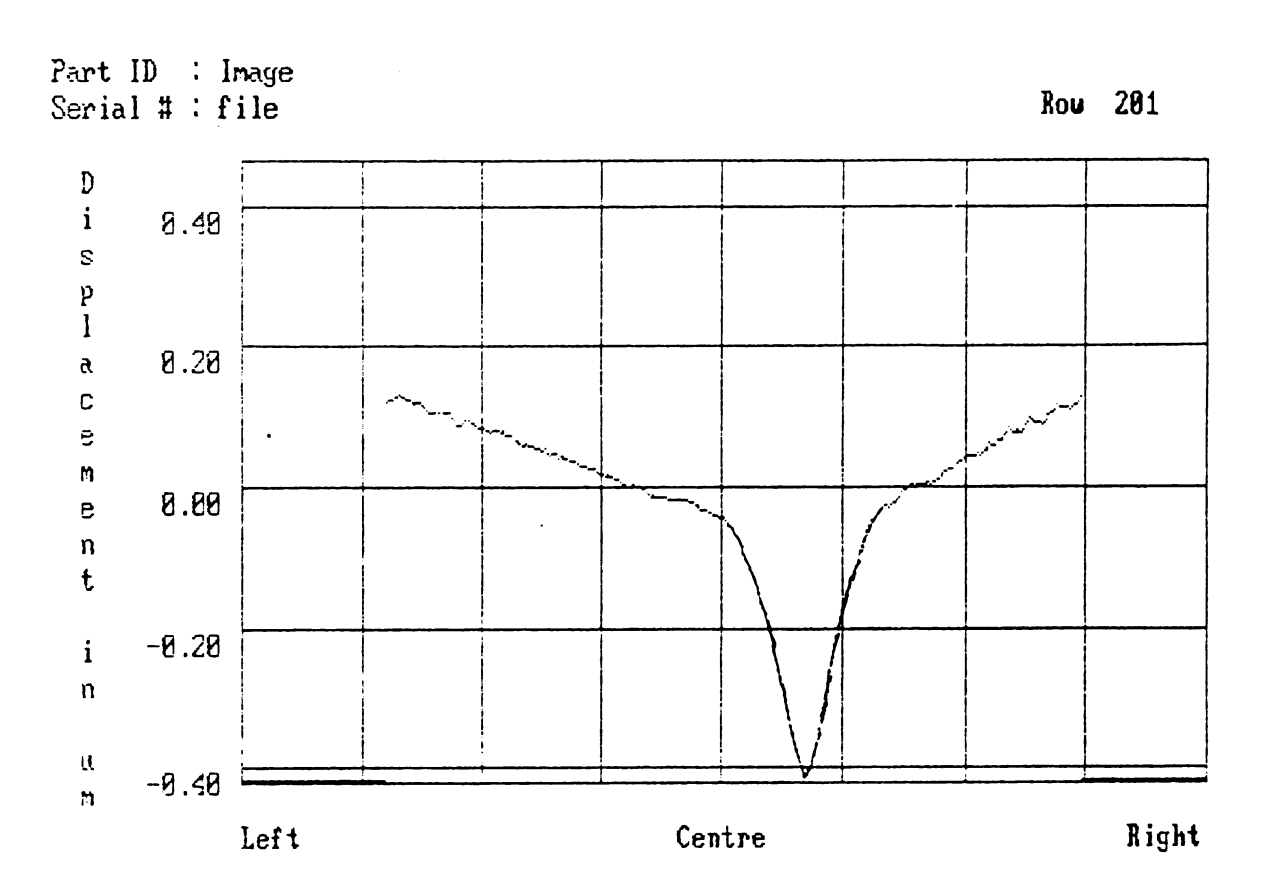


Fig. 4.10
2D plot of Figure 4.8 of the section where the damage spot is located.

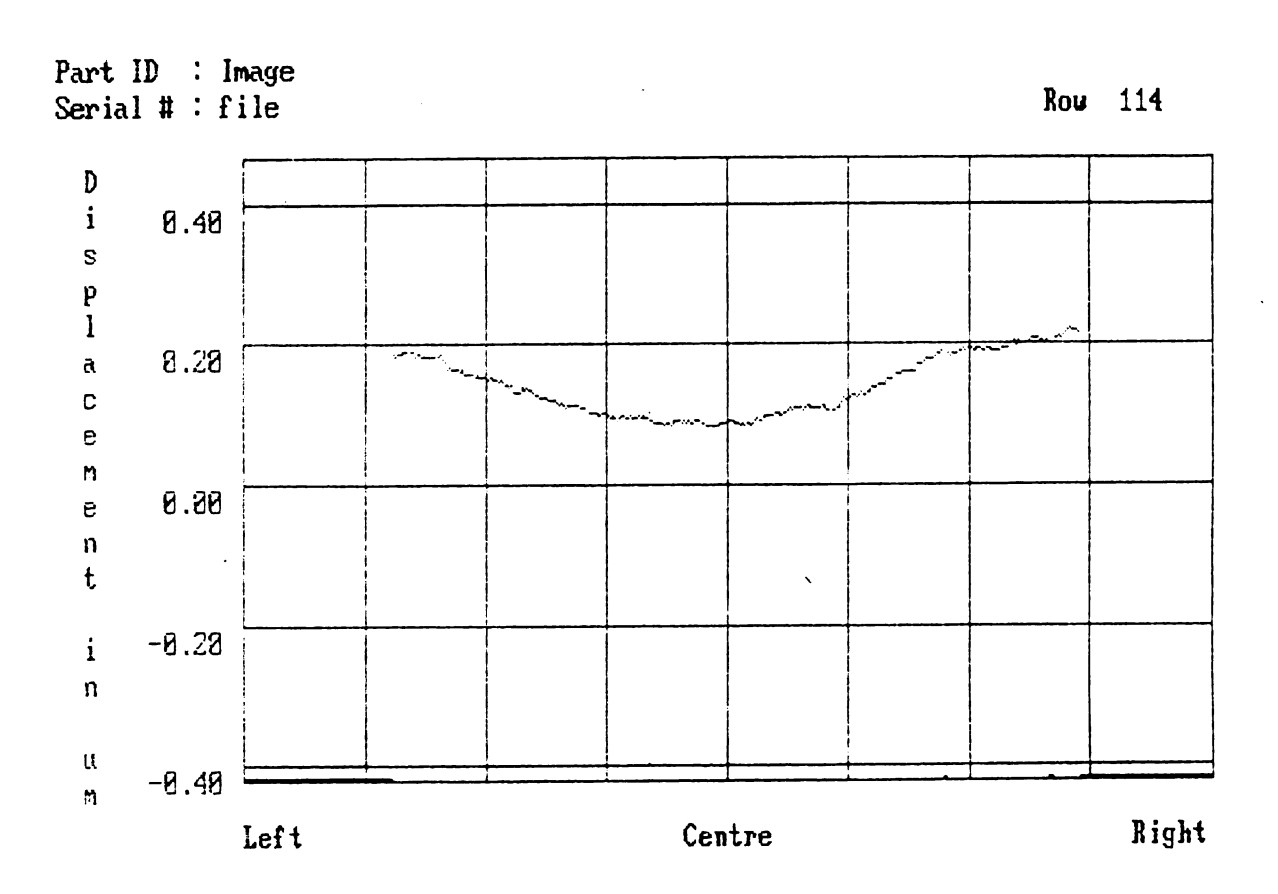


Fig. 4.11
2D plot of Figure 4.8 of a arbitrary section away from the damaged spot.

combination of thermal and creep effects.

4.2.1.4 Discussion and Summary

For an undamaged plate, when the heat source is removed, the created fringe pattern will tend to trace back into the original (or primary) heat point or the area which generates those fringes, and the speed of the 'trace back' is very fast (several seconds). If there is damage, the damaged zone will block this 'trace back' and act as another heat source creating some 'secondary' fringes, and these 'secondary' fringes will rest there for quite some time. These phenomena were checked on different specimens using different heating location. This happens because in the damaged zone the matrix is loosened, some fiber may be broken and likely there will be some air trapped in the matrix and between laminates. Overall, these will decease the thermal conductivity in the damaged zone area. When we monitor the live change of this phenomena it is quite obvious. To characterize the size of the damage and the depth of the damage more work need to be done.

The steamer we used is very simple. A more sophisticated device can be built to have adjustable heat flow.

4.2.2 Using Gravity (creeping)

This is unique and simple to do, and it seems especially suitable for composite materials. Figure 4.12 is the setup.

All polymers exhibit time dependence of material response. This manifests itself by the increase with time of deformations under constant load, which is called creep, and conversely, by the decrease with time of stresses under deformation constraints, which is called relaxation. These phenomena may be used to do NDT for a composite material.

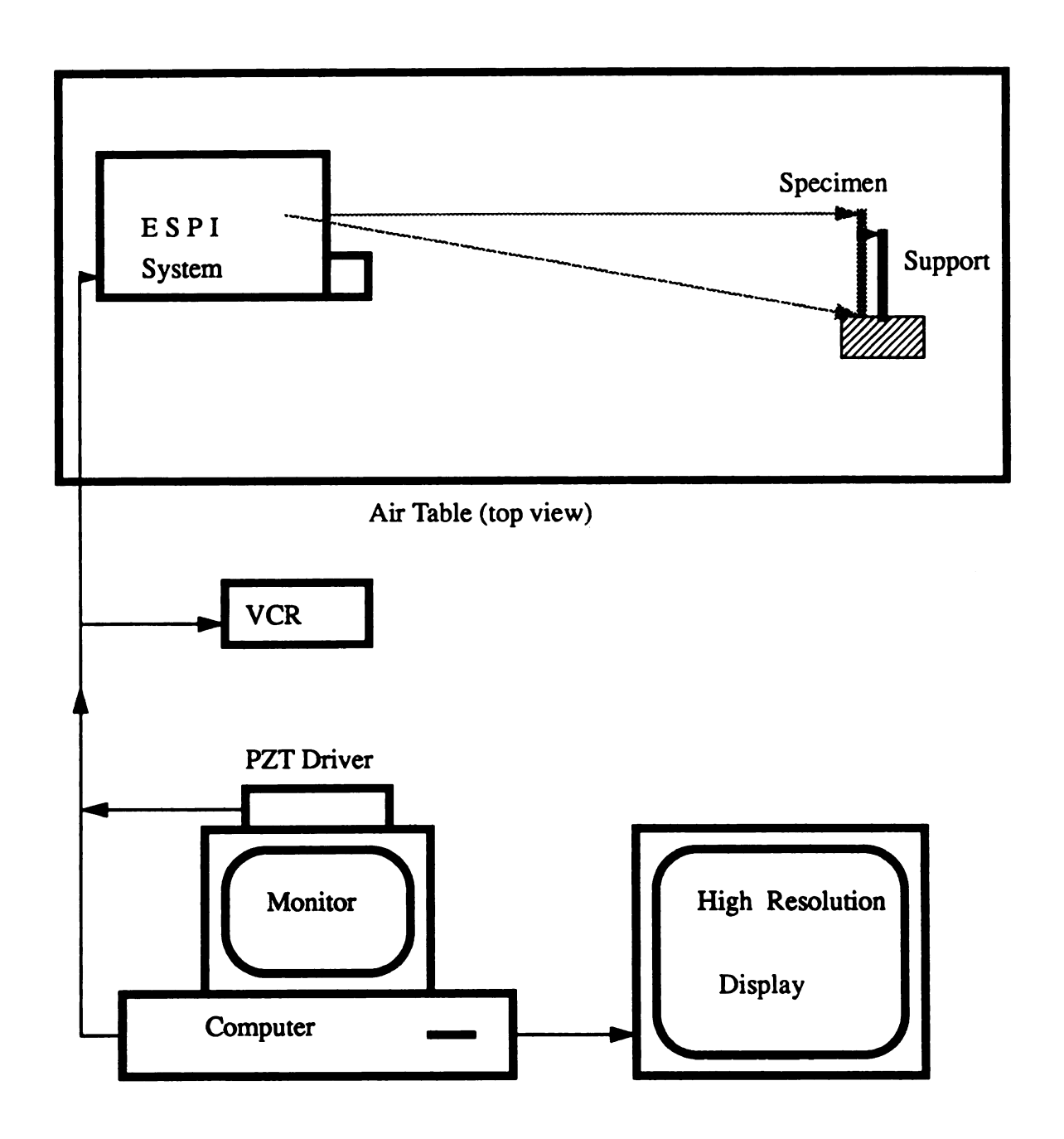


Fig. 4.12
Setup for gravity creeping test of composite using ESPI

The effects described are of considerable engineering importance for fiber-reinforced composite structures, because stresses and deformations determined on the basis of elastic analysis may change considerably with time because of polymeric matrix time dependence. ESPI can be used to monitor those time-induced deformations in real time, and, therefore, provide more understanding about composite materials.

All polymeric matrix viscoelastic properties, such as creep and relaxation, are significantly temperature dependent, so, creep and thermal techniques can be combined to create a new NDT method for composite.

We found that even at room temperature the damaged and undamaged composite plate will give significant difference in terms of the number of fringes and shape of the fringes accumulated in certain time period. Those fringes are induced only by gravity force. Certainly, this has something to do with the nature of the damage and the size of the damage zone. Some results are presented in Figures 4.13 - 4.15.

4.2.3. Using Vibration Method

The experiments we did were on impact damaged glass/epoxy plates with various layouts. Two samples are presented here (Figure 4.16). A speaker was used as the excitation for this study (Figure 4.17). Results shown in Figures 4.18 - 4.26. Unidirectional carbon fiber plates (A s-4/828 mPDP) with cuts were also studied (Figure 4.27), and results are presented in Figures 4.28 - 4.29.

We found that:

- (1) At low frequency, damaged and undamaged plates have similar vibration modal shapes. At higher frequency, the vibration modal shape becomes very different.
- (2) Many resonant frequencies are under 1000 Hz., and the excitation of those frequencies is easy.

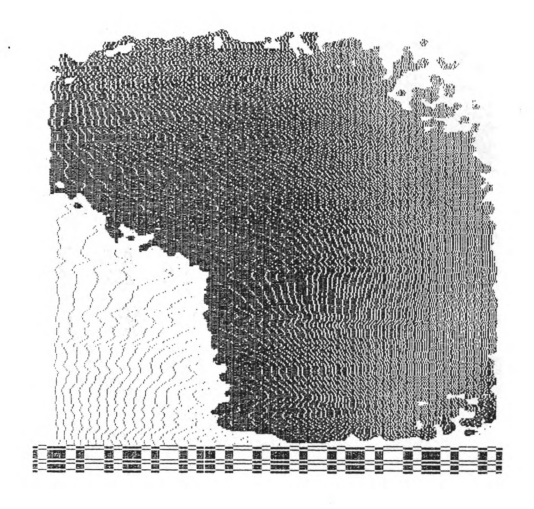


Fig.~4.13 Plate #3 creeping at room temperature with fringe accumulation time $\Delta t=5~s.$

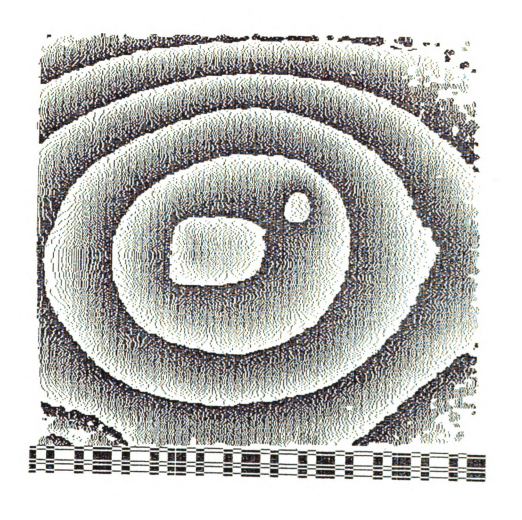


Fig.~4.14 Plate #9 creeping at room temperature with fringe accumulation time $~\Delta t = 30~s.$

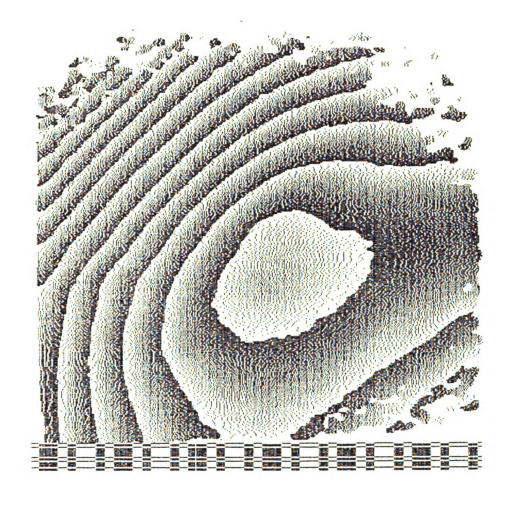
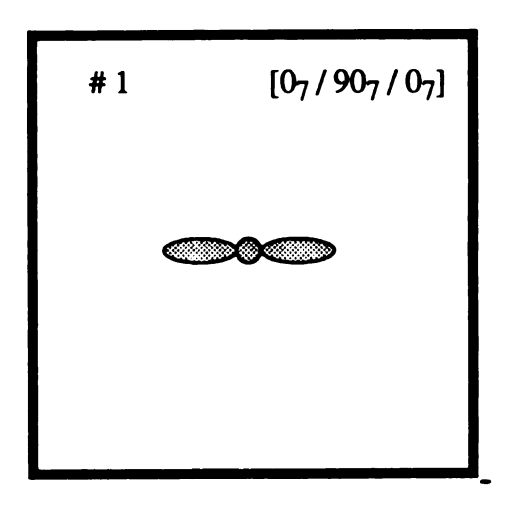


Fig.~4.15 Plate #7 creeping at room temperature with fringe accumulation time $~\Delta t=30~s.$



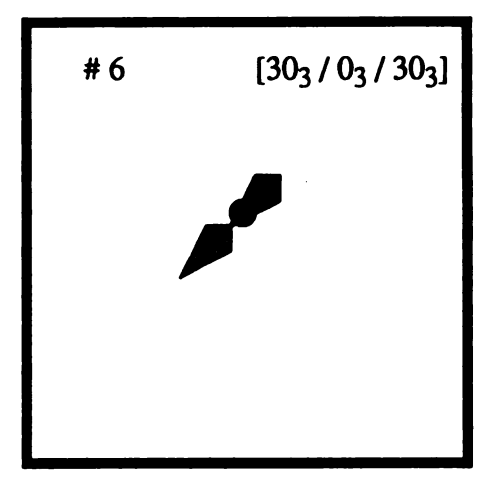


Fig. 4.16
Impact damaged composite (glass/epoxy)specimens used in NDT using ESP time-average mode, speaker was used for excitation.
Dimension is 6" x 6".

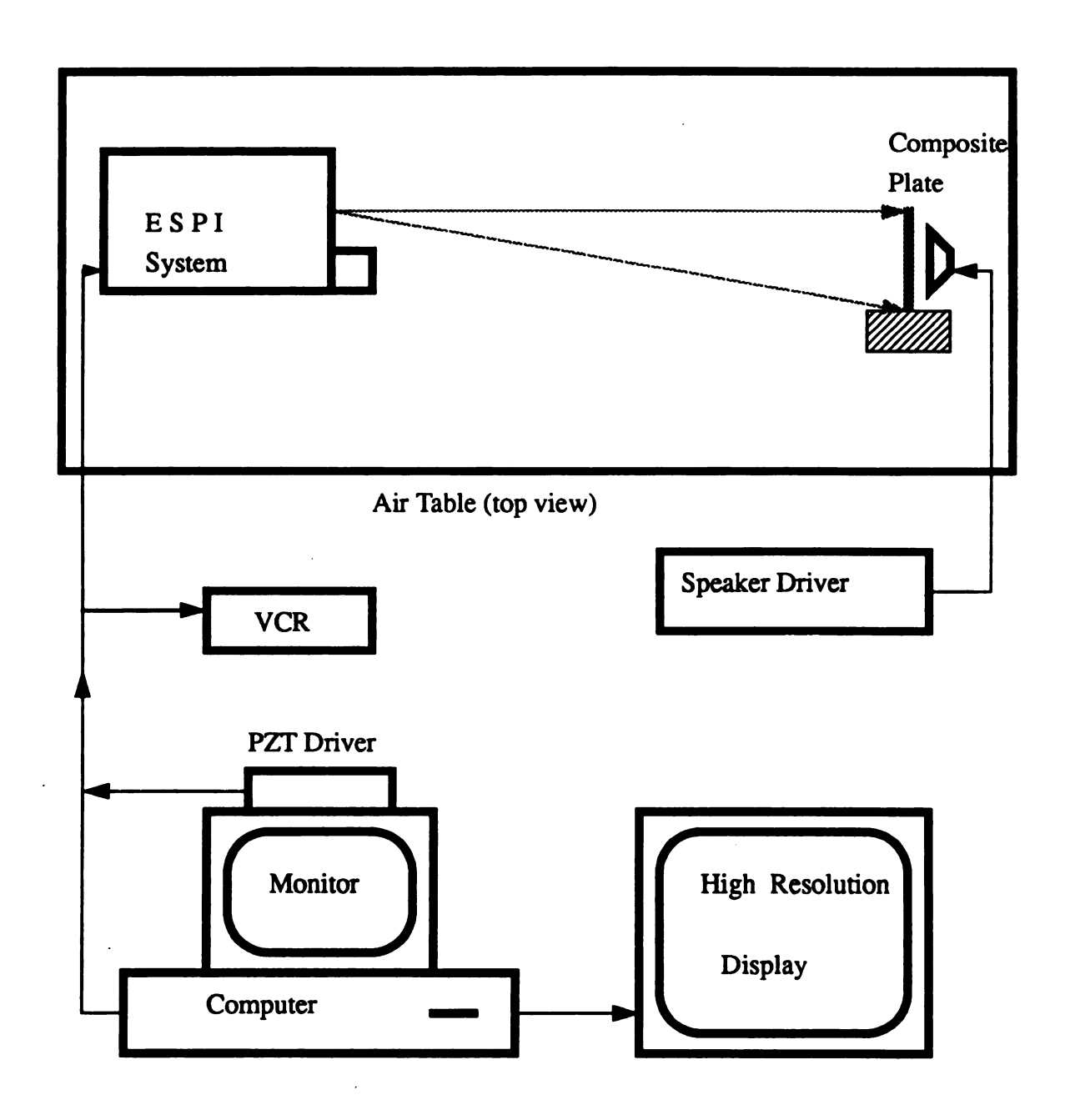


Fig. 4.17
Setup for vibration test using a speaker

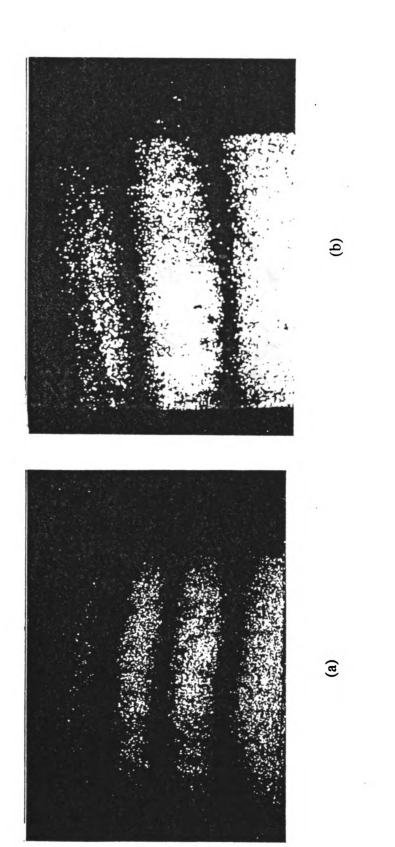


Plate #1 vibrating at 173 Hz, (a) before impact, (b) after impact.

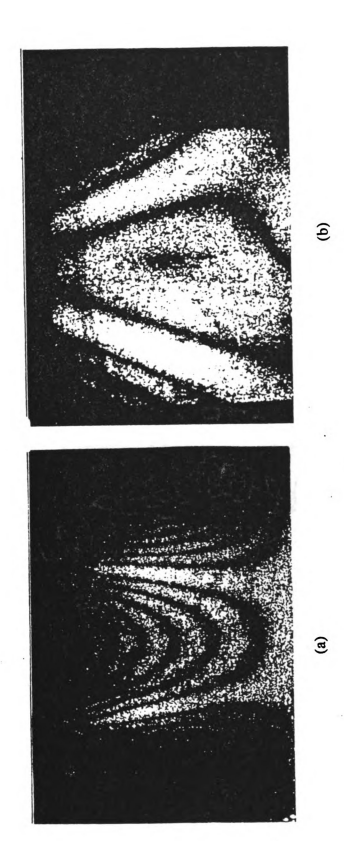


Plate #1 vibrating at 707 Hz, (a) before impact, (b) after impact.

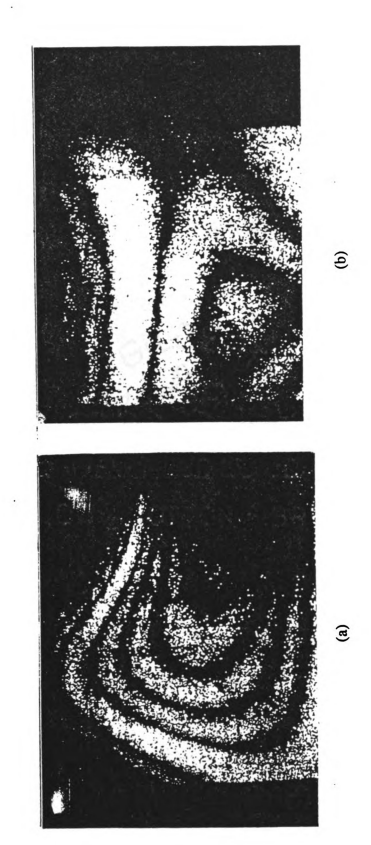


Plate #1 vibrating at 942 Hz, (a) before impact, (b) after impact.

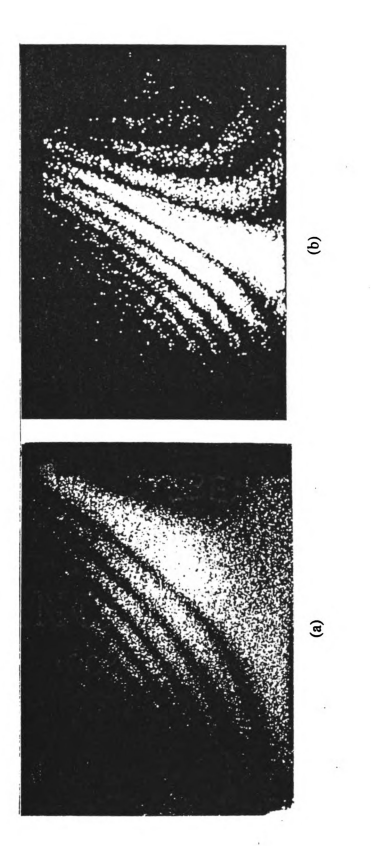


Plate #6 vibrating at 100 Hz, (a) before impact, (b) after impact.

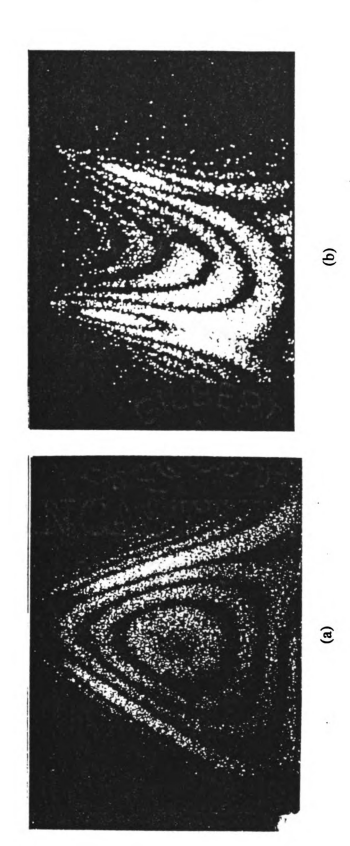


Plate #6 vibrating at 300 Hz, (a) before impact, (b) after impact.

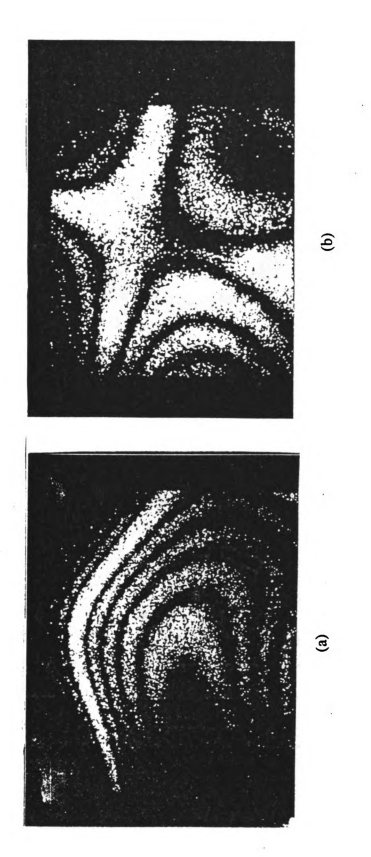


Plate #6 vibrating at 388 Hz, (a) before impact, (b) after impact.

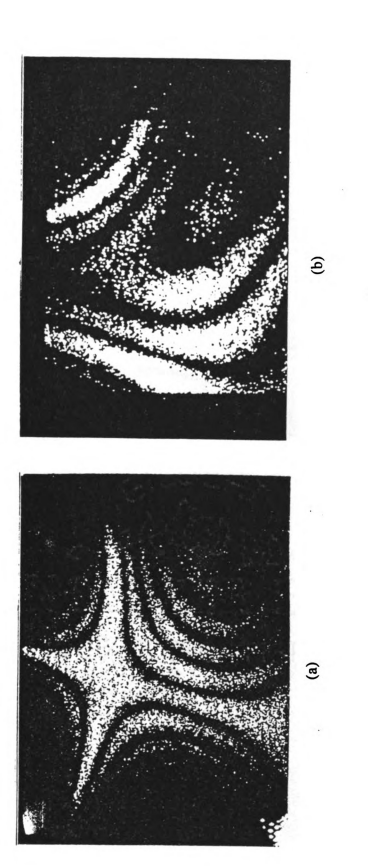
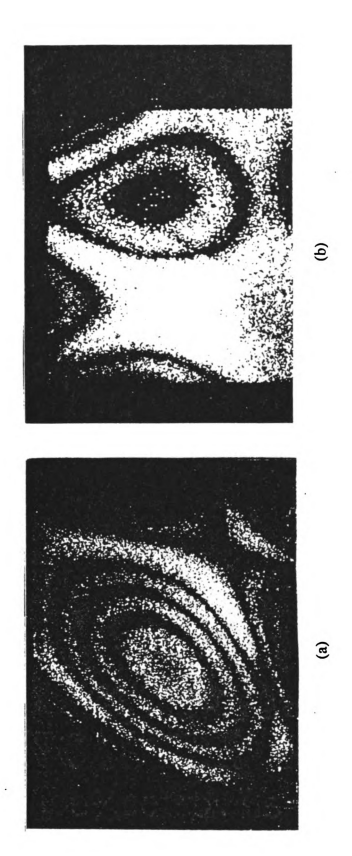


Fig. 4.24
Plate #6 vibrating at 451 Hz, (a) before impact. (b) after impact.



 $\overline{\text{Fig. 4.25}}$ Plate #6 vibrating at 761 Hz, (a) before impact, (b) after impact.

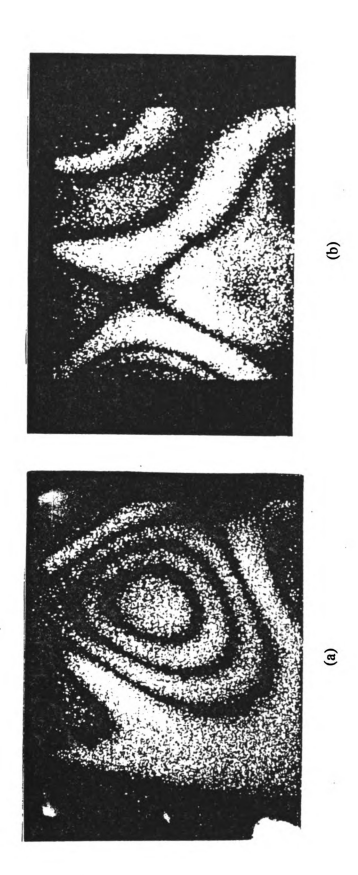


Plate #6 vibrating at 805 Hz, (a) before impact, (b) after impact.

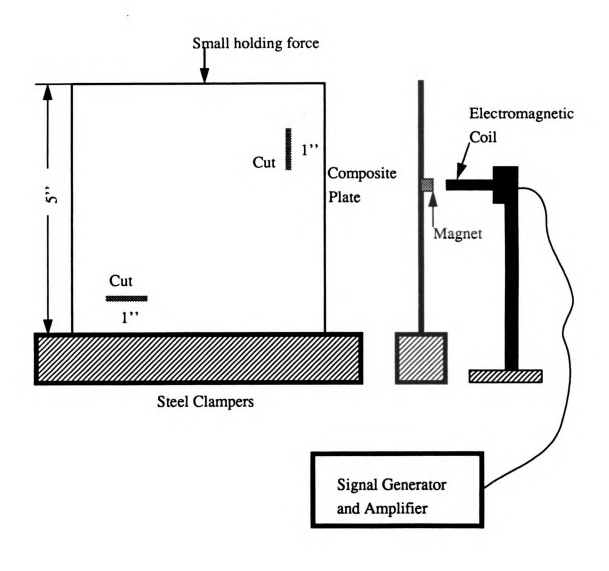
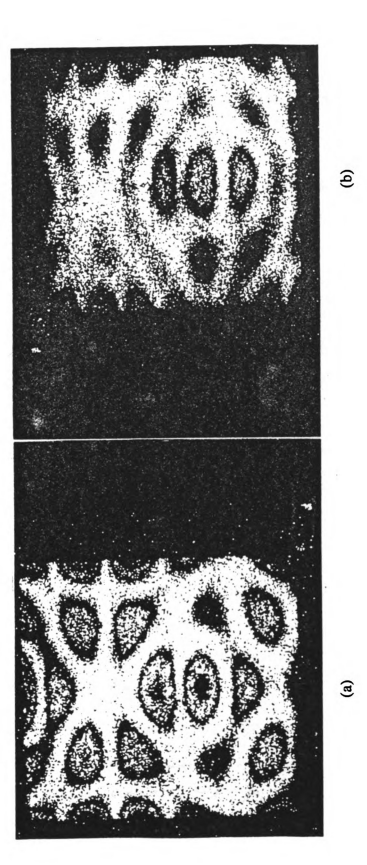


Fig. 4.27
Experimental setup for nondestructive inspection using
ESPI's time average vibration mode. The composite being
tested is A s-4/828 mPDA, 18 plies, the depth of cut is 9 plies.



Fig. 4.28

Carbon fiber plate vibrating at 2057 Hz, (a) plate without cuts, (b) plate with cuts.



Carbon fiber plate vibrating at 8150 Hz, (a) plate without cuts, (b) plate with cuts.

CONCLUSIONS AND RECOMENDATIONS

The improvement in image processing techniques, development of high resolution cameras, and creation of faster and efficient algorithms have enabled ESPI to reach a stage where it can be employed as a usable and reliable measuring tool. However, use of ESPI in the industrial environment would be enhanced by maximizing cost effectiveness and compactness while minimizing the need for a stable environment. The advantages dictating the choice of ESPI over conventional methods are its non-contacting nature and fast displacement and vibration modal shape presentation combined with high accuracy and repeatability.

Compared with decorrelation of speckles, the 'memory loss' is more important. At the present time, a standard TV system is used in ESPI, and it imposes some limits on the capability of ESPI. The vertical resolution and horizontal resolution of a standard TV system are about 20 μ m with respect to the CCD's image target.

To reduce environmental effects, basically there are two ways to go. (1) Shortening picture taking time, designing a special TV system, and improving the image taking camera. (2) Making a 'self-compensation' setup, as used, for example, in the principle of operation of shearography.

On the other hand, more study in the area of NDT of composite materials and other materials should be carried out using the current ESPI system. Effort should be exerted to get more insight and understanding of the different stressing techniques and their effectiveness in testing various materials.

LIST OF REFERENCES

LIST OF REFERENCES

- 1. R. L. Powell and K. A. Stetson, "Interferometry vibration analysis by wavefront reconstruction," Journal of the Optical Society of America, 55 (12) 1593-1598 (Dec. 1965).
- 2. C. M. Vest, E. L. Mckague, and A. A. Friesem, "Holographic detection of microcracks," Trans. ASME, Ser. D-J, Basic Engineering, 93, 237-246 (1971).
- 3. A. D. Luxmoore, "Holographic detection of cracks in concrete," Nondestr. Test 6, 258-263 (1973).
- 4. M. J. Salkind, "Early detection of fatigue damage in composite materials," J. Aircr., 13, 764-769 (1976).
- 5. C. S. Bartolotta and B. J. Pernick, "Holographic nondestructive evaluation of interference fit fasteners," Appl. Opt., 12, 885-886 (1973).
- 6. C. M. Vest and D. W. Sweeney, "Applications of holographic interferometry to nondestructive testing," Int. Adv. Nondestr. Test., 5, 17-21 (1977).
- 7. R. J. Parker and D.G.Jones, "Holography in an industrial environment," Optical Engineering, p055-063, vol. 27 No. 1 (January 1988).
- 8. A. Macovske, Appl. Opt. 16, 2722 (1971)
- 9. O. Schwomma, Austrian patent 298,830 (1972)

- 10. J. N. Butters and J. A. Leendertz, Opt. Laser. Technol. 3, 26 (February 1971)
- 11. J. W. Goodman, "Laser Speckle and Related Phenomena," Chapter 2, ed. J. C. Dainty, Springer-Verlag: Berlin (1975).
- 12. J. D. Rigden and E. I. Gordon, Proc. I. R. E. 50, 2367 (1962)
- 13. B.M. Oliver, Proc. IEEE 51, 220 (1963)
- 14. J.W. Goodman, Proc. IEEE 53, 1688 (1965).
- 15. E. Wolf, Proc. Roy. Soc. (London) A225, 96 (1954).
- 16. S. Lowenthal and H.H. Arsenault, J. Opt. Soc. Am. 60, 1478 (1970).
- 17. F. Eernike, Physica 5, 785 (1938)
- 18. J. C. Dainty, "Topics in Applied Physics", Vol 9. p209.
- 19. J.M. Burch, Optical Instruments and Techniques, 1970 p213-229
- 20. J. C. Dainty, "Topics in Applied Physics", Vol 9. p211.
- 21. Chaules M. Vest, "holographic Inerferometry," John Wiley and sons, Inc. (1979).
- 22.. D. Herbert, private communication.
- 23. Robert Jones and Catherine Wykes, "Holographic and Speckle Interferometry," Cambridge University Press, p167, 1983.
- 24. Robert Jones and Catherine Wykes, "Holographic and Speckle Interferometry," Cambridge University Press, p170 (1983)

- 25. Boxiang Lu, Xiangyang Yang, Harald Abendroth and Heiner Eggers, "Time-average subtraction method in electronic speckle pattern interferometry," Opt. Comm. Vol 70, 3, 177-180 (March 1989).
- 26. K. Hogmoen and O. J. Lokber, Appl. Opt., 16, 1869-1875 (1977).
- 27. T. J. Cookson, J. N. Butters and H. C. Pollard, Optics and Laser Technology, 10, 119-128 (1978).
- 28. O. J. Lokberf and K. Hogmoen, Appl. Opt., 15, 2701-2704 (1976).
- 29. G. A. Slettemoen, Opt. Commun., 23, 213-16 (1977).
- 30. J. C. Wyant, C. L. Koliopoulos, B. Bhushan and O. E. George, ASLE Trans. 27, 101 (1984).
- 31. P. Carre, Metrologia 2, 13 (1966).
- 32. J. H. Bruning, D. R. Herriott, J. E. Gallagher, D. P. Rosenfild, A. D. white and D. J. Brangaccio, Appl. Opt. 13, 2693.(1974).
- 33. C. E. Sommargren, J. Opt. Soc. Am. 65, 960 (1975).
- 34. J. C. Wyant, Appl. Opt. 14, 2622 (1975).
- 35. J. H. Bruning, "Fringe scanning interferometers," in Optical Shop Testing, ed. D. Malacara (Wiley, New York)(1978).
- 36. N. A. Massie, Appl. Opt. 19, 154 (1980).
- 37. R. C. Moore and F. H. Slaymaker, Appl. Opt. 19, 2196 (1980).
- 38. J. C. Wyant, Laser Focus, p. 65 (May, 1982).

- 39. J. C. Wyant, and K. Creath, Laser Focus, p. 188 (November, 1985).
- 40. R. N. Shagam, and J. C. Wyant, Appl. Opt. 17, 3034 (1978).
- 41. H. Z. Hu, Appl. Opt. 22, 2052 (1983).
- 42. K. Creath, Appl. Opt. 24, 3053 (1985).
- 43. G. E. Sommargren, Appl. Opt. 20, 610 (1981)
- 44. C. J. Morgan, Opt. Lett. 7, 368 (1982).
- 45. C. J. Greivenkamp, Opt. Eng. 23, 350 (1984).
- 46. G. T. Reid, Opt. Lasers Eng. 7, 37 (1986).
- 47. Guanming lai and Toyohiko Yatagai, J. Opt. Soc. Am. A/Vol. 8, 822 (May, 1991)
- 48. D. Kerr, F. Mendoza Santoyo, and J. R. Tyrer, J. Opt. Soc. Am. A/Vol. 7, 820, (May, 1990).
- 49. K. Creath, "Hologram interfeometry and speckle metrology," 473-497, SEM (1990)
- 50. K. Grunewald, W. Fritzsch, A. V. Harnier, and E. Roth, "Nondestructive testing of plastics by means of holographic interferometry," Polym. Sci. Eng., 15, 16-28 (1975).
- 51. W. J. Harris and D. C. Woods, "Thermal stress studies using optical holographic interferometry," Mater, Eval., 32, 50-56 (1974).
- 52. J. R. Crawford and R. Benson, "Holographic interferometry of circuit board component failure," Appl, Opt., 15, 24-25 (1976).

- 53. I. S. Klimenko, E. G. Matinyan, and L. G. Dubitskii, "Use of focused image holography for the nondestructive testing of electronic parts," Sov. J. Nondestr. Test., 10, 696-699 (1975).
- 54. O. J. Burchett, "Analysis techniques for the inspection of structures by holographic interferometry," Mater. Eval., 30, 25-31 (1972).
- 55. G. M. Brown, "Pneumatic tire inspection," in Holographic Nondestructive Testing, R. K. Erf (Ed.), Academic Press, New York, pp. 355-364 (1974).
- 56. L. A. Kersch, "Advanced concepts of holographic nondestructive testing," Mater. Eval., 29, 125-140 (1971).

